CIVIL ENGINEERING STUDIES
Structural Research Series No. 249

AN EXPERIMENTAL STUDY OF A FLAT SLAB FLOOR REINFORCED WITH WELDED WIRE FABRIC

by

J. O. JIRSA
M. A. SOZEN
C. P. SIESS

A Report to

THE REINFORCED CONCRETE RESEARCH COUNCIL
OFFICE OF THE CHIEF OF ENGINEERS, U. S. ARMY
GENERAL SERVICES ADMINISTRATION,
PUBLIC BUILDINGS SERVICE
HEADQUARTERS, U. S. AIR FORCE,
DIRECTORATE OF CIVIL ENGINEERING

and

U. S. NAVY, ENGINEERING DIVISION,
BUREAU OF YARDS AND DOCKS

UNIVERSITY OF ILLINOIS
URBANA, ILLINOIS
JUNE 1962

AN EXPERIMENTAL STUDY OF A FLAT SLAB FLOOR REINFORCED WITH WELDED WIRE FABRIC

by

J. O. Jirsa
M. A. Sozen
C. P. Siess

A Report on a Research Project
Conducted by the

CIVIL ENGINEERING DEPARTMENT
UNIVERSITY OF ILLINOIS

in cooperation with the

REINFORCED CONCRETE RESEARCH COUNCIL

OFFICE OF THE CHIEF OF ENGINEERS, U. S. ARMY

GENERAL SERVICES ADMINISTRATION, PUBLIC BUILDINGS SERVICE

HEADQUARTERS, U. S. AIR FORCE
Contract AF 33(658)-47

and

U. S. NAVY, ENGINEERING DIVISION, BUREAU OF YARDS AND DOCKS
NBy 37633

UNIVERSITY OF ILLINOIS

URBANA, ILLINOIS

JUNE 1962

TABLE OF CONTENTS

TABLE OF CONTENTS (Cont'd.)

LIST OF TABLES

LIST OF FIGURES

LIST OF FIGURES (Cont'd)

LIST OF FIGURES (Cont'd)

LIST OF FIGURES (Cont'd)

1. INTRODUCTION

1.1 Object and Scope

The object of the work reported is to study the behavior and strength of a flat slab reinforced with welded wire fabric which is a high-strength reinforcement.

Tests were carried out on a nine-panel flat slab designed in accordance with Section 1004 of ACI 318-56. The test structure is described in Chapter 2, its construction in Chapter 3, and its instrumentation in Chapters 4 and 5. The test structure was part of an extensive investigation of multiple panel reinforced concrete floor slabs. Descriptions of the various components of the test apparatus were given in previous reports (Refs. 2, 3, 4, 5 and 6). The details will not be repeated here.

The program of testing was established to determine the performance of the structure at design load, overload and failure. The test procedure and chronology are discussed in Chapter 6. Chapter 7 presents the behavior of the structure and the distribution of measured moments is discussed in Chapter 8 along with comparisons of the measured moments with static and theoretical moments. An analysis of the strength of the structure is presented in Chapter 9.

1.2 Acknowledgments

The studies included in this report were made as part of an investigation conducted in the Structural Research Laboratory of the Civil Engineering Department at the University of Illinois in cooperation with the following organizations:

Reinforced Concrete Research Council
Directorate of Civil Engineering, Headquarters, U. S. Air Force
General Services Administration, Public Buildings Service
Office of the Chief of Engineers, U. S. Army
Bureau of Yards and Docks, Engineering Division, U. S. Navy

The program of investigation has been guided by an Advisory Committee on which the following persons have served:

Douglas McHenry, Chairman of the Advisory Committee, Portland Cement Association
L. H. Corning, Portland Cement Association
G. B. Begg, Jr., Public Buildings Service, General Services Administration
W. J. Bobisch, BuDocks, Department of the Navy
Frank Brown, Wire Reinforcement Institute, Inc.
J. Di Stasio, Sr., Consulting Engineer, Di Stasio and Van Buren
A. S. Neiman, Headquarters, U. S. Air Force
N. M. Newmark, University of Illinois
D. H. Pletta, Virginia Polytechnic Institute
J. R. Powers, Headquarters, U. S. Air Force
Paul Rogers, Consulting Engineer, Paul Rogers and Associates
E. J. Ruble, Association of American Railroads
W. E. Schoem, Office of the Chief of Engineers, U. S. Army
M. P. Van Buren, Consulting Engineer, Stasio and Van Buren
C. A. Willson, American Iron and Steel Institute

The project has been under the direction of Dr. C. P. Siess, Professor of Civil Engineering, and the immediate supervision of Dr. M. A. Sozen, Associate Professor of Civil Engineering.

Invaluable assistance in the instrumentation of the test structures and in the development and operation of the data recording equipment was given by Professor V. J. McDonald and his staff.

The following research personnel assisted in the construction and testing of the test structure and in presentation of the data: E. J. Strougal, H. L. Smith, A. L. Heard, and L. D. Stroup.

2. DESCRIPTION OF TEST STRUCTURE

2.1 Description of Prototype Structure

The test structure was a quarter-scale model of a typical flat slab structure. The prototype was a nine-panel structure with three bays in each direction. Each panel was 20 feet on column centerlines. An over-all layout of the prototype is shown in Fig. 2.1.

The prototype slab was designed by the engineering firm of DiStasio and Van Buren according to the provisions of the empirical method in Section 1004 of the 1956 ACI Building Code. The slab was designed for a live load of 200 psf, and a dead load of 84 psf, giving a total design load of 284 psf. The design stress for the concrete was 1350 psi (f'_c = 3000 psi). The design stress for the steel was 20,000 psi.

The discontinuous edges of the structure were supported on spandrel beams. Two adjacent edges were supported on deep, narrow beams which were relatively stiff in flexure. The other two edges were supported on wide, shallow beams. The structure was symmetrical about one diagonal.

The slab was reinforced with 1/2-in. square bars. The placement of the bars in the prototype is shown in Figs. 2.2 and 2.3.

2.2 Description of the Test Structure

The over-all layout of the test structure is shown in Fig. 2.4. The structure was a nine-panel slab, with the panels spanning 5'-0" center to center of columns.

All dimensions were scaled down directly from the plans for the prototype structure by a factor of one quarter. The slab was 1 3/4 in. thick. The over-all thickness of the drop panels was 2 1/2 in. The interior drop panels were 1 ft 8 in. square. The interior column capitals were 1 ft square.

The shallow beams were 4 1/2 in. wide and 2 1/2 in. deep. The deep beams were 2 in. wide and 6 in. deep. All beams were reinforced with #2 deformed bars. The beam stirrups were made of 1/8 in. square bars and were closed. The beam reinforcement and stirrups are shown in Fig. 2.5.

The corner columns were 3 1/2 in. square, the side columns were 3 1/2 in. by 5 in. and the interior columns were 3 3/4 in. square. The length of the columns was 21 3/8 in. The columns were reinforced to provide a stiffness equal to that of the prototype structure columns which extend above the floor. The column reinforcement is shown in Fig. 2.6.

The slab was reinforced with welded wire fabric. The wire mats were fabricated of various gages of wire to provide the required steel area at each design section. The location of the mats and the wire sizes are shown in Fig. 2.7a, b, c.

2.3 Relationship of the Test Structure to the Prototype

First, it must be emphasized that the prototype was designed using 1/2 in. square bars as reinforcement. In the previous flat slab structure built from this prototype design, a direct bar for bar substitution was made using 1/8 in. square bars. However, for this test structure, such a direct substitution was not practical.

The method for establishing the wire size and spacing was to determine the area of steel provided per foot at each design section in the prototype. The wire size and spacing needed to provide the same area of steel was then determined.

Since the test structure was a quarter-scale model, the diameters of the individual wires were scaled down by a factor of one quarter. The spacing of the wires was also scaled down. This resulted in an equivalent wire for

wire substitution of the reinforcement for a prototype structure reinforced with welded wire fabric. This design was done by Mr. Frank B. Brown of the Wire Reinforcement Institute.

Since it was not possible to select wire sizes that would provide the exact areas of steel at the design sections in the original prototype, the closest size was chosen. A comparison of the area of steel provided by the welded wire fabric at each section in the model with the area of steel in a similar structure reinforced with 1/8 in. square bars is shown in Figs. 2.8 and 2.9.

The concrete used in the slab was composed of a small-size aggregate. The stress-strain curve in compression for the concrete was similar to that for concrete used in full-sized reinforced concrete structures.

3. MATERIALS AND CONSTRUCTION OF THE TEST STRUCTURE

3.1 Reinforcing Steel

(a) Slab Reinforcement

The slab reinforcement consisted of specially manufactured small-scale welded wire fabric. The wire sizes ranged from 9.5 (diameter 0.142 in.) to 16 (diameter 0.0625 in.) gage. The wires were formed into mats by welding at each intersection. The mats were crated in flat layers rather than rolled. The fabric was manufactured by the Joliet plant of the American Steel and Wire Division of the United States Steel Corperation.

Measured stress-strain curves for each of the sizes of wires used in the test structure are shown in Fig. 3.1 through 3.7. Each curve represents the average of three samples cut from the pertinent mats. The strain at fracture measured over 4 in. including the zone of fracture ranged from 1.5 for the 15 gage wire to 2.5 for the 9.5 gage wire. The apparent initial modulus of elasticity was very close to 30×10^6 psi. Welding did not seem to have affected the stiffness appreciably. The ultimate stress ranged from 70,000 to 81,000 psi.

To improve the bond properties of the steel, the wire mats were placed in a moist room for several days and allowed to rust. The mats were then wire brushed to remove the loose rust.

(b) Beam Reinforcement

All of the beams were reinforced with No. 2 deformed bars. This steel had an average yield stress of 54,000 psi. A typical stress-strain curve for the bars is shown in Fig. 3.8.

(c) Column Reinforcement

The columns were reinforced with No. 3 deformed bars. The yield stress of these bars was 55,000 psi.

(d) Stirrup Steel

The stirrups were fabricated of 1/8-in. square plain bars. The average yield stress of the steel was 47,000 psi.

3.2 Concrete

The close spacing of the slab reinforcement necessitated the use of a mix containing only small aggregate. Since the requirements for this structure were the same as the previous four structures, no trial batching was necessary.

The concrete was mixed in 600-lb. batches in a non-tilting drum rotary mixer of 6 cu-ft. capacity. The aggregate was 80 percent Wabash River gravel and 20 percent fine lake sand by weight. The aggregate to cement ratio was 4.9. Type 1 cement was used.

Two sizes of test cylinders were cast. Fifty-four 2 by 4-in. cylinders and thirty-six 4 by 8-in. cylinders were cast. In addition, 24 beams 1 3/5 in. deep, 2 in. wide and 17 in. long were cast to provide data on the modulus of rupture.

Table 3.1 contains a tabulation of the data on the water:cement ratios, compressive strength and modulus of rupture of the test specimens at the beginning (56 days) and end (100 days) of tests on the structure.

Thirty-three 2 by 4-in. cylinders were tested when they were 56 days old. The average strength was 2760 psi with values ranging from 3290 to 4850 psi. The initial modulus of elasticity was 3.0×10^6 psi. Eighteen 4 by 8-in. cylinders tested at this time had an average strength of 3900 psi with a range of 3440 to 4350 psi. The modulus of elasticity of these specimens was 3.0×10^6 psi. The average modulus of rupture at 56 days was 750 psi. Individual values ranged from 710 to 800 psi.

At the conclusion of testing, 100 days after casting, the remainder of the specimens were tested. Twenty-two 2 by 4-in. cylinders averaged 3670 psi with a spread of values from 3020 to 4780 psi. Eighteen 4 by 8-in. cylinders averaged 3880 psi and ranged from 3330 to 4640 psi. The modulus of rupture at 100 days was 804 psi with individual values from 693 to 882 psi.

3.3 Formwork

Most of the formwork was composed of 3/4 in. plywood sheets supported on 2 by 6 in. joists spaced at 15 in. The 2 by 6 in. joists were in turn supported by 4 by 8 in. beams at 20 in. centers. The column forms and drop panel forms were also made of 3/4 in. plywood. The exterior faces of the beams were formed by steel channels.

The columns and beam forms were aligned and the plywood slab forms were checked in order to maintain a uniform slab thickness.

The forms were coated with "Slippit" before the reinforcement was placed.

3.4 Placement of Reinforcement

The column and beam reinforcement was assembled in cages to facilitate placement. No. 7 gage wires were welded to the ends of the column steel in the exterior columns to provide additional anchorage. The length of these wires was about 8 in. Following placement of all of the steel, the No. 7 wires on the exterior columns were bent over and checked to insure proper cover. The wires were bent in the form of a 90° hook. The purpose of the wires was to provide a means of transferring stress to the columns.

The beams framing into the corners were assembled together with the corner column and placed as a unit. The remainder of the exterior columns had been placed prior to the positioning of the corner beam and column assembly.

The middle beam cage was then placed. This cage had been fabricated without the negative steel. Finally, the negative steel in the middle span was tied into place.

The slab reinforcement was already formed into mats. The mats were located in their proper position and all transverse wires lying outside the design section were cut so that they would still serve as anchorage but not as reinforcement. Strain gages were placed on the wires and waterproofed before the mats were tied into place.

The mats were supported by 1/4-in. square bars at 8 to 12-in. intervals. Slots were cut in these bars at various depths so that all the steel would have proper cover. The opening of the slots was slightly smaller than the diameter of the wires to enable the support to be clamped to the wire. All mats were tied to the plywood forms.

3.5 Casting and Curing

The structure was cast on 14 March 1961. The first batch was mixed at 8:15 a.m. and the last batch was placed at 11:30 a.m.

The concrete was placed using buckets, pushed into place by hand and consolidated with an electric internal vibrator. Three temporary screed supports were used, and they divided the slab into four parallel strips. The location of each of the batches of concrete is shown in Fig. 3.9.

The concrete in the columns and beams was consolidated with the internal vibrator. The vibrator was placed along the exterior surface of the forms to insure a well consolidated member. The concrete in the slab was consolidated with a vibrating screed made by attaching an electric vibrator to a 4-in. channel. This vibrator was supported by the channels forming the edge beams and by the temporary screed supports. The surface was given a second screeding with a wooden screed. The temporary screeds were then removed and

the trough left after their removal was filled with concrete and troweled smooth. Finally the entire surface was troweled with a steel trowel.

Eight hours after completion of the casting, the structure was covered with wet burlap. The burlap was removed after seven days and the forms were struck. The entire surface of the structure was painted with "Traffic White" to reduce moisture loss. The test specimens were cured and painted in the same way as the structure and were then stored under the structure.

3.6 Condition of the Structure At The Start of Testing

At the start of testing, the thickness of the slab was measured using a level at 141 points located at critical sections. The maximum positive deviation was 1/8 in. and the maximum negative deviation was 1/16 in. Figure 3-10 shows a contour plot of the thickness deviation from the desired 1 3/4 in. The contour interval is 1/32 in.

Examination of the structure for shrinkage cracks indicated that none had formed. The corner columns had lifted off the reaction dynamometers because of shrinkage and it was necessary to shim the dynamometers up until contact was restored.

4. LOADING SYSTEM

4.1 Loading Frame and Reaction Piers

An elevation of the reaction and loading frames is shown in Fig. 4.1. The 16 reaction piers were concrete blocks 18 in. square and 5 ft. high. These piers were tied together at the top by steel beams cast in the concrete to resist overturning forces.

The loading frame was made of three steel bents which crossed the slab in the north-south direction. The vertical members of the frames were 10-in. WF columns, and the cross beams were pairs of 18-in. channels, to which the nine loading jacks were bolted. The vertical members were bolted to floor beams on each side of the test setup and the floor beams were bolted to the laboratory floor.

4.2 Load Distributing System

The load on each panel was applied by one jack and distributed equally to 16 loading points by means of a pyramidal system of bars. A loading plate, 8 by 8 by 3/4 in., was used at each loading point. Reasonably uniform pressure under these plates was effected by 3/8-in. sheets of gray sponge rubber between the plates and the slab. An elevation of this system is shown in Fig. 4.2.

The nine 20-ton capacity hydraulic jacks were connected to an electric pump. A control manifold was used so that any combination of panels could be loaded.

5. INSTRUMENTATION

5.1 Strain Measurements

(a) Steel Strains

In the previous four test structures, the strain gages on the reinforcement were mounted after casting of the slab. The reinforcement was made accessible at the required locations by using cork blockouts which were subsequently removed. In this test structure, the same method could not be used because the diameter of most of the wires was very small making it difficult to attach the gages once the wires were embedded in concrete unless very large blockouts were used. Consequently, the strain gages were mounted prior to casting.

The most critical problem was that of waterproofing of the gages. The waterproofing had to meet several requirements in addition to sealing the strain gage from moisture. It was necessary that the material used could provide an adequate seal without exceeding the cover thickness of the concrete. Also it was essential that the waterproofing be tough enough to withstand handling during placement and casting of the concrete.

As a trial, several gages were mounted on wires and covered with a layer of Epoxoid*. These wires were then loaded and the strains indicated by the gages embedded in epoxoid were compared with strains measured mechanically. There was no adverse affect of the epoxoid layer on the reliability of the strain gages.

The waterproofed gages were next placed in water for two days and then checked for electrical short circuits. Several of the gages were inoperative following this test. The epoxoid was found to have hairline cracks.

---

*An adhesive produced by the International Prestressing Corporation, Los Angeles, California.

The cracking was apparently due to the relative flexibilities of the wire and the epoxoid. The wires were very flexible and the epoxoid was cracked in handling. Even though the epoxoid lacked the needed flexibility, it did provide the necessary resistance to abrasion that was needed, so the final step in the waterproofing was to find a material that would seal the hairline cracks.

The most easily applied material appeared to be wax. The gages were heated and molten wax was applied on the epoxoid. The wax used was Sinclair 300, an industrial wax product used in waterproofing milk cartons. These wax-coated gages were found to be adequate in providing a moisture seal and this method was subsequently used for all the steel gages in addition to the epoxoid.

The welded wire mats were marked at the locations of strain gages and the wires were cleaned at these points. A total of 323 strain gages were mounted. The location and notation of these gages as shown in Figs. 5.1, 5.2, and 5.3. All gages were Type A-7 SR4 electric strain gages.

Following mounting of the gages, the mats were placed in the forms. As each mat was placed, the strain gage leads were led through holes drilled in the forms. The holes were located so that several leads could be led through the same hole. The holes were large enough to allow the forms to be pulled over the wires when the forms were struck. In order to prevent concrete from entering the holes, each hole was sealed with a small piece of ordinary modeling clay which remained soft and allowed the wire to pull through.

After the structure was cast and the forms stripped, 320 of the 323 gages applied on the reinforcement were found to be operative.

(b) Concrete Strains

Following curing of the concrete, a total of 30 strain gages were mounted on the concrete. Ten gages were placed on the top of the slab at the

edge. The location of these gages is shown in Fig. 5.4. Twenty gages were placed on the bottom surface on the drop panel at column 7. The location of these gages is shown in Fig. 5.5.

5.2 Reaction and Load Measurements

The column reactions were measured in three orthogonal directions by specially built tripod dynamometers which can be seen in Figs. 5.6 and 5.7. The design, manufacture, and method of operation of these dynamometers have been described in Refs. 2, 3 and 5. A needle deflection of one dial division on the strain indicator corresponded to a vertical reaction of 60 lb. or about 2.5 psf on the structure.

The applied load was measured by means of two sets of dynamometers. Load was measured by recording the strains in the 5-in. WF main beam of the load distributing system in each panel. This procedure resulted in a sensitivity of about 90 lb. per dial division on the strain indicator (approximately 3.5 psf).

A specially built horizontal ring dynamometer was placed between the jack and the main loading beam in each panel. The sensitivity of this dynamometer was 25 lb. per dial division on the strain indicator (1 psf). These dynamometers were removed in the test to failure since the rated capacity of each dynamometer was 13,000 lb.

Detailed description of these dynamometers have been given in Refs. 5 and 8.

5.3 Deflection Measurements

The vertical deflections of the structure were measured at 33 locations with 0.001-in. dial gages in all of the tests. Fig. 5.8 shows the locations and designations of the dial gages. The gages were located at the midpoint of each panel and at the midpoints of all beams and column centerlines.

The dial gages at the midpoint of the panels were supported on adjustable stands resting on the floor. The stands for the gages located at the midpoints of beams and column lines were supported on the steel beams of the reaction frame.

5.4 Torsional Rotation of the Beams

The torsional rotation of two corner panel beams, one shallow and one deep, were measured during the test to failure. Eight 0.001-in. dials were placed on the side of each beam, two dials measuring the rotation at the center, two at the one quarter-point, and two at each end.

5.5 Reading and Recording

All strain gages were wired to a large switchboard in which one switch point was provided for each load dynamometer, strain gage, reaction dynamometer leg and check gage. The check gages were used to provide information on the magnitude and direction of electrical drift during testing.

The switch bank was connected to a portable strain indicator, which was balanced semiautomatically by an external servomechanism mechanically coupled to the indicator. The servomechanism was a Leeds and Northrup Type G. Speedomax, which was wired to sense the deflection of the strain indicator dial and then drive the slide wire of the strain indicator until the dial deflection was reduced to zero.

From the strain indicator, the strain data was fed directly into an analog-to-decimal converter unit (Benson - Lehner Decimal Converter). The strain data were taken directly from the decimal converter into an IBM card punch and into an automatic typewriter. The strains were thus punched into IBM cards and tabulated as well. The strain data, including computation of reactions, were reduced using IBM equipment.

The load dynamometers were read and recorded manually both before and after each load increment. There were 18 load dynamometers and 413 other strain gages which were automatically balanced and recorded, so a total of 449 strain readings were taken for each load increment. The deflection dial gages were read and the data recorded and reduced manually.

In addition, observations of the behavior of the structure and data on cracking were also recorded.

6. TEST PROCEDURE AND CHRONOLOGY

6.1 Test Procedure

Each test consisted of the application of load to a given load level. The load was applied in predetermined increments. The number of increments depended on the maximum level of loading, the previous loading history and the expected behavior of the slab. In the tests where no failure occurred, the load was removed and the maximum load during the test was again applied in one increment. Data was recorded at the initial zero load, at each load increment, and again at zero loads following the initial and rebound loadings.

The magnitude of the load increment was controlled by monitoring a particular load dynamometer. After this dynamometer indicated the desired load had been reached, the hydraulic pump was stopped and the main valve leading to the control manifold was closed. The load on each of the remaining panels was checked. If no adjustment of load was necessary, the individual valves leading from the manifold were closed. If some adjustment was needed, the valves of the panels that were loaded properly were closed and the load on the remainder of the panels was adjusted to the desired level. This operation took approximately 10 minutes.

When the loading operation was completed, the deflection and strain readings were begun simultaneously. Deflection readings were completed in about 10 minutes.

Strain readings were read and recorded in the following order: (1) the six check gages, (2) bottom steel gages, (3) top steel gages, (4) beam steel gages, (5) concrete gages, (6) tripod reaction dynamometers, (7) the six check gages. The strain readings took from twenty-two to thirty minutes.

After all the strain gages had been read, the deflections at the midspan of the panels and the load dynamometers were read and recorded.

The structure was checked for cracking whenever the load was expected to cause additional cracks. Seven-power magnifying lenses were used in looking for cracks. The cracks were marked with pencil and the test number and load increment were marked beside the crack. About one hour was taken to mark cracks.

Photographs of the crack patterns in the structure were taken at various times during the testing period.

6.2 Chronology

A total of 14 tests were carried out on the structure over a period of about 8 weeks. A complete tabulation of the panels loaded in each test, load level and date of test is contained in Table 6.1.

Testing began on 3 May 1961 when the first load was applied and concluded on June 21. A total of 49 days was required to complete the load test.

Test 500 involved only the strain and deflection readings before and after the loading frames were placed on the slab. The combined weight of the slab and the loading frame was 44 psf.

Test 501 consisted of applying a load of 56 psf making a total load of 100 psf. This load did not exceed the estimated cracking load of the structure. The test also provided a means of checking all loading equipment and instrumentation.

The structure was loaded to design load for the first time in test 502. The applied load was 240 psf making a total load of 284 psf.

The loading during test 503 was increased to 384 psf or 1.5 live loads plus 1.0 dead load. Following test 503, a series of tests, 504-511 were

conducted with various combinations of panels loaded. These tests were all carried out at a total load of 384 psf.

Test 512 was terminated when three of the interior reaction dynamometers failed. In test 513, all four interior column dynamometers were replaced by short steel pipe columns. In this test, the structure carried a total load of 955 psf when an exterior row of panels failed. Test 514 involved the loading of the interior panel E to failure with loads of approximately 500 psf applied on the remaining eight panels to provide restraint along the edges of panel E.

7. BEHAVIOR OF THE TEST STRUCTURE

7.1 Introductory Remarks

The behavior of the test structure observed in four tests is described in this chapter. The tests described are the following: (1) Test 502, all panels loaded to design load (284 psf); (2) Test 503, all panels loaded to 384 psf; (3) Test 512, all panels loaded to 674 psf; (4) Test 513, all panels loaded to 955 psf. The behavior of the structure is presented in terms of deflections, steel strains and cracking.

In this chapter, the response of the structure is evaluated in terms of the applied load or the load applied by the hydraulic jacks. The dead load of the test structure including the weight of the load distributing system is 44 psf, 40 psf less than the assumed dead load of the full-sized structure. It is important to note that the remainder of the design dead load (40 psf) was applied by the hydraulic jacks and is considered as part of the applied load.

7.2 Test 502 (Design Load)

(a) Loading

The load was applied in four increments to the following load levels: 60, 117, 174, and 242 psf. Thus, the maximum total load was 242 + 44 = 286 psf. This was the first test in which the design load was reached. The complete test took 6 1/2 hours. Previous tests had been below the estimated cracking load of the structure.

(b) Deflections

The maximum recorded deflection in Test 502 was 0.096 in. This deflection was recorded at the center of panel A, the corner panel supported by two shallow beams. The interior panel deflected 0.042 in. The maximum beam deflections were 0.049 and 0.019 in. for the shallow and deep beams, respectively. These are the deflections due to the applied load in this test only.

Several load-deflection curves are shown in Fig. 7.1. The first five curves are for mid-panel deflections. Curves A1 and J3 are beam deflections and H1 is the deflection at the midpoint of the centerline between two interior columns. The load deflection curves are nearly linear throughout the loading range indicating that there had been only a small amount of cracking during this test.

A schematic deflection diagram showing the deflections measured under the maximum applied load is presented in Fig. 7.2.

(c) Strains

The strains presented for test 502 are those measured under the applied load. No measurable residual strains existed since previous loadings were below the cracking load.

Measured load-strain curves at various points in the slab are shown in Fig. 7.3 for gages on the bottom steel and in Fig. 7.4 for gages on the top steel. These curves were selected to give examples of the different types of load-strain curves observed.

The load-strain curves for the bottom steel (Fig. 7.3) are linear for gages E24, F15, and J15. This observation is consistent with the state of the slab which was uncracked at the bottom. The bending over of the load-strain curve for gages A24, B22, and C22 indicated possible cracking. However, a detailed search for cracks in these regions during the test revealed no cracks that could be detected.

As would be expected, the strains measured in the top steel were significantly larger than those measured in the bottom steel (Fig. 7.4). The only load-strain curves which remained linear were those measured in the slab reinforcement at the faces of the spandrel beams (gage B62). Cracking strains were measured in all other sections although only one crack was actually

discovered on the top of the slab. As explained in Section 6.1, cracks were sought using illuminated seven-power magnifying glasses.

The distribution of strains in the positive moment sections is shown in Fig. 7.5. The only strains in the bottom reinforcement that exceeded the cracking strain were across section 2-2. The maximum strain in the bottom reinforcement was 20×10^{-5} and was recorded in an exterior column strip. There was no measurable strain in the bottom reinforcement adjacent to the deep beams.

In Fig. 7.5 the strains measured across section 2-2 are considerably larger than those measured across section 6-6. However, this does not mean that the bending moments across these sections differed in the same proportion. The reinforcement in the middle strips of section 6-6 was closer to the neutral axis of the uncracked slab than the corresponding reinforcement in section 2-2. Furthermore, the measured strains were in the vicinity of the cracking strain; the moment-strain relationship was not linear at every section.

The distribution of strains in the negative moment sections is shown in Fig. 7.6. Strains in the top reinforcement ranged from a maximum of 37×10^{-5} to nearly zero strain. Maximum strains in the top steel were recorded at the faces of the interior column capitals and ranged from 20 to 30×10^{-5}. Strains in the reinforcement over the exterior columns on the shallow and deep beam sides were 25×10^{-5} and 15×10^{-5}, respectively. Strains in the top steel at the edges were all less than 10×10^{-5} except for one gage which reached 15×10^{-5}.

The maximum strains recorded in the deep beams were 18×10^{-5} and strains in the shallow beams reached 30×10^{-5}.

(d) Cracking

The structure was examined for cracks after the application of each load increment. No cracks were found in the bottom of the slab during this

test. A few very short cracks were found over column 2 extending toward column 6 after the final load increment (242 psf) had been applied. The load-strain curves indicated more extensive cracking in the negative moment sections but no further cracks were observed.

7.3 Test 503 (1.5 Live Loads + Dead Load)

(a) Loading

The load was applied in four increments to the following load levels: 117, 239, 290, 336 psf. The maximum total load on the structure was 336 + 44= 380 psf. The two increments applied after the design load had been reached were smaller (about 50 psf) than the first two increments (about 120 psf). The test was completed in 8 hours.

(b) Deflections

The maximum mid-panel deflection measured during test 503 was 0.16 in. in panel A, the corner panel supported by two shallow beams. The interior panel deflected 0.065 in. The maximum shallow beam deflection was 0.70 in. and the maximum deep beam deflection 0.025 in.

Representative load-deflection curves are shown in Fig. 7.7. The first five curves represent mid-panel deflections. Curves A1 and J3 depict beam deflections and H1 the deflection between two interior columns. All of the curves are linear up to an applied load of 240 psf. Since the structure had been loaded to this level (240 psf) previously, no further cracking or inelastic action would be expected to that load.

A schematic deflection is shown in Fig. 7.8 for test 503. The deflections given in this diagram include residual deflections from test 502 and thus represent the values that would have been measured if the structure had been loaded to 336 psf applied in one test.

(c) Strains

Load-strain curves are presented in Figs. 7.9 and 7.10. The load-strain curves are linear up to an applied load of 240 psf. Since the structure had been loaded to this load in previous tests, a linear load-strain curve was expected. Nonlinearity beyond 240 psf indicates further cracking at or near the gage locations. Several of the gages which indicated significant cracking during test 502 remained nearly linear in test 503. The load-strain curve for gage X10 in Fig. 7.4 indicated cracking at or near that gage. In Fig. 7.10, gage X10 had much less residual strain. This indicated a crack of sufficient height at gage X10 had formed during test 502 so that only a small amount of further cracking occurred during test 503. This behavior should not be confused with the behavior of curves E24 and F15. A comparison of the load strain curves for gages E24 and F15 in Figs. 7.9 and 7.3 shows that the strains remained linear throughout both test 502 and 503. No cracking had taken place at these locations.

The distribution of strains in the positive moment sections is shown in Fig. 7.11. The plotted strains include the residual strains in the preceding test 502. The strains in section 4-4 increased by approximately 30-50 percent over the corresponding strains in test 502. Strains in section 6-6 increased by about 50 percent and those in section 2-2 increased by about 100 percent over the strains measured in test 502. The differences in the increase in strain between tests 502 and 503 is primarily the result of cracking. Once cracking occurs, the rate of increase of strain is greater than the rate of increase of an uncracked section. Therefore, those sections that were cracked in test 502 (section 2-2) had a greater percentage increase in strain in test 503 than those sections that remained uncracked throughout tests 502 and 503.

The maximum strain in the bottom reinforcement was 53 x 10^{-5}. This occurred in an exterior column strip in section 2-2. Strains across section 4-4 were all below the cracking strain. Strains in the reinforcement adjacent to the deep beams remained relatively unchanged from test 502 and were nearly zero.

The distribution of strains in the negative moment sections is shown in Fig. 7.12. Residual strains are included in this figure. Strains in the top steel generally increased about 50-70 percent over the strains in test 502.

The maximum strains in the top steel were recorded at the face of the interior column capital. These strains reached a value of 67 x 10^{-5}. The strain in the middle strips at all the sections was less than the cracking strain. The highest strains were in the reinforcement over the columns and ranged from 20 to 40 x 10^{-5}.

The maximum strains in the deep and shallow beams were 37 x 10^{-5} and 45 x 10^{-5}, respectively.

(d) Cracking

Figure 7.13 shows the pattern of observed cracks in the bottom of the slab. The cracks were confined to about the middle third of the exterior panels and were parallel to the beams. The cracking on the bottom of the panels adjacent to the shallow beams was more extensive than in those adjacent to the deep beams. Cracking extended into the shallow beams in the corner panel. The bottom of the interior panel showed no cracking.

Figure 7.14 shows the crack pattern in the top of the slab. All cracking was confined to the area around the columns. Most of the cracks around the interior columns were parallel to the edges of the column capitals and drop panels. A few cracks began to appear along the column centerlines. All the cracks were very short. The cracks over the exterior columns were

perpendicular to the edge and extended toward the interior columns. The length of these cracks was also very short. They were generally confined to the surface above the exterior drop panels.

Flexural cracking occurred in the beams. The negative moment sections of the beams at the columns showed the most cracking. The flexural cracks in the beams were extensions of the cracks in the top surface above the columns. The cracks in the positive moment sections of the beams were confined to the corner spans. The deep beams supporting panel J were cracked the most extensively in the positive moment region. The length of the cracks in all the beams was about one-half the depth of the beam. The negative moment flexural cracks were confined to the width of the column and the positive moment cracks were generally within the middle third of the span.

The exterior surfaces of the columns were cracked during test 503. The cracks were spaced at 3-5 in. and were located in the upper two-thirds of the columns. The cracks penetrated about one-half of the way through the columns.

All cracks in the structure could be classified as hairline cracks; the maximum crack width did not exceed 0.005 in.

7.4 Test 512

(a) Condition of the Structure Before Test 512

Tests 504 to 511 were tests with various patterns of loading at dead load plus 1.5 live load (384 psf). The patterns of loading were chosen to produce maximum moments at critical sections and, consequently, some additional cracking was produced. However, this additional cracking was largely confined to short extensions of existing cracks and the over-all crack pattern remained the same.

Tests 504 to 511 produced only slight changes in the crack patterns of the beams and columns. Very few new cracks were formed. Almost all additional cracking was confined to extension of the existing flexural cracks in these members.

(b) Loading

The maximum load was reached in five increments with the applied load at each level as follows: 240, 338, 433, 522 and 630 psf. The last load level (630 psf) was the maximum load applied when three of the interior reaction dynamometers failed.

(c) Deflections

Because of the sudden failure of the reaction dynamometers, no deflection data was obtained at an applied load of 630 psf. As a result, all following discussion is based on deflection measurements recorded at an applied load of 522 psf.

The maximum deflection recorded in test 512 was 0.36 in. at the mid-point of panel A. The interior panel mid-point deflection was 0.14 in. The shallow beam deflection was 0.15 in. and the deep beam deflection was 0.05 in. Load-deflection curves for test 512 are shown in Fig. 7.15. The first five are mid-panel deflections and curves A1 and J3 are at the mid-point of beams.

All of the curves are linear up to 340 psf which was the magnitude of the load in previous tests. Beyond this load, the curves bend over. All curves except J3 exhibit some definite increase in the rates of deflection after a load level of 433 psf has been reached. Curves A0 and J0 show large increases in deflection with the application of load increment 5 (522 psf) indicating that cracking had reduced the stiffness of these panels considerably. There are no residual deflections shown since many dial gages were inoperative following the failure of the reaction dynamometers.

A schematic deflection diagram showing the deflections at 522 psf is given in Fig. 7.16. These deflections include any residual deflections resulting from tests prior to test 512. The deflections shown are greater than the maximum deflections observed during test 512. The cumulative residual deflections at the mid-points of the panels varied from 0.10 in. in panel A to 0.035 in. in panel E. The cumulative residual deflections in the shallow beams ranged drom 0.016 to 0.046 in. and in the deep beams the values ranged from 0.005 to 0.01 in.

(d) Strains

Representative load strain curves are presented in Figs. 7.17 and 7.18 for gages on the bottom and top steel, respectively. The curves are essentially linear up to 340 psf, the level of loading reached in preceding tests. The initial slopes of the curves indicate greater flexibility than those measured in tests 502 and 503, indicating the effect of progressive cracking in tests 504-511. Curve E24 indicated that the first cracking was produced at that location during test 512. Curve B62 is linear throughout test 512. This gage was on the top reinforcement in a middle strip between exterior columns and cracking never occurred at that point. No residual strains are shown for test 512 since the failure of the reaction dynamometers produced unrealistic strains.

Figure 7.19 shows the strain distribution at the positive moment sections. These distributions include residual strains which resulted from previous tests. The maximum strain was 120×10^{-5} and was measured in section 2-2 which had the highest strains. As before, the smallest strains were measured in section 4-4. In all sections, the strains were highest in or immediately adjacent to the column strips and were nearly zero in the reinforcement near the deep beams.

The strain distribution in the negative moment sections is shown in Fig. 7.20. Residual strains have been included in these strain distributions. The largest strains were recorded in the top steel over the interior columns. The maximum strain was at the face of an interior column capital and reached a value of 150 x 10^{-5}. The strains across the interior negative moment sections indicated that cracking had occurred along the entire section. The strains at the exterior columns ranged from 50 to 120 x 10^{-5}. The strains on the exterior middle strips were all below cracking strain.

Strains in the shallow beams varied from 31 to 97 x 10^{-5}. Strains in the deep beams ranged from values of 22 to 60 to 10^{-5}.

(e) Cracking

At an applied load of 433 psf, the crack pattern became more extensive on both the top and bottom of the structure. Existing cracks were widened and extended and new cracks formed. Figures 7.21 and 7.22 show the cracks which had formed in the slab at the maximum applied load in test 512. These figures do not show the abnormal cracks which opened as a result of the failure of the three interior column dynamometers.

The cracks on the bottom of the structure began to spread to almost all positive moment sections (Fig. 7.21). In addition, a series of cracks were formed which extended from the mid-point of the corner panels to the corner columns. Crack widths on the bottom of the slab were less than 0.005 in.

Cracking on the top of the slab was concentrated around the columns (Fig. 7.22). Cracks radiated in all directions from the interior columns. The "diagonal" cracks were close to 0.01 in. in width and had the largest width of any of the cracks on the top of the slab. Cracks extended the entire distance between interior columns. The negative moment sections between interior and

exterior columns also exhibited some cracking although this was generally not a continuous crack as it was between the interior columns (Fig. 7.22 shows final state). The width of these cracks was about 0.005 in. Cracks over the corner columns were confined to short cracks across the corner of the structure. The cracking on top of the slab over the remainder of the exterior columns was arranged in a triangular configuration. Cracks started at the edge of the structure as parts of the torsion cracks in the beams and radiated inward concentrating at a point at about the edge of the drop panel.

The flexural cracking in the beams and columns was confined mainly to an increase in the extent of existing cracks. Maximum crack widths in these members measured to be 0.005 in.

(f) Conditions Leading to the Failure of Reaction Dynamometers

The failure of the dynamometers supporting the interior columns was initiated by distress in the beam-column connections which caused a transfer of load and bending moment to the interior columns.

Torsional cracking in the beams was first noted at 433 psf. Torsional cracks were observed at all beam-column connections but they appeared to be most pronounced in the shallow beams. However, these cracks were hairline cracks and there was no sign of distress.

The following load level (522 psf) produced considerable widening and development of these cracks. There was a large concentration of rotation at the torsional cracks at columns 2 and 3 supporting shallow beams. The torsional cracks at columns supporting deep beams were not extensive.

Application of the fifth load increment which increased the total applied load to 630 psf caused further severe rotation at columns 2 and 3. As soon as the load of 630 psf was reached, three reaction dynamometers

supporting columns 6, 7, and 11 failed. The condition of the dynamometers after failure indicated that they had failed under the action of a resultant force which was oblique to the horizontal. These dynamometers were calibrated under vertical loads corresponding to 750 psf and designed to carry 1000 psf on the slab and would not have failed unless a fairly large horizontal thrust was involved along with the applied load of 630 psf.

After the tripod dynamometers failed, the structure was deflected in an abnormal pattern and deflection and strain data were no longer realistic.

Photographs of the cracks at the beam column connections are shown in Fig. 7.23. These pictures were taken prior to test 513. The black steel rods seen in the pictures are clamps used to reinforce the beam-column connection. These were installed after test 512. The cracks in the shallow beams are shown in Figs. 7.23a and b and the deep beam is shown in Fig. 7.23c. The torsional failure at columns framing into shallow beams was well defined by the spalling of the concrete in the zone of failure. The deep beam (Fig. 7.23c) had several well defined torsional cracks but still retained considerable torsional capacity at the connection.

7.5 Test 513 (Test to Failure)

(a) Preparation of Structure for Test 513

It was necessary to replace the damaged reaction dynamometers before further testing proceeded. The slab was lifted off the interior dynamometers by a lift system consisting of two screw type jacks and a wood framework. The two jacks were placed on opposite sides of the interior column enabling the slab to be lifted uniformly. The reaction dynamometers at all four interior columns were removed. A short section of 4-in. steel pipe was placed into position. This pipe had a plate fitted for a one inch steel ball welded to the upper end. The slab was lowered onto the pipe and the pipe was

welded into place. The columns retained a pin-ended condition and the slab was returned to proper height with replacement of the dynamometers.

The comparison of the initial slopes of the load-deflection curves measured in tests 512 (Fig. 7.15) and 513 (Fig. 7.24) indicates that the eight exterior panels of the structure underwent a reduction in stiffness of about 40 percent after test 512. However, this reduction is not unusual in view of the fact that extensive additional cracking occurred in the final stages of test 512 and the exterior beam-column connections were damaged. Evidently, the abnormal cracks, which opened in the bottom of the slab in the immediate vicinity of the interior columns as a result of the failure of the dynamometers, were sufficiently closed when the columns were restored to their original elevations. If these cracks did affect the response of the structure, their effect was not appreciable.

The beam-column connections were strengthened by an external prestressing device. A vertical force was applied to the exterior edge of the side columns by means of clamps. The clamps were made of two steel plates, one at each end of a one inch diameter threaded rod. The threaded rods slipped through holes at the middle of the steel plates. One end of the plates fit against the top and bottom of the column and a 1 in. diameter rod fit between the other end of the plates. Tension was applied to the rod by turning one of the nuts. A view of this clamp is shown in Figs. 7.23a and b. The clamps provided a means of transferring load to the columns at those connections where severe torsional cracking had already taken place and retarded failure in the columns that were not severely damaged.

(b) Loading

The load was applied to all panels. Measurements were made at the following load levels: 247, 343, 529, 625, 720, 791 and 911 psf. At 911 psf

(955 psf total), failure was observed in panels ABC. An attempt was made to place additional load on the remaining panels but failure was imminent in all panels except panel E. Hence, loading was continued only on panel E. At 1200 psf, the main beam of the load distributing system in panel E yielded. Thus, the loading was stopped without complete collapse of the interior panel. This panel was loaded to failure in test 514 after the load distributing system was strengthened. The panel failed at 1500 psf.

(c) Deflections

The last deflection measurements for applied load during test 513 were made at a load of 791 psf. Following the failure of panels ABC, only scattered measurements were obtained. Representative load-deflection diagrams are given in Fig. 7.24. The first four show mid-panel deflections. Curves A1 and J3 show beam deflections and curve H1 indicates deflections measured between interior columns. Curves A0 and B0 show large increases in deflection in the final stage of loading. Curve E0 did not show signs of a significant decrease in stiffness of that panel, although a definite bend in the curve was noted at the higher loads. The deflection of the deep beam (curve J3) increased nearly linearly throughout test 513. The shallow beam (curve A1) showed signs of decreasing stiffness, especially with the application of the final load increment.

A schematic deflection diagram is shown in Fig. 7.25. This diagram does not include any residual deflections from previous tests. The deflections shown are for an applied load of 791 psf. The diagram shows a "trough" developing in panels ABC. The deflection at the midspan of these panels was nearly 1 in. The similar panels on the opposite side of the diagonal of symmetry through columns 1 and 16 had deflections of about 0.70 in. The deflection of the shallow beams spanning columns 1 through 4 were also greater than the beams spanning columns 1, 5, 9, and 13.

(d) Development of Yield Lines and Mode of Failure

In a slab reinforced with intermediate grade reinforcement, the development of a yield line is marked by the extensive opening of one or two adjacent cracks in a zone of maximum moment and by the noticable concentration of rotation in that region. It is possible to judge whether a given section has developed its yield capacity simply by visual inspection. In a slab reinforced with welded wire fabric, the phenomenon of "yielding" is different because of the stress-strain curve and positive anchorage of the wires.

The stress-strain curve for the fabric does not have a "flat-top" region. Any increase in rotation at any section meets with increased resistance at all levels of loading; a stage when rotation occurs freely is never reached. Thus, the cracks do not open wide even at final stages of loading. Furthermore, the elongation required at the level of the reinforcement is concentrated over a short length of the wire bounded by cross-wires. For a given crack opening large strains are developed. Thus, the steel fractures before the development of cracks wide enough to be diagnosed positively as yield lines.

In accordance with the preceding discussion, it appears that the best measure of whether a given section in the test structure has developed its yield capacity is the distribution of stresses across that section. Although the welded wire fabric does not exhibit a well defined yield point, the reaching of the 0.2 percent offset stress may be designated as "yielding". For the steel used in the slab, the ultimate stress was about ten percent greater than the 0.2 percent offset stress.

The distribution of the steel stresses across four critical sections is shown in Figs. 7.26-7.29. The plotted diagrams depict the variation of the total (including residual stresses) applied load stress across a section for load levels of 434, 720 and 791 psf applied. The 0.2 percent offset stress of the reinforcement in each strip is indicated in the figures.

From these stress distributions, it can be seen that at all load levels the stresses were highest in the positive moment section of panels ABC (Fig. 7.27). The stresses across column line 5-8 (Fig. 7.28) were higher than the corresponding stresses across column line 3-15 (Fig. 7.29). On the basis of the stress distribution, the moments in the positive moment sections and interior negative moment sections of the exterior panels supported by shallow beams were greater than those supported by the deep beams. Since the shallow beam-column connections were more severely damaged than the deep beam connections, their stiffness was reduced thus causing a larger moment in the remaining sections.

The structure was inspected carefully for crack widths that could be classified as yield lines. At an applied load of 720 psf, no cracks opened sufficiently to be diagnosed as yield lines. The stress distributions at 720 psf confirmed this observation. The stresses reached magnitudes slightly greater than 60,000 psi at several locations, however, the stresses in these sections were still below the 0.2 per cent offset stress.

As the load was increased to 791 psf, cracks of sufficient width to be considered yield lines were observed. In general, the stress distributions corroborated this observation.

The crack widths indicated that a yield line formed at the center of panel B. The stress distribution at this section (Fig. 7.26) indicates that 0.2 per cent offset stresses were reached in the column strip between panels A and B.

The crack widths between columns 6 and 7 indicated that a yield line formed in that region (See Fig. 2.4 for designation of columns.). The stresses across the centerline between columns 6 and 7 did not reach the yielding level, however, it is important to point out that the maximum moment does not exist

across that line. The line of maximum moment shifts gradually from the face of the capital to the column centerline at mid-panel. Thus, the low stresses measured across the column centerline do not preclude the formation of a yield line at a short distance from the centerline. The cracks in the structure indicated that a yield line had formed at the face of the capital at column 6 and extended into panel B toward column 7.

Further increase in load above 800 psf resulted in apparent yield lines at other locations. As the load increased, cracks opened sufficiently at the center of panel H and between columns 10 and 11 to indicate the formation of a yield line. The loading was terminated when a line of fracture formed in panels A and B. At the time of the occurrence of the fracture, the maximum applied load was 911 psf, determined from monitoring one load dynamometer. The strains measured after the failure had occurred were no longer realistic and stresses could not be utilized to verify the formation of any additional yield lines. However, the stress distributions at a load of 791 psf indicated stresses at the negative moment section between columns 7 and 11 (a similar section on the opposite side of the diagonal of symmetry) such that additional load could be expected to raise the stresses to the 0.2 per cent offset stress.

The fracture which occurred in the center of panels A and B at 911 psf coincided with the yield line at the location. The stresses in the column strip between panels A and B reached 75,000 psi at a load of 791 psf. With additional load, the reinforcement fractured at that location. The fracture probably originated at the column strip and spread into panel B. The length of the fracture was about 45 in.

The fracture was accelerated by the loss of moment capacity at columns 2 and 3. The moment was redistributed to the positive moment and interior negative moment sections of panels ABC, which in turn resulted in

higher stresses at those sections. The fracture resulted in a sudden rotation of the slab about the interior and exterior columns. This rotation caused the complete collapse of column 2. The condition of column 2 after failure is shown in the photograph in Fig. 7.30a. The capital broke away from the column and spalled as a unit. Figure 7.30b shows wide cracks through the column and crushing of the concrete at the base of the capital indicating that the rotation was about the base of the capital. Rotation about that point caused an outward deflection of column 2. The whole reaction was transmitted to the column through the bottom corner of the capital which was sheared off simultaneously with the fracture of the slab reinforcement.

Further loading was attempted on the remaining panels (DEF and GHJ). However, the load caused very large deflections in panels G and H and it was impossible to reach the previous load of 911 psf on these panels.

The large deflections were accompanied by a widening of the yield lines in panel H and between columns 10 and 11. In addition, large rotations were observed at column 14. Figure 7.30c shows the crack pattern at column 14. The large crack which formed along the top outside corner of the beam extended about 20-25 in. in both directions from the column. The crack propagated through the slab. A bottom view at column 14 is shown in Fig. 7.30d. Crushing of the concrete can be seen at the base of the column capital indicating rotation was taking place about that point.

The failure of column 14 was unlike the failure of columns 2 and 3 in that the beam-column connection remained largely intact. Failure at columns 2 and 3 was characterized by the beams and slab twisting away from the column. However, at column 14 it appeared that the slab rotated without a further transmittal of moment to the beams or column. As can be seen in Fig. 7.30c, a large crack formed around the top plate of the prestressing clamp. (The

clamp was removed when the photograph was taken.) It is evident that the clamp strengthened the beam-column connection sufficiently to prevent a failure of the connection similar to that at column 2.

Since no further load could be applied to the exterior panels only the interior panel was loaded with the remaining panels retaining from 500-800 psf. As the load was increased on the interior panel, the drop panels at columns 10 and 11 began to spall. The spalling of concrete at column 10 is shown in Fig. 7.31. The cracks between the drop panels and the slab were first observed at a load 791 psf. As the loading increased the cracks became wider with some minor spalling occurring at a load of 911 psf. The final loading of the interior panel resulted in almost complete destruction of the drop panel. Large portions of the drop panels spalled and the remainder of the drop panels were loose and could be removed by hand.

The loading on panel E was terminated when the main beam of the load distributing system began to yield. On the following day, the beam was strengthened and loading was resumed. The maximum total load on panel E when it failed was 1500 psf. The failure was marked by yield lines forming at the negative moment sections of the panel. The entire center panel appeared to have been "pushed through" the slab.

Following all loadings to failure, the load distributing system was removed and photographs were taken of the crack pattern on the top and bottom of the slab. These crack patterns are shown in Figs. 7.32 and 7.33. The dark lines indicate cracks that formed prior to test 513.

8. DISTRIBUTION OF MOMENTS IN THE STRUCTURE

8.1 Introductory Remarks

The moment distributions presented in this chapter were analyzed from strains measured during test 502. The moments are related to the total load on the structure including the dead load. Test 502 consisted of four load levels in which the total loads were 104, 161, 218, and 286 psf; the last load was the design load of the structure.

In this chapter, the distribution of moments across the full width of the structure are discussed. In addition, the moments at the design sections are compared with the ACI design moment at those sections. The moments in the interior panel are compared with theoretical solutions available for a typical interior panel. The moments in individual panels are given and the total moments across strips consisting of three panels are compared to the static total moment in these three-panel strips.

8.2 Determination of Moments

In reinforced concrete structures, the conversion of measured strains to moments is not straightforward. The complication arises primarily from the tensile strength of the concrete which contributes to the capacity of the section. For structures with low reinforcement ratios, the tensile properties of the concrete have a significant influence on the capacity. Therefore, it is necessary to determine moment-strain relationships which include the effect of the concrete tensile strength.

A typical moment-strain relationship for a section reinforced with welded wire reinforcement is shown qualitatively in Fig. 8.1. Such curves were developed for each section in which the wire diameter, reinforcement ratio or steel depth changed. Each curve consists of two straight lines.

Two points in addition to the origin are needed to describe the relationship. The coordinates of the intermediate point are the cracking moment and strain. The coordinates of the end point are the moment at the proportional limit of the wire and the corresponding strain. The method of producing the moment-strain diagrams is based on the conclusions of small beam tests conducted in connection with this structure and the previous structures in this series.

The cracking moments were computed using the ordinary flexure formula, $\sigma = Mc/I$. The moment of inertia was based on a transformed section. The strain distribution was assumed to be linear. The cracking strain was taken to be 0.00019. The cracking stress assumed in these computations was 600 psi. This was somewhat less than the modulus of rupture of the test control specimens which gave values of 775 psi. However, it should be pointed out that the control specimens were not reinforced. The steel in the slab offered a restraint to the concrete shrinkage and resulted in a lowering of the tensile strength. Furthermore, the assumed tensile strength was chosen to correlate with results obtained from a study of the static moment in the interior panel which could be computed accurately.

The strains measured in the slab reinforcement during test 502 were all less than the proportional limit of the wire. Therefore, the proportional limit stress was used in computing the moment at the third point for the moment-strain diagram. The cracking was assumed to have developed sufficiently at this level that the influence of the concrete in tension was negligible. The values of proportional limit stress and strain were obtained from the stress-strain curves for the wire (Figs. 3.1-3.7).

Separate moment-strain curves were developed for the beams. Typical moment-strain curves for the beams are shown in Fig. 8.2. The cracking moment was computed in the same manner as that used for the wire reinforcement. The

deep beam was assumed to have an effective compression flange width of 4t (four times the thickness of the slab) and to be restrained from twisting about its longitudinal axis. The cracking stress and strain remained the same as for the slab. The yield stress and strain were used in computing the terminal point of the moment-strain relationship. Since the steel used in the beams had a well-defined yield point (Fig. 3.8), the yield point values were analogous to the proportional limit values used previously.

The moments were computed for total load. Dead load strains were added to the strains measured at the applied load levels. The dead load strain was determined by projecting the load-strain curves for each gage location to a zero load. The total load strains were used to obtain a moment from the moment-strain diagrams.

8.3 Distribution of Moments Across the Full Width of Structure

The moments were determined at critical sections across the full width of the structure. The location of the critical sections is shown in Fig. 8.3. Sections 1, 3, 5 and 7 are negative moment sections and sections 2, 4 and 7 are positive moments sections.

The distribution of moments across the sections are shown in Figs. 8.4 through 8.12. The moments are shown for the four load levels in test 502. The beam moments at the corresponding load levels are indicated by the solid circles and their magnitudes are given in parentheses. It is important to note that the beam moments are given in kip-in. while the slab moments are plotted in kip-in. per foot. The moments across the column capitals are distinguished by the additional vertical lines within the column strips denoting the edge of the capital. The curves are discontinuous at the column capitals. The curves are formed by straight line segments connecting the values of moments computed at each gage location.

In general the highest moments were reached in those sections with the greatest stiffness, that is, the column strips and wall strips. The middle strips which had the lowest stiffness had the lowest moments. From the moment curves, it can be seen that the moments at the positive and exterior negative moment sections (1, 2, 4, 6 and 7) were zero adjacent to the deep beam.

The negative moments at the interior column capitals were higher at the exterior face of the capital than at the interior face. The negative moments at sections 3 and 5 (excluding moments across the column capitals) reached a maximum just outside the capital and decreased at the edge of capital. The point of maximum moment was at the edge of the drop panels and a higher moment was expected at that location since the drop panel was stiffer.

The exterior negative moment distributions (sections 1 and 7) show that the moments at the columns were much higher than at the remainder of the exterior sections. The torsional stiffness of the beams was less than usually assumed in design procedures.

Since the strains did not exceed the proportional limit values, there was no significant reduction in the stiffness of any section. This is evident from the moment distributions which showed that the moment at all sections increased almost proportionally with the load.

8.4 Comparison of Measured Moments with Theoretical Moments in Interior Panel E

Theoretical solutions for plates supported on columns are available for a limited number of cases. The theoretical solution is based on the differential equation which describes the deflection of the plate. The equation and various solutions and references to literature on the subject can be found in Ref. 7.

The differential equation was solved by the method of finite differences to obtain the theoretical moments presented in this discussion.

If small finite lengths are considered instead of the differentials, difference equations are obtained which correspond to the differential equation. The solutions obtained by difference equations approach the exact solutions as the finite length approaches zero. The number of difference equations needed to express the differential equation increases as the boundary conditions increase, as a result few solutions for edge panels are available since the boundary conditions are more involved in the edge panels than they are in a typical interior panel.

In Ref. 7, the results of Nielsen's theoretical solutions obtained by finite differences are given for an interior panel of an infinite array of uniformly loaded panels. The distribution of moment across the negative and positive moment sections are shown in Fig. 8.13. Two solutions are shown in the figure. For one solution Nielsen assumed the column reaction to be uniformly distributed over the area of the capital which imparted no additional stiffness to the slab. In the second solution the stiffness of the capital was assumed to be equal to the slab stiffness at the edge and infinitely stiff at the mid-point of the capital. The shear in this solution was assumed to be distributed linearly around the perimeter of the capital.

The measured moment is shown by the broken line in Fig. 8.13. The measured negative moment is higher than the theoretical moment at the column capitals and is nearly the same in the middle third of the panel width. The higher moment at the capital is due to a greater stiffness of the capital than assumed in the theoretical solution. The drop panels in the structure also contribute to the stiffness. The negative moment reaches a peak at the edge of the drop panel and decreases slightly at the edge of the column capital. The measured positive moment is lower than the theoretical values as a result of the increased measured moment at the negative moment section.

Theoretical solutions have also been obtained for a typical interior panel at the University of Illinois. These solutions are presented in Ref. 7. The theoretical solution for a panel similar to the interior panel in the test structure is shown in Fig. 8.14. The theoretical solution is based on the reaction being concentrated at the corners of the capitals. The capitals were assumed to be infinitely stiff.

The measured negative moments indicate that the capital is not infinitely stiff since the moment did not approach zero at the edge of the capital. The peak theoretical moment at the corner of the capital due to the concentrated reaction at that point is not evident in the measured moment. The theoretical structure did not have any drop panels. Thus the measured moment reaches a peak at the edge of the drop panel which is not present in the theoretical solution. The positive measured moment is lower than the theoretical values largely due to the greater moment measured across the drop panel in the negative moment sections.

In general the theoretical solutions and measured moments show the same trends. The distribution of moment between the negative and positive moment sections varied slightly from the theoretical moments. The major reason for discrepancy is the drop panels in the test structure which caused the measured negative moment to be higher than theoretical values. Also, it is quite evident that the actual stiffness of the column capitals is extremely difficult to predict and any assumption is subject to question.

8.5 Comparison of Measured Moments with ACI Design Moments

In order to compare the measured moments with the design moments, it was necessary to convert moment distributions across a section to the total moment across that section. This was done by determining the area under the curves shown in Figs. 8.4-8.12 within a given design section. Thus, the

moments were obtained in the wall, middle, and column strips at the critical sections. The measured moments in the design sections are presented in Tables 8.1-8.4. The moments are given for the load levels in test 502. The moment is given at each critical section (See Fig. 8.3). The moment measured at the design load is compared to the design moment computed according to Article 1004, ACI 318-56. The design moments are computed for the load level measured in the test (286 psf).

(a) Moments in the Wall Strip

The moments in the wall strips are divided into the moment carried by the slab and beam. For each load level, the total moment carried by the slab and beam in the wall strip is given in Table 8.1.

The ACI beam design moments are based on the code provisions of Article 1004 of ACI 318-56 which give the percentage of panel load carried by the beam. The beam moment coefficients are given in Article 701.

The relative magnitudes of the measured total moments at 286 psf shown in Table 8.1 are reasonable. The end moments appear to be unusually high, especially the moment at the end adjoining the shallow beam (section 1). Nevertheless, these high values may be ascribed to the stiffness of the column relative to the shallow beam. On the basis of the figures listed, no strong case may be made for nonsymmetry of the section about section 4. The moment at section 7 is lower than that at section 4. This relationship is corroborated by the relative magnitudes of the moments at sections 3 and 5. However, it is unlikely that this is a direct effect of the difference between the geometry of the two beams perpendicular to the strip considered.

The comparison of the total measured and design moments is not favorable (Table 8.1). The design moments were lower at the interior negative

sections 3 and 5 and higher at all other sections. The greatest relative difference occurred at section 4.

The relative magnitudes of the moments measured in the slab and beams at each section differed considerably from the proportions assumed in design. At sections 3 and 5, the design moments in the beam and slab are of comparable magnitude. The measured ratio of slab to beam moment at those sections was on the order of two. At the exterior sections 1 and 7, the design moments for the beam and slab are also comparable while the measured ratio of slab to beam moment was about one-half.

The measured and design moments for the wall strip including the deep beam are listed in Table 8.2. At 286 psf, they compare in the same manner as the moments listed in Table 8.1. The difference between the measured and design moments is very large in sections 1 and 7. The measured distribution of moment to the beam and slab is approximately the same as assumed in design. However, it should be noted that in interpreting the test data, the deep beam was assumed to have a flange of four times the slab thickness in addition to the width of the beam.

(b) Moments in the Column Strip

The measured moments in both column strips in the structure are presented separately. They are given in Fig. 8.3. In this way, each strip can be compared individually with the ACI design moments which are the same for both column strips.

In both strips the exterior negative design moments were slightly over-estimated. The interior negative measured moments were about 25-30 per cent greater than the design moments. The exterior positive moments were greater in the test structure than the design moments while the interior positive moment is about the same in both cases.

(c) Moments in the Middle Strip

The measured moments are given separately for each of the three middle strips and compared individually with the design moments, which are the same for two of the middle strips. The moments in the middle strip are shown in Table 8.4.

In general, the exterior negative measured moments were less than the design moment and the interior negative measured moments were considerably greater than provided in design. The positive measured moments were generally higher than the design moments.

8.6 Comparison of Computed, Measured, and Design Static Moments

This section is devoted to the comparison of three quantities: computed, measured, and design values of the static moments in the test structure. The static moment is defined as the moment caused by the load about a section at mid-span. In a beam, the static moment is equal to the sum of the positive moment at mid-span and the average of the negative moments at the ends of the span. The static moment in a rectangular panel of a slab is resisted not only by the bending moments acting on planes perpendicular to the span but also by the twisting moments acting on edges parallel to the span considered. Furthermore, the centroid of the reaction is influenced by the distribution of shears along the supported edges.

A panel in a flat slab structure is not a basic structural unit even if the columns are arranged in a regular pattern. However, one advantage of considering the flat slab panel by panel is that an approximation to the static moment may be obtained in a given panel on the basis of equilibrium conditions alone.

None of the column centerlines in the test structure were lines of symmetry. Therefore, the boundary forces along the column centerlines could

not be ascertained without a rigorous analysis. However, if the shears and twisting moments along the adjoining panel edges are arbitrarily assumed to be zero, it is possible to obtain an approximate evaluation of the static moment in the panel. If a reasonable assumption is made about the distribution of shears along the supported edges of the slab in each panel and twisting moments along these edges are ignored, the static moment in the panel can be calculated directly.

Two different assumptions were made as to the distribution of the shear at the supported edges. One set of computed static moments was based on a uniform distribution of shear along all supported edges including those supported by beams. These are denoted as M_s in all the following tables. The second set of computed static moments was based on a uniform distribution of shear along the edges of the columns or capitals depending on the panel considered. Moments based on this assumption are given as M'_s. The true static moment in the panels lies between the values of M_s and M'_s. Since no precise determination of the distribution of shear can be made, this range of values provides a means of estimating the actual static moment.

The measured static moment in each panel was determined by adding the positive measured moment at the centerline of the panel to the average of the negative moments in the panel. The measured moments for all panels of the structure are listed in Tables 8.6 to 8.14. The percentage of total moments at the sections considered is given. The total moments are also given as coefficients of WL, the product of the total load on the panel and the span center to centerline of the supporting constants. The value of WL was constant for all panels.

The design static moment was determined by summing design positive moment and the average of the design negative moments in each panel.

In the following tables, the computed, measured, and design static moments are listed for each panel individually. However, in comparing the static moments, it is preferable to consider a strip of three panels such that the boundary conditions are known. Therefore, the panels are grouped to give a section across the full width of the structure if they are considered together.

Static Moments in Panels ABC

	Panel A M/WL	Panel B M/WL	Panel C M/WL	Panels ABC M/3WL
M_s	0.098	0.093	0.098	0.096
M'_s	0.101	0.090	0.101	0.097
M_{meas}	0.107	0.091	0.105	0.101
$M_{des.}$	0.102	0.070	0.111	0.094

There was little difference between the computed static moments based on the two different assumptions. In the corner panels A and C, the centroid of the reaction was near the face of the beam if the shear was assumed to be distributed along the beams and columns. However, if the shear was distributed along the columns only, the centroid of the reaction was closer to the edge of the panel (to the outside of the face of the beam). Thus, the value of M'_s was larger than M_s. The centroid of the reaction at the interior column capitals remained the same for both assumptions.

The measured static moment in the individual panels deviated somewhat from the computed static moments and the measured moment across the full width of the structure was slightly higher. Figure 8.15 shows the variation in the measured from the computed static moments at the four load levels in test 502.

The design static moments were nearly the same as the computed static moment in panel A. However, in panels B and C there was considerable difference in the values. Panel B was under-designed while panel A was over-designed but it is important to note that in the section across the entire structure, the design static moment compared favorably with the computed and measured values.

Static Moments in Panels DEF

	Panel D M/WL	Panel E M/WL	Panel F M/WL	Panels DEF M/3WL
M_s	0.096	0.088	0.096	0.93
M'_s	0.097	0.088	0.097	0.94
M_{meas}	0.98	0.087	0.110	0.98
M_{des}	0.96	0.065	0.106	0.89

The end support conditions were the same for the individual panels and in panels D and F, the computed static moments were equal. Although panels D and F were supported by different spandrel beams, these beams did not affect the support conditions in the span parallel to the beam.

The measured moments compare favorably with the computed static moments in panels D and E but in panel F the measured moment was considerably greater (13 per cent). The measured static moment across the entire section was 4 per cent higher than the computed values, largely as a result of the high measured moment in panel F. The variation between measured and computed static moments across the section is shown in Fig. 8.15.

The design moment in panels D and F are approximately equal to the computed values, however, in panel E the design moment is 26 per cent less than the computed static moment. The design moments for the section across

the full width are 5 per cent lower than the computed static moments and 9 per cent less than the measured value.

Static Moments in Panels GHJ

	Panel G M/WL	Panel H M/WL	Panel J M/WL	Panels GHJ M/3WL
M_s	0.106	0.100	0.106	0.104
M'_s	0.101	0.090	0.101	0.097
M_{meas}	0.102	0.081	0.127	0.103
M_{des}	0.103	0.069	0.112	0.095

The computed static moment in the panels was considerably different depending on the assumptions for shear distribution in these panels. As can be seen from the table, M_s was higher in all panels. If the shear was considered to be distributed along the beams and columns, the centroid of the reaction was shifted toward the edge of the panel. The centroid of the reaction was near the edge of the beam and since the deep beam was narrow the reaction was almost at the edge of the panel. The result was a higher value of M_s in these panels.

The values of measured moment in the individual panels varied considerably, especially in panel H and J. However, the measured moment across the entire structure falls within the range of computed moments. The measured static moments in test 502 are shown in Figs. 8.15.

The value of design moment in panels G and J appears to be reasonable but panel H appears to be under-designed. The design moment across the entire structure falls below the range of computed static moments.

A summary of the static moments is given in Table 8.15. The measured moments in the individual panels were considerably different from the

computed static moments in those panels. However, as was pointed out in the preceding discussion, the measured moment across the full width compared favorably with the static moments. Referring to Fig. 8.15, it can be seen that in all sections across the entire structure the measured and computed moments were very close. In general, the measured static moment increased as the load increased but this is not unreasonable since the load may cause sufficient deflection of the capitals to shift the reaction to the edge of the panels. As a result, the moments tend to increase.

Comparison of the computed and design static moments in the individual panels (Table 8.15) shows that the design is adequate in the panels with some beam support in the direction of the span. The three panels which had no spandrel beams in the direction of design moment (Panels BEH) were considerably under-designed. The method for design of the beams provides a considerable addition to the capacity of the panel. On the basis of these results, it can be concluded that as the number of panels which have no beam support in the direction of the span increases, the design static moment across the full width of the structure decreases. The over-all result will be a reduced factor of safety for the structure since the beams are the major reason for attaining a design static moment that is close to the computed static moments.

9. STRENGTH ANALYSIS

9.1 Introductory Remarks

The strength of the structure was determined by considering various failure mechanisms similar to the method suggested by A. Ingerslev and improved by K. W. Johansen (Ref. 9). This method is commonly referred to as the yield-line analysis.

Three different failure mechanisms are considered. The first is a collapse mechanism designated as a "structural failure" shown in Fig. 9.1. The mechanism is distinguished by the formation of yield lines or hinges across the full width of the structure including the beams. The exterior hinge is assumed to form at or near the face of the beam.

The second collapse mechanism is a slab failure shown in Fig. 9.2. The exterior hinge is assumed to form across the full width of the structure, excluding the beams. The interior yield line forms between the interior columns and extends to about the center of corner panels along the diagonal. the positive moment yield line is located near the center of the panels and extends along the diagonals to the corner columns.

The third failure mechanism shown in Fig. 9.3 is for the interior panel. The positive yield lines form an X coinciding with the diagonals of the panel. The negative yield lines are parallel to the column centerlines but do not coincide with these centerlines.

The resisting moments across the sections at which yield lines formed were computed using the straight line formula

$$M = A_s f_s jd$$

where M = resisting moment of the section

A_s = area of tension reinforcement

f_s = stress of the reinforcement

jd = effective internal moment arm

The welded wire fabric used in reinforcing the slab did not have a flat-top stress-strain curve. Therefore in keeping with the discussion of Section 7.5(d), the strength of the slab was calculated based on the 0.2 per cent offset stress in the reinforcement. Since the wire still has some strength after it reaches the 0.2 per cent offset stress, the strength was also computed using the ultimate stress in the wire. The straight line formula was used for the ultimate resisting moments of the sections. The ultimate resisting moments could have been computed by defining the internal moment arm as

$$d\ (1 - 0.4\ k_u)$$

where $$k_u = \frac{(p - p')}{f_{cu}}\ f_y$$

f_{cu} = average compressive strength of concrete at failure ($f_{cu} = 0.7\ f'_c$)

p = tension reinforcement ratio

p' = compression reinforcement ratio

However, the moments computed on this basis were numerically the same as those given by the straight-line formula.

The yield moment was used in determining the strength of the beams since the beam reinforcement had a well defined yield point. For the deep beams a flange width was assumed equal to the width of the beam plus four times the slab thickness, or 9 in.

9.2 Comparison of Calculated and Measured Strength

The loads determined from each of the assumed modes of failure are shown in the table below. The loading was assumed to be concentrated at sixteen points which was the actual loading on the test structure. However, computations based on uniform loading gave almost identical results.

Two different assumptions were made as to the distribution of shear. One set of computations was based on a uniform distribution of shear along all supported edges. Another set of computations was based on the assumption that the shear was concentrated at the corners of the column capitals.

Failure Mode	Assumed Shear Distribution	Capacity Based on 0.2% offset stress psf	Capacity Based on Ultimate Stress psf
1. Structure			
(a) Row adjacent to shallow beam	Uniform	1040	1090
(b) Row adjacent to deep beam	Uniform	970	1030
2. Slab			
(a) Row Adjacent to shallow beam	Uniform	873	964
	Conc.	1100	1200
(b) Row Adjacent to deep beam	Uniform	776	876
	Conc.	1100	1220
3. Interior Panel	Uniform	1330	1480
	Conc.	2100	2320

As can be seen from the table, the critical failure mechanism was a slab failure adjacent to the deep beam. However, the assumption that the shear is concentrated along all supported edges tends to make the span of the slab too great and results in a low capacity. A more realistic value of the

capacity at failure would appear to be that for the slab failure in the row of panels adjacent to the shallow beam. With a uniform distribution of shear along all supported edges the ultimate load was computed as 964 psf. The ultimate load with the shear concentrated at the corners of the capitals was 1200 psf. The assumption that the shear is concentrated at the corners is also unrealistic because the capitals deflect considerably at high loads and thereby cause a shift in the reaction toward the beam. The span increase is accompanied by a corresponding decrease in the capacity. It is also important to remember that the development of the slab mechanism depends upon the ability of the beam-column connections to withstand torsional rotations which in many cases may control the strength of the structure.

On the basis of the calculations for capacity it appears that a reasonable value of the strength is about 900 psf. This load gives a factor of safety for the structure of 3.2 based on the design load of 284 psf. It is interesting to note that the actual failure in the structure occurred as a slab failure in the panels adjacent to the shallow beam at a load of 955 psf. However, the beam-column connections were reinforced prior to this load and, even with this extra reinforcement, were responsible for the failure.

The structural failure load was considerably higher than the slab failure load largely due to the beams. The beams add considerable strength to the structure and as a result do not participate in the failure mechanism.

The ultimate load for the interior panel was calculated as 1480 psf based on a uniform distribution of shear. The value based on concentrated shear is very high but the assumption is unrealistic because of deflections in the column capitals. The factor of safety based on the design load (284 psf) is 5.2. The actual failure load of the interior panel was about 1500 psf.

It should be pointed out that the X-shaped failure mode assumed in the interior panel occurs only if the failure mechanism is confined to a single panel. A series of like panels in an infinite array of panels would have a different failure mode. Such a failure mode is characterized by hinges or yield lines along the column and panel centerlines and includes more than one panel. The failure load would be 948 psf if the reinforcement in each panel was similar to the interior panel in the test structure.

From a comparison of the computed ultimate loads with the actual failure loads on the test structure, it can be concluded that the structure was able to develop its rated capacity. The maximum moments in the slab failure mode were not fully developed because of the torsional failures in the beam column connections. However, the load at the 0.2 per cent offset stress was reached in the section that failed and the factor of safety for the measured failure load was 3.4.

From the viewpoint of the strength of the structure it appears unreasonable to use the same working stresses for high-strength as for intermediate grade reinforcement.

10. SUMMARY

10.1 Object and Scope

This report describes and analyzes the tests on a nine-panel flat slab structure reinforced with welded wire fabric. The work was carried out as part of an extensive investigation of multiple-panel reinforced concrete floor slabs.

The panels were arranged three by three. Each panel measured five feet square on column centers. The slab was 1 3/4 in. thick. The dimensions of the slab, the spandrel beams, and columns are given in Fig. 2.4-2.6.

The design of the structure was made according to Section 1004 of ACI 318-56 for a live load of 200 psf on the slab. The arrangement of the slab, beam, and column reinforcement is shown in Fig. 2.5-2.7. The average 0.2 per cent offset stress for the steel was 70 ksi. The properties of the concrete are listed in Table 3.1.

Each panel was loaded at 16 symmetrically located points (Fig. 4.2 and 5.6). A series of tests, including pattern loadings, were carried out as indicated in Table 6.1. The structure was instrumented with 323 strain gages on the reinforcement and 30 on the concrete (Fig. 5.1-5.5). Deflections were measured at 33 locations (Fig. 5.8).

10.2 Behavior of the Test Structure Under Service Load

The performance of the structure under service load was characterized by very low stresses and deflections. The maximum deflection was 0.096 in. or L/625 (Fig. 7.2) and the maximum stress in the reinforcement was 11,000 psi (Figs. 7.4 and 7.5) at the design load.

The distribution of moments across the full width of the structure are shown in Figs. 8.4 to 8.12. Comparisons of the measured moment with the

design moment are given in Table 8.1 to 8.4. The comparison of the design moments with those measured was poor. The ratio of the measured to design moment at a total load of 286 psf ranged from 0.22 to 1.79 for the slab and 0.31 to 1.48 for the beam sections.

10.3 Strength

The test structure failed at a total load of 955 psf on all panels. The failure was initiated by distress at the exterior beam-column connections and consummated by fracture of the reinforcement across the mid-span of a row of three exterior panels. The ratio of the ultimate to design load was 3.4.

Calculation of the capacity of the structure on the basis of the yield-line analysis indicated a load of about 900 psf predicated on a negative yield-line forming at the face of the exterior beam. However, the beam-column connection failed in combined bending, shear, and torsion before the slab reinforcement yielded at the face of the beam. As long as the designer provides for the moment and shear to be transmitted to the supporting columns, the yield-line analysis should give a safe estimate of the capacity.

REFERENCES

1. American Concrete Institute, Building Code Requirements for Reinforced Concrete, (ACI 318-56).

2. Mayes, G. T., M. A. Sozen, and C. P. Siess, "Tests on a Quarter-Scale Model of a Multiple-Panel Reinforced Concrete Flat Plate Floor," Structural Research Series No. 181, Dept. of Civil Engineering, Univ. of Illinois, September 1959.

3. Hatcher, D. S., M. A. Sozen, and C. P. Siess, "An Experimental Study of a Reinforced Concrete Flat Slab Floor," Structural Research Series No. 200, Dept. of Civil Engineering, Univ. of Illinois, June 1960.

4. Hatcher, D. S., M. A. Sozen, and C. P. Siess, "A Study of Tests on a Flat Plate and a Flat Slab," Structural Research Series No. 217, Dept. of Civil Engineering, Univ. of Illinois, July 1961.

5. Gamble, W. L., M. A. Sozen, and C. P. Siess, "An Experimental Study of a Two-Way Floor Slab," Structural Research Series No. 211, Dept. of Civil Engineering, Univ. of Illinois, June 1961.

6. Vanderbilt, M. D., M. A. Sozen, and C. P. Siess, "An Experimental Study of a Reinforced Concrete Two-Way Floor Slab with Flexible Beams," Structural Research Series No. 228, Dept. of Civil Engineering, Univ. of Illinois, November 1961.

7. Corley, W. G., M. A. Sozen, and C. P. Siess, "The Equivalent Frame Analysis for Reinforced Concrete Slabs," Structural Research Series No. 218, Dept. of Civil Engineering, Univ. of Illinois, June 1961.

8. Gamble, W. L., M. A. Sozen, and C. P. Siess, "Measured and Theoretical Bending Moments in Reinforced Concrete Floor Slabs," Structural Research Series No. 246, Dept. of Civil Engineering, Univ. of Illinois, June 1962.

9. Johansen, K. W., "Beregning of krydsarmerede Jarenhetonpladers Brudmoment," Bygningsstateske Meddelelser (Copenhagen), Vol. 3, 1931. (See also: Hognestad, Eivind, "Yield-Line Theory for the Ultimate Flexural Strength of Reinforced Concrete Slabs," Proc. ACI, Vol. 49, 1953, p. 637).

TABLE 3.1

PROPERTIES OF CONCRETE

Batch	Water/Cement	Compressive Strength								Modulus of Rupture			
		56 days				100 days				56 days		100 days	
		2x4 cyl. No.of Tests	f'_c psi	4x8 cyl. No.of Tests	f'_c psi	2x4 cyl. No.of Tests	f'_c psi	4x8 cyl. No.of Tests	f'_c psi	No.of Tests	f_r psi	No.of Tests	f_r psi
1	0.72	2	4380			2	4140						
2	0.72	2	3590	3	3440			3	3330	3	800	3	812
3	0.73	3	4470			2	4780						
4	0.73	3	4850	3	4350	2	4060	3	4640	3	718	3	882
5	0.72	3	3490			2	3380						
6	0.73	3	3940	3	3830	2	3580	3	3870				
7	0.72	3	3670			2	3240						
8	0.72	3	3720	3	3850	2	3020	3	3760	3	778	3	822
9	0.72	3	3290			2	3180						
10	0.72	2	3770	3	3910			3	4180	3	711	3	693
11	0.72	3	3560			2	3970						
12	0.72	3	3390	3	4000	2	3410	3	4180				
Averages			3760		3900		3670		3990		750		804

f'_c = compressive strength of a 6 x 12 in. cylinder

f_r = modulus of rupture

TABLE 6.1

CHRONOLOGY OF TESTS

Test No.	Date	Panels Loaded	Remarks
500	20 April 1961	All	Readings taken during assembly of load distribution system.
501	3 May	All	100 psf*
502	4	All	LL + DL 284 psf
503	11	All	1.5LL + DL 384 psf
504	16	ABC-GHJ	384 psf on ABC-GHJ, 84 psf on others
505	18	DEF	384 psf on DEF, 84 psf on others
506	23	ADG-CFJ	384 psf on ADG-CFJ, 84 psf on others
507	25	BEH	384 psf on BEH, 84 psf on others
508	6 June	ABC-DEF	384 psf on ABC-DEF, 84 psf on others
509	9	DEF-GHJ	384 psf on DEF-GHJ, 84 psf on others
510	12	ADG-BEH	384 psf on ADG-BEH, 84 psf on others
511	13	BEH-CFJ	384 psf on BEH-CFJ, 84 psf on others
512	15	All	674 psf
513	20	All	955 psf
514	21	E	1500 psf

* All values of nominal uniform load given in the table include the weight of the slab and the load distributing system.

TABLE 8.1

MEASURED MOMENTS IN WALL STRIP INCLUDING SHALLOW BEAM

		Shallow Beam						Deep Beam		
		1	2	3	3'	4	5'	5	6	7
Load, psf		Moments, kip-in.								
104	Slab	1.0	1.2	3.6	3.6	0.6	4.3	4.3	1.1	0.8
	Beam	1.0	1.5	1.7	1.6	0.9	1.6	1.7	1.8	1.4
	Total	2.0	2.7	5.3	5.2	1.5	5.9	6.0	2.9	2.2
161	Slab	1.5	2.0	5.9	5.9	0.9	6.6	6.6	1.8	1.1
	Beam	2.5	2.7	2.7	2.5	1.3	2.3	3.5	3.0	2.0
	Total	4.0	4.7	8.6	8.4	2.2	8.9	10.1	4.8	3.1
218	Slab	2.0	2.6	7.7	7.7	1.3	8.9	8.9	2.5	1.6
	Beam	4.5	4.0	5.0	3.4	1.9	3.2	5.0	4.2	3.5
	Total	6.5	6.6	12.7	11.1	3.2	12.1	13.9	6.7	5.1
286	Slab	3.3	3.3	10.1	10.1	1.8	11.2	11.2	3.3	2.4
	Beam	5.3	4.9	6.3	5.1	2.5	4.6	6.8	4.8	4.9
(Design Load)	Total	8.6	8.2	16.4	15.2	4.3	15.8	18.0	8.1	7.3
DESIGN MOMENT for 286 psf	Slab	5.3	3.6	7.6	6.7	2.8	6.7	7.6	3.6	4.3
	Beam	5.1	5.8	8.2	7.2	5.0	7.2	8.2	5.8	5.1
	Total	10.4	9.4	15.8	13.9	7.8	13.9	15.8	9.4	9.4

TABLE 8.2

MEASURED MOMENTS IN WALL STRIP INCLUDING DEEP BEAM

Load, psf		Shallow Beam						Deep Beam	
		1	2	3	3'	4	5'	5	6	7
		Moments, kip-in.								
104	Slab	0.2	0.4	1.5	1.5	0.3	1.0	1.0	0.3	0.4
	Beam	1.0	3.0	5.2	5.0	1.6	5.3	6.7	5.5	1.8
	Total	1.2	3.4	6.7	6.5	1.9	6.3	7.7	5.8	2.2
161	Slab	0.3	0.5	2.0	2.0	0.4	1.6	1.6	0.4	0.5
	Beam	1.6	4.5	7.1	8.0	2.6	7.8	10.3	11.0	2.9
	Total	1.9	5.0	9.1	10.0	3.0	9.4	11.9	11.4	3.4
218	Slab	0.5	0.7	3.2	3.2	0.5	2.2	2.2	0.6	0.7
	Beam	2.2	7.5	12.8	11.0	3.6	10.8	14.0	15.2	3.9
	Total	2.7	8.2	16.0	14.2	5.1	13.0	16.2	15.8	4.6
286	Slab	0.6	1.0	4.1	4.1	0.7	4.2	4.2	0.9	1.0
	Beam	2.9	11.2	17.4	15.0	4.6	14.3	18.3	15.7	4.9
(Design Load)	Total	3.5	12.2	21.5	19.1	5.3	18.5	22.5	16.6	5.9
DESIGN MOMENT for 286 psf	Slab	2.7	1.8	3.9	3.6	1.4	3.6	3.9	1.8	2.2
	Beam	9.3	10.6	14.9	13.1	9.0	13.1	14.9	10.6	9.3
	Total	12.0	12.4	18.8	16.7	10.4	16.7	18.8	12.4	11.5

TABLE 8.3

MEASURED MOMENTS IN COLUMN STRIP

	Shallow Beam						Deep Beam	
	1	2	3	3'	4	5'	5	6	7
Load, psf	Moments, kip-in.								
Column Strip 1 (Closer to parallel shallow beam)									
104	3.8	2.8	8.3	5.9	1.9	7.7	7.4	1.7	3.2
161	5.7	4.4	13.1	9.2	3.0	12.4	11.9	4.3	4.9
218	7.1	5.9	16.1	12.0	4.0	16.6	17.0	5.7	6.8
286	10.1	10.1	20.0	17.3	5.4	21.7	21.8	9.9	8.6
Design Moment for 286 psf	12.0	6.7	15.6	13.9	5.6	13.9	15.6	6.7	10.0
Column Strip 2 (Closer to parallel deep beam)									
104	2.7	3.7	7.8	7.6	2.0	7.7	8.2	2.4	3.3
161	4.3	4.9	13.4	11.6	3.3	12.0	12.7	3.8	5.0
218	5.6	6.7	16.9	17.3	4.4	16.6	17.0	5.3	6.9
286	8.0	9.7	20.7	20.6	6.0	19.1	20.8	9.3	8.8
Design Moment for 286 psf	12.0	6.7	15.6	13.9	5.6	13.9	15.6	6.7	10.0

TABLE 8.4

MEASURED MOMENTS IN MIDDLE STRIPS

	Shallow Beam						Deep Beam		
	1	2	3	3'	4	5'	5	6	7
Load, psf	Moments, kip-in.								
Middle Strip 1 (Closer to parallel shallow beam)									
104	0.7	2.9	2.4	2.4	1.2	2.3	2.3	1.9	1.0
161	1.1	4.4	3.9	3.9	1.8	3.7	3.7	3.2	1.3
218	1.3	5.9	5.5	5.5	2.3	5.0	5.0	4.3	1.8
286	1.8	8.4	7.5	7.5	3.2	7.1	7.1	6.4	2.4
Design Moment for 286 psf	3.6	6.5	5.6	4.8	4.8	4.8	5.6	6.5	6.5
Middle Strip 2									
104	1.0	2.7	2.9	2.9	1.4	1.8	1.8	2.7	0.7
161	1.5	4.2	4.4	4.4	2.3	2.9	2.9	4.3	1.2
218	2.1	5.7	5.9	5.9	3.0	4.0	4.0	5.7	1.5
286	2.7	8.6	7.5	7.5	4.1	7.0	7.0	7.4	2.2
Design Moment for 286 psf	3.1	5.6	4.7	4.2	4.2	4.2	4.7	5.6	5.6
Middle Strip 3 (Closer to parallel deep beam)									
104	0.6	1.6	2.0	2.0	1.2	2.1	2.1	1.8	1.1
161	1.0	2.9	3.2	3.2	1.6	3.1	3.1	2.8	1.7
218	1.4	3.8	4.2	4.2	2.3	4.4	4.4	3.8	2.4
286	1.9	5.0	6.0	6.0	4.7	5.8	5.8	5.3	3.2
Design Moment for 286 psf	3.1	5.6	4.7	4.2	4.2	4.2	4.7	5.6	5.6

TABLE 8.5

MOMENTS ACROSS FULL WIDTH OF THE STRUCTURE

	Shallow Beam								Deep Beam
	Moments, kip-in.								
Load, psf	1	2	3	3'	4	5'	5	6	7
104	-12.02	19.77	-35.38	-32.50	10.99	-33.77	-35.36	20.11	-13.68
161	-19.48	30.51	-56.00	-50.50	17.16	-52.40	-56.24	34.69	-20.78
218	-26.52	42.73	-77.34	-70.21	23.19	-71.59	-77.34	47.26	-29.14
286	-36.55	62.04	-99.65	-93.14	32.85	-94.79	-101.46	63.37	-38.39
Measured Total Moment									
104		43.47			44.14			44.63	
161		68.25			68.61			73.20	
218		94.66			94.09			100.50	
286		130.14			126.82			133.30	
	Moment Coefficients in Terms of WL								
Load, psf	1	2	3	3'	4	5'	5	6	7
104	0.026	0.042	0.075	0.069	0.024	0.072	0.076	0.043	0.029
161	0.027	0.042	0.077	0.070	0.024	0.072	0.078	0.048	0.029
218	0.027	0.044	0.080	0.072	0.024	0.074	0.080	0.049	0.030
286	0.028	0.048	0.078	0.073	0.025	0.074	0.079	0.049	0.030
Total Moment Coefficient									
104		0.093			0.094			0.095	
161		0.094			0.095			0.101	
218		0.097			0.097			0.108	
286		0.101			0.098			0.104	

TABLE 8.6

MOMENTS AT DESIGN SECTIONS, CORNER PANEL A, DESIGN LOAD

	Measured Moment (kip-in.)				Percentage of Total Moment			
Load, psf	104	161	218	286	104	161	218	286
Exterior Negative Moment								
Column Strip	1.94	2.91	3.35	4.68	12.9	11.9	9.9	10.2
Middle Strip	0.67	1.06	1.31	1.75	4.5	4.3	3.9	3.8
Wall Strip	1.00	1.48	1.95	3.30	6.7	6.1	5.8	7.2
Beam	1.00	2.50	4.50	5.30	6.7	10.2	13.4	11.5
Interior Negative Moment								
Column Strip	3.53	5.63	7.13	9.61	23.5	23.1	21.2	20.9
Middle Strip	2.41	3.87	5.45	7.52	16.1	15.9	16.2	16.4
Wall Strip	3.64	5.88	7.73	10.10	24.3	24.1	22.9	22.0
Beam	1.70	2.70	5.00	6.30	11.3	11.1	14.8	13.7
Total Ext. Neg. Moment	4.61	7.95	11.11	15.03	30.7	32.6	33.0	32.7
Total Int. Neg. Moment	11.28	18.08	25.31	33.53	75.2	74.0	74.5	73.0
Average Negative Moment	7.95	13.02	18.21	24.28	53.0	53.3	54.0	52.9
Positive Moment								
Column Strip	1.46	2.29	3.04	5.08	9.7	9.4	9.0	11.1
Middle Strip	2.90	4.40	5.88	8.38	19.3	18.0	17.4	18.3
Wall Strip	1.19	2.01	2.58	3.26	7.9	8.2	7.7	7.1
Beam	1.50	2.70	4.00	4.90	10.0	11.1	11.9	10.7
Total Positive Moment	7.05	11.40	15.50	21.62	47.0	46.7	46.0	47.1
Total Moment	15.00	24.42	33.71	45.90	100.0	100.0	100.0	100.0
Moment Coefficient, WL	0.096	0.101	0.103	0.107				

TABLE 8.7

MOMENTS AT DESIGN SECTIONS, EDGE PANEL B, PERPENDICULAR TO THE SHALLOW BEAM, DESIGN LOAD

	Measured Moment (kip-in.)				Percentage of Total Moment			
Load, psf	104	161	218	286	104	161	218	286
Exterior Negative Moment								
Column Strip	3.52	5.41	7.08	10.27	25.2	24.8	24.9	26.2
Middle Strip	1.00	1.52	2.05	2.72	7.2	7.0	7.2	6.9
Interior Negative Moment								
Column Strip	9.23	14.56	17.93	21.40	66.1	66.8	63.1	54.6
Middle Strip	2.91	4.36	5.94	7.45	20.8	20.0	20.9	19.0
Total Ext. Neg. Moment	4.52	6.93	9.13	12.99	32.4	31.8	32.2	33.2
Total Int. Neg. Moment	12.14	18.92	23.87	28.85	87.0	86.8	84.1	73.6
Average Negative Moment	8.33	12.93	16.50	20.92	59.7	59.3	58.1	53.4
Positive Moment								
Column Strip	2.96	4.63	6.23	9.68	21.2	21.2	21.9	24.7
Middle Strip	2.67	4.25	5.67	8.58	19.1	19.5	20.0	21.9
Total Positive Moment	5.63	8.88	11.90	18.26	40.3	40.7	41.9	46.6
Total Moment	13.96	21.81	28.40	39.18	100.0	100.0	100.0	100.0
Moment Coefficient, WL	0.090	0.090	0.087	0.091				

TABLE 8.8

MOMENTS AT DESIGN SECTIONS, EDGE PANEL B, PARALLEL TO THE SHALLOW BEAM, DESIGN LOAD

	Measured Moment (kip-in.)				Percentage of Total Moment			
Load, psf	104	161	218	286	104	161	218	286
Negative Moment								
Column Strip	3.28	5.25	6.79	9.28	22.2	22.7	21.9	22.0
Middle Strip	2.35	3.76	5.20	7.30	15.9	16.2	16.8	17.3
Wall Strip	3.96	6.23	8.31	10.64	26.8	26.9	26.8	25.3
Beam	1.60	2.40	3.30	4.83	10.8	10.4	10.6	11.5
Total Negative Moment	11.19	17.64	23.60	32.05	75.8	76.2	76.0	76.1
Positive Moment								
Column Strip	0.96	1.47	1.96	2.63	6.5	6.4	6.3	6.2
Middle Strip	1.17	1.84	2.32	3.16	7.9	7.9	7.5	7.5
Wall Strip	0.56	0.88	1.25	1.76	3.8	3.8	4.0	4.2
Beam	0.88	1.32	1.91	2.50	6.0	5.7	6.2	5.9
Total Positive Moment	3.57	5.51	7.44	10.05	24.2	23.8	24.0	23.9
Total Moment	14.76	23.15	31.04	42.10	100.0	100.0	100.0	100.0
Moment Coefficient, WL	0.095	0.096	0.095	0.098				

TABLE 8.9

MOMENTS AT DESIGN SECTIONS, CORNER PANEL C, PERPENDICULAR TO THE SHALLOW BEAM, DESIGN LOAD

	Measured Moment (kip-in.)				Percentage of Total Moment			
Load, psf	104	161	218	286	104	161	218	286
Exterior Negative Moment								
Column Strip	1.06	1.67	2.24	3.14	7.3	7.6	6.9	7.0
Middle Strip	0.63	1.03	1.39	1.89	4.3	4.7	4.3	4.2
Wall Strip	0.20	0.30	0.45	0.60	1.4	1.4	1.4	1.3
Beam	1.00	1.60	2.20	2.90	6.9	7.3	6.8	6.4
Interior Negative Moment								
Column Strip	3.28	6.34	7.99	9.75	22.6	28.8	24.5	21.6
Middle Strip	1.95	3.16	4.17	5.98	13.4	14.3	12.8	13.3
Wall Strip	1.53	2.40	3.20	4.14	10.5	10.9	9.8	9.2
Beam	5.20	7.10	12.80	17.40	35.8	32.2	39.3	38.6
Total Ext. Neg. Moment	2.89	4.60	6.28	8.53	19.9	20.9	19.3	18.9
Total Int. Neg. Moment	11.96	19.00	28.16	37.27	82.4	86.2	86.5	82.7
Average Negative Moment	7.43	11.80	17.22	22.90	51.2	53.6	52.9	50.8
Positive Moment								
Column Strip	2.08	2.42	3.30	4.99	14.3	11.0	10.1	11.1
Middle Strip	1.61	2.78	3.80	4.97	11.1	12.6	11.7	11.0
Wall Strip	0.40	0.53	0.73	1.00	2.8	2.4	2.2	2.2
Beam	3.00	4.50	7.50	11.20	20.7	20.4	23.0	24.9
Total Positive Moment	7.09	10.23	15.33	22.16	48.8	46.4	47.1	49.2
Total Moment	14.52	22.03	32.55	45.06	100.0	100.0	100.0	100.0
Moment Coefficient, WL	0.093	0.091	0.099	0.105				

TABLE 8.10

MOMENTS AT DESIGN SECTIONS, CORNER PANEL C, PERPENDICULAR TO THE DEEP BEAM, DESIGN LOAD

	Measured Moment (kip-in.)				Percentage of Total Moment			
Load, psf	104	161	218	286	104	161	218	286
Exterior Negative Moment								
Column Strip	1.63	2.63	3.32	4.28	11.2	11.1	10.2	9.7
Middle Strip	1.01	1.31	1.83	2.44	7.0	5.5	5.6	5.6
Wall Strip	0.76	1.14	1.58	2.43	5.2	4.8	4.9	5.5
Beam	1.45	2.00	3.50	4.90	10.0	8.5	10.8	11.2
Interior Negative Moment								
Column Strip	3.90	6.33	8.49	10.70	26.8	26.8	26.1	24.4
Middle Strip	2.28	3.65	4.95	7.07	15.7	15.4	15.2	16.1
Wall Strip	4.28	6.58	8.88	11.18	29.5	27.8	27.4	25.5
Beam	1.70	3.50	5.00	6.80	11.7	14.8	15.4	15.5
Total Ext. Neg. Moment	4.85	7.08	10.23	14.05	33.4	30.0	31.5	32.0
Total Int. Neg. Moment	12.16	20.06	27.32	35.75	83.7	84.9	84.1	81.4
Average Negative Moment	8.51	13.57	18.78	24.90	58.6	57.4	57.8	56.7
Positive Moment								
Column Strip	1.24	2.08	2.70	4.46	8.5	8.8	8.3	10.2
Middle Strip	1.85	3.15	4.27	6.44	12.7	13.3	13.2	14.7
Wall Strip	1.13	1.83	2.52	3.32	7.8	7.7	7.8	7.6
Beam	1.80	3.00	4.20	4.80	12.3	12.7	12.9	10.9
Total Positive Moment	6.02	10.06	13.69	19.02	41.4	42.6	42.2	43.3
Total Moment	14.53	23.63	32.47	43.92	100.0	100.0	100.0	100.0
Moment Coefficient, WL	0.093	0.098	0.099	0.102				

TABLE 8.11

MOMENTS AT DESIGN SECTIONS, INTERIOR PANEL E, DESIGN LOAD

	Measured Moment (kip-in.)				Percentage of Total Moment			
Load, psf	104	161	218	286	104	161	218	286
Negative Moment								
Column Strip	7.25	11.35	15.94	20.21	57.5	55.7	56.8	54.2
Middle Strip	2.35	3.62	4.95	7.20	17.4	17.8	17.6	19.3
Total Negative Moment	9.60	14.97	20.89	27.41	74.9	73.8	74.4	73.5
Positive Moment								
Column Strip	1.97	3.17	4.19	5.81	14.6	15.5	14.9	15.6
Middle Strip	1.42	2.25	2.98	4.05	10.5	11.0	10.6	10.9
Total Positive Moment	3.39	5.42	7.17	9.86	25.1	26.5	25.6	26.5
Total Moment	12.99	20.39	28.06	37.27	100.0	100.0	100.0	100.0
Moment Coefficient, WL	0.083	0.084	0.086	0.087				

TABLE 8.12

MOMENTS AT DESIGN SECTIONS, EDGE PANEL F, PERPENDICULAR TO THE DEEP BEAM, DESIGN LOAD

	Measured Moment (kip-in.)				Percentage of Total Moment			
Load, psf	104	161	218	286	104	161	218	286
Exterior Negative Moment								
Column Strip	3.16	4.75	6.79	8.67	27.6	26.2	27.0	25.0
Middle Strip	0.67	1.18	1.50	2.17	5.9	6.5	6.0	6.3
Interior Negative Moment								
Column Strip	6.40	10.16	14.97	20.41	56.0	56.0	59.5	58.8
Middle Strip	1.78	2.87	3.95	5.48	15.6	15.8	15.7	15.8
Total Ext. Neg. Moment	3.83	5.93	8.29	10.84	33.5	32.7	32.9	31.2
Total Int. Neg. Moment	8.18	13.03	18.92	25.89	71.6	71.8	75.2	74.6
Average Negative Moment	6.01	9.48	13.62	18.37	52.6	52.3	54.1	52.9
Positive Moment								
Column Strip	2.75	4.33	5.89	8.93	24.0	23.9	23.4	25.7
Middle Strip	2.67	4.33	5.66	7.41	23.4	23.9	22.5	21.3
Total Positive Moment	5.42	8.66	11.55	16.34	47.4	47.7	45.9	47.1
Total Moment	11.43	18.14	25.17	34.71	100.0	100.0	100.0	100.0
Moment Coefficient, WL	0.073	0.075	0.077	0.081				

TABLE 8.13

MOMENTS AT DESIGN SECTIONS, EDGE PANEL F, PARALLEL TO THE DEEP BEAM, DESIGN LOAD

	Measured Moment (kip-in.)				Percentage of Total Moment			
Load, psf	104	161	218	286	104	161	218	286
Negative Moment								
Column Strip	3.93	5.98	8.56	9.79	23.9	23.8	24.5	20.6
Middle Strip	2.00	3.15	4.27	5.90	12.2	12.6	12.2	12.4
Wall Strip	1.37	1.82	2.69	4.17	8.3	7.3	7.7	8.8
Beam	5.13	7.90	10.90	14.65	31.2	31.5	31.1	30.9
Total Negative Moment	12.43	18.85	26.42	34.51	75.5	75.2	75.5	72.7
Positive Moment								
Column Strip	1.00	1.65	2.20	3.01	6.1	6.6	6.3	6.3
Middle Strip	1.16	1.58	2.25	4.66	7.0	6.3	6.4	9.8
Wall Strip	0.27	0.40	0.53	0.67	1.6	1.6	1.5	1.4
Beam	1.60	2.60	3.60	4.60	9.7	10.4	10.3	9.7
Total Positive Moment	4.03	6.23	8.58	12.94	24.5	24.8	24.5	27.3
Total Moment	16.46	25.08	35.00	47.45	100.0	100.0	100.0	100.0
Moment Coefficient, WL	0.105	0.103	0.107	0.110				

TABLE 8.14

MOMENTS AT DESIGN SECTIONS, CORNER PANEL J, DESIGN LOAD

	Measured Moment (kip-in.)				Percentage of Total Moment			
Load, psf	104	161	218	286	104	161	218	286
Exterior Negative Moment								
Column Strip	1.68	2.60	3.60	4.47	9.0	8.3	8.4	8.2
Middle Strip	1.13	1.74	2.41	3.18	6.0	5.5	5.6	5.8
Wall Strip	0.39	0.53	0.71	0.95	2.1	1.7	1.7	1.7
Beam	1.80	2.90	3.90	4.90	9.6	9.2	9.1	9.0
Interior Negative Moment								
Column Strip	5.30	8.09	10.59	11.50	28.4	25.7	24.7	21.1
Middle Strip	2.05	3.13	4.37	5.82	11.0	10.0	10.2	10.7
Wall Strip	1.02	1.63	2.19	4.20	5.5	5.2	5.1	7.7
Beam	6.65	10.30	13.95	18.30	35.6	32.8	32.5	33.5
Total Ext. Neg. Moment	5.00	7.77	10.62	13.50	26.8	24.7	24.8	24.7
Total Int. Neg. Moment	15.02	23.15	31.10	39.82	80.4	73.7	72.5	72.9
Average Negative Moment	10.01	15.46	20.86	26.66	53.6	49.2	48.6	48.7
Positive Moment								
Column Strip	1.07	1.73	2.37	4.86	5.7	5.5	5.5	8.9
Middle Strip	1.82	2.82	3.81	5.30	9.7	9.0	8.9	9.7
Wall Strip	0.28	0.42	0.64	0.85	1.5	1.3	1.5	1.6
Beam	5.50	11.00	15.20	17.00	29.4	35.0	35.4	31.1
Total Positive Moment	8.67	15.97	22.02	28.01	46.4	50.8	51.4	51.3
Total Moment	18.68	31.43	42.88	54.67	100.0	100.0	100.0	100.0
Moment Coefficient, WL	0.120	0.130	0.131	0.127				

TABLE 8.15

SUMMARY OF STATIC MOMENT COEFFICIENTS

Panel		A	B	C	D	E	F	G	H	J
M_{meas} @	104 psf	0.096	0.090	0.093	0.095	0.083	0.105	0.093	0.073	0.120
	161	0.101	0.090	0.091	0.096	0.084	0.103	0.098	0.075	0.130
	218	0.103	0.087	0.099	0.095	0.086	0.107	0.099	0.077	0.131
	286	0.107	0.091	0.105	0.098	0.087	0.110	0.102	0.081	0.127
M_s		0.098	0.093	0.098	0.096	0.088	0.096	0.106	0.100	0.106
M'_s		0.101	0.090	0.101	0.097	0.088	0.097	0.107	0.090	0.101
M_{des}		0.102	0.070	0.111	0.096	0.065	0.106	0.103	0.069	0.112

M_s: Uniform distribution of reaction along all supported edges.

M'_s: Uniform distribution of reaction along edges of capitals and/or columns.

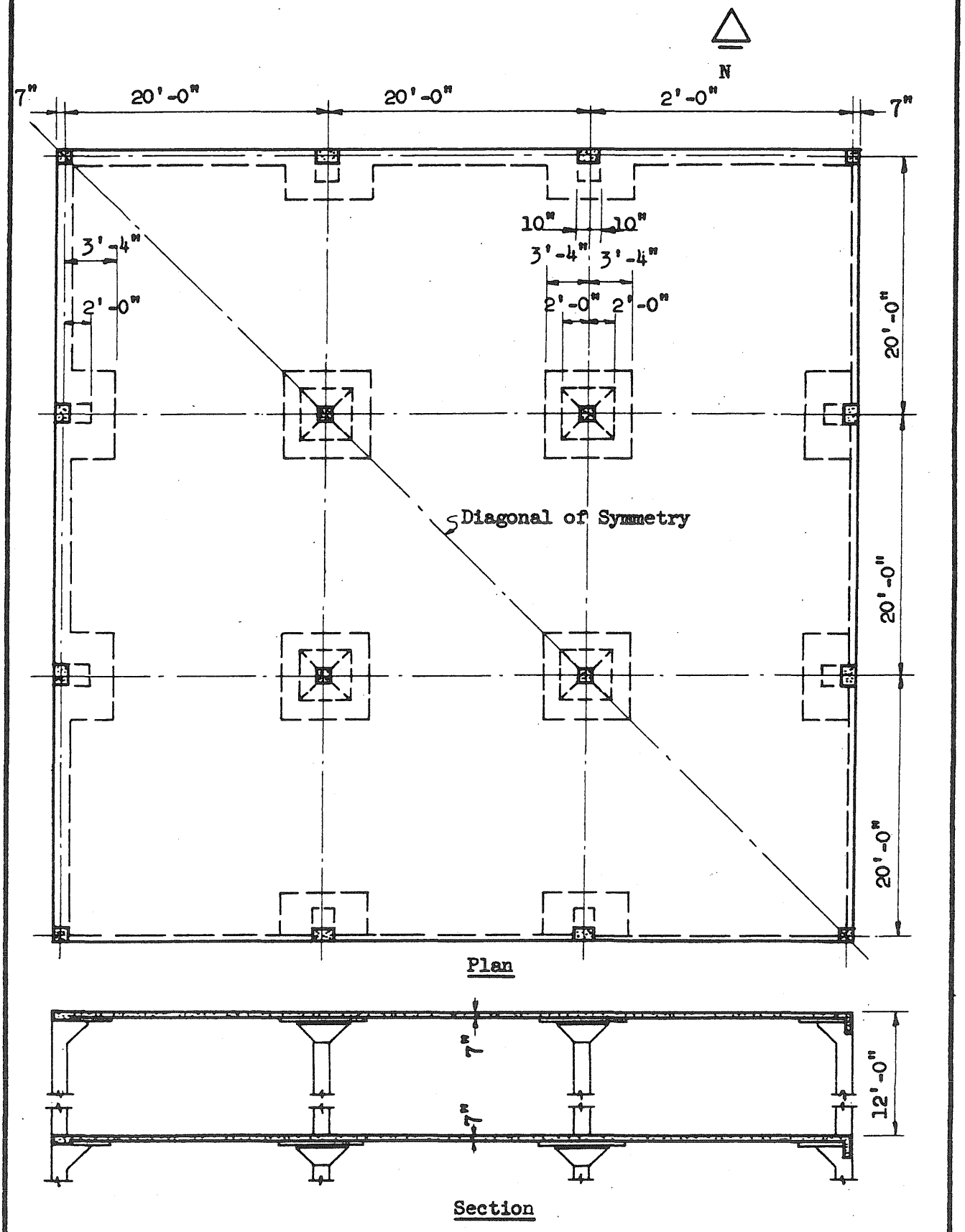

FIG. 2.1 LAYOUT OF PROTOTYPE STRUCTURE

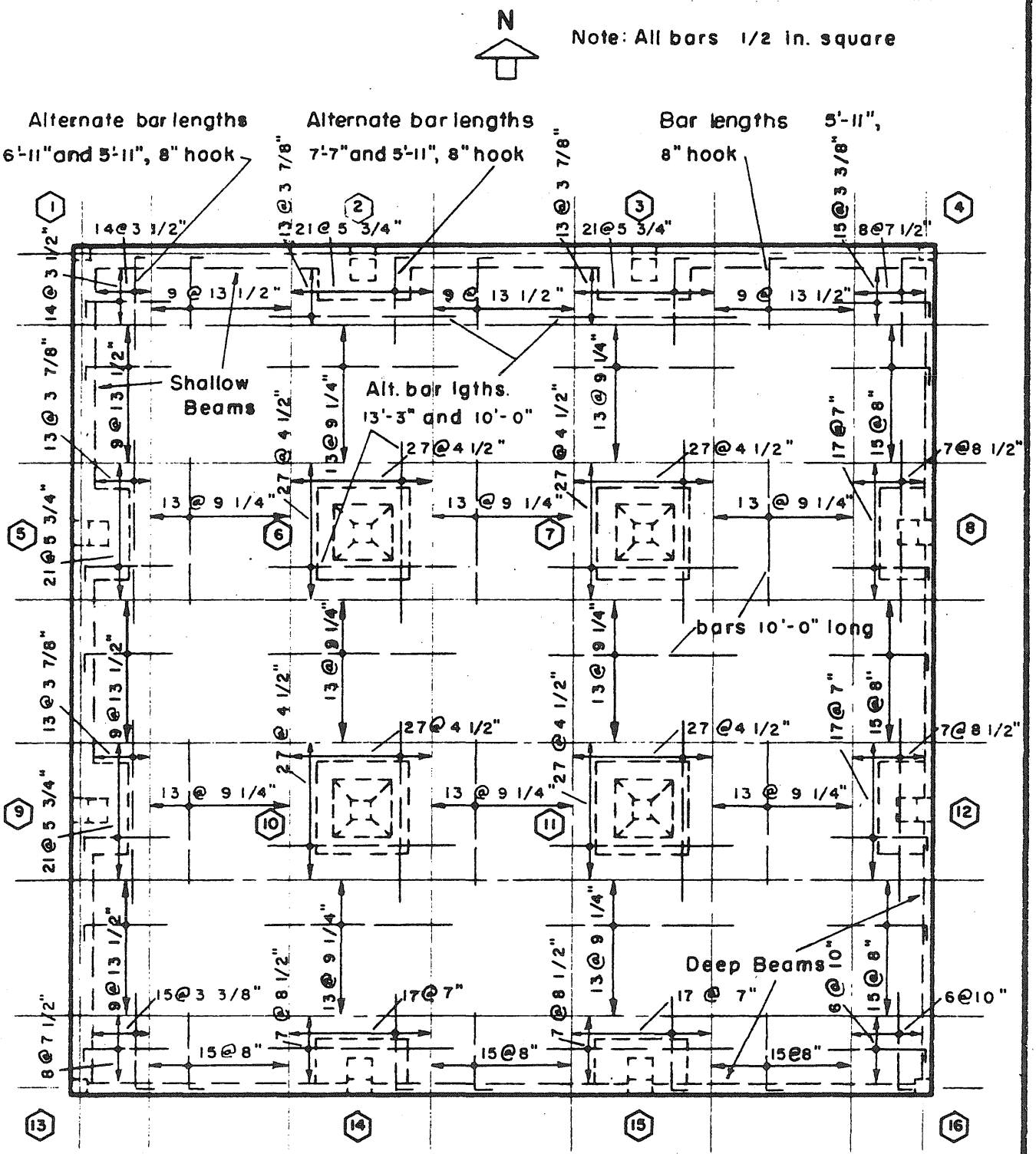

FIG. 2.2 PROTOTYPE STRUCTURE TOP STEEL

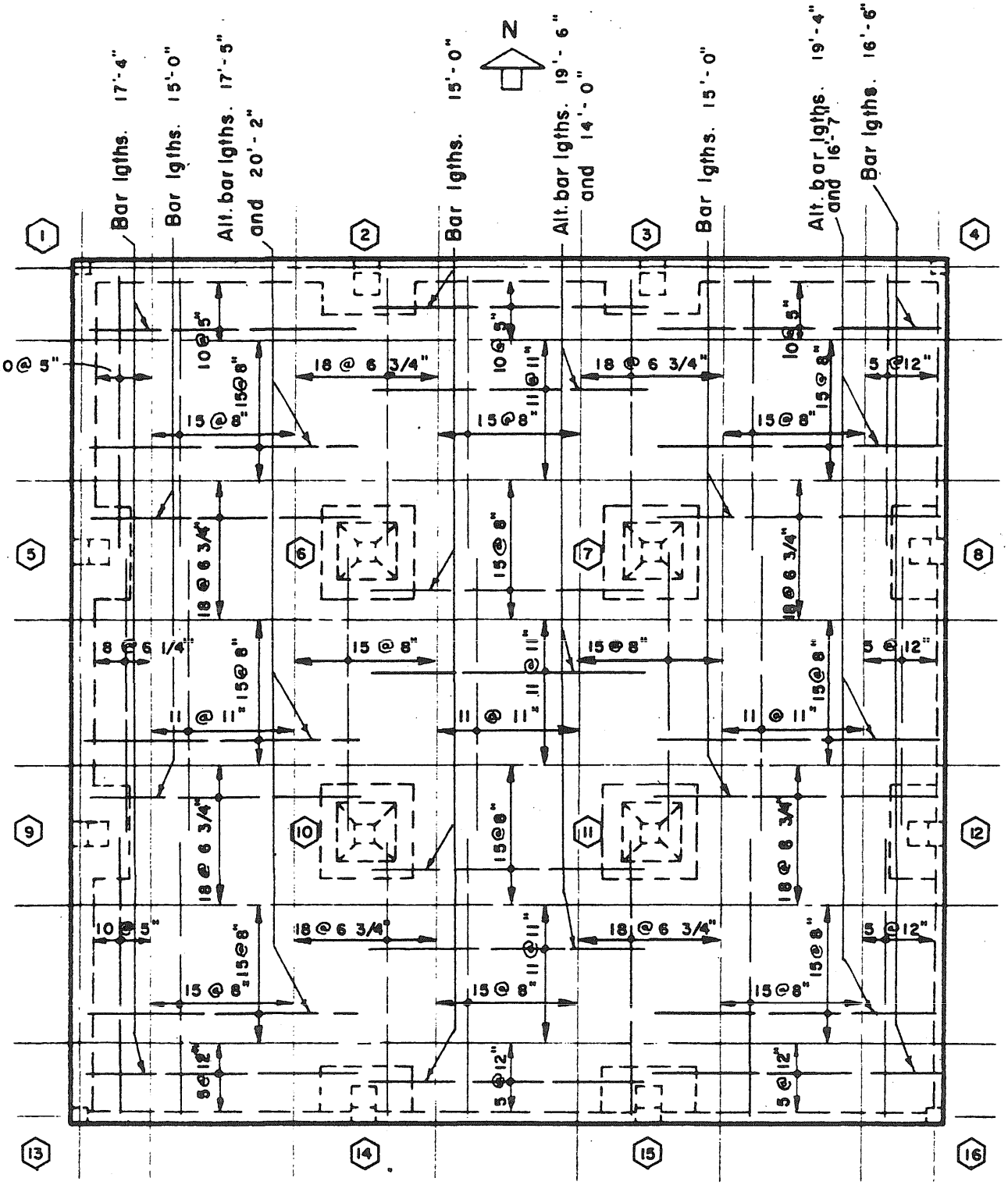

Note: All bars 1/2 in. square

FIG. 2.3 PROTOTYPE STRUCTURE BOTTOM STEEL

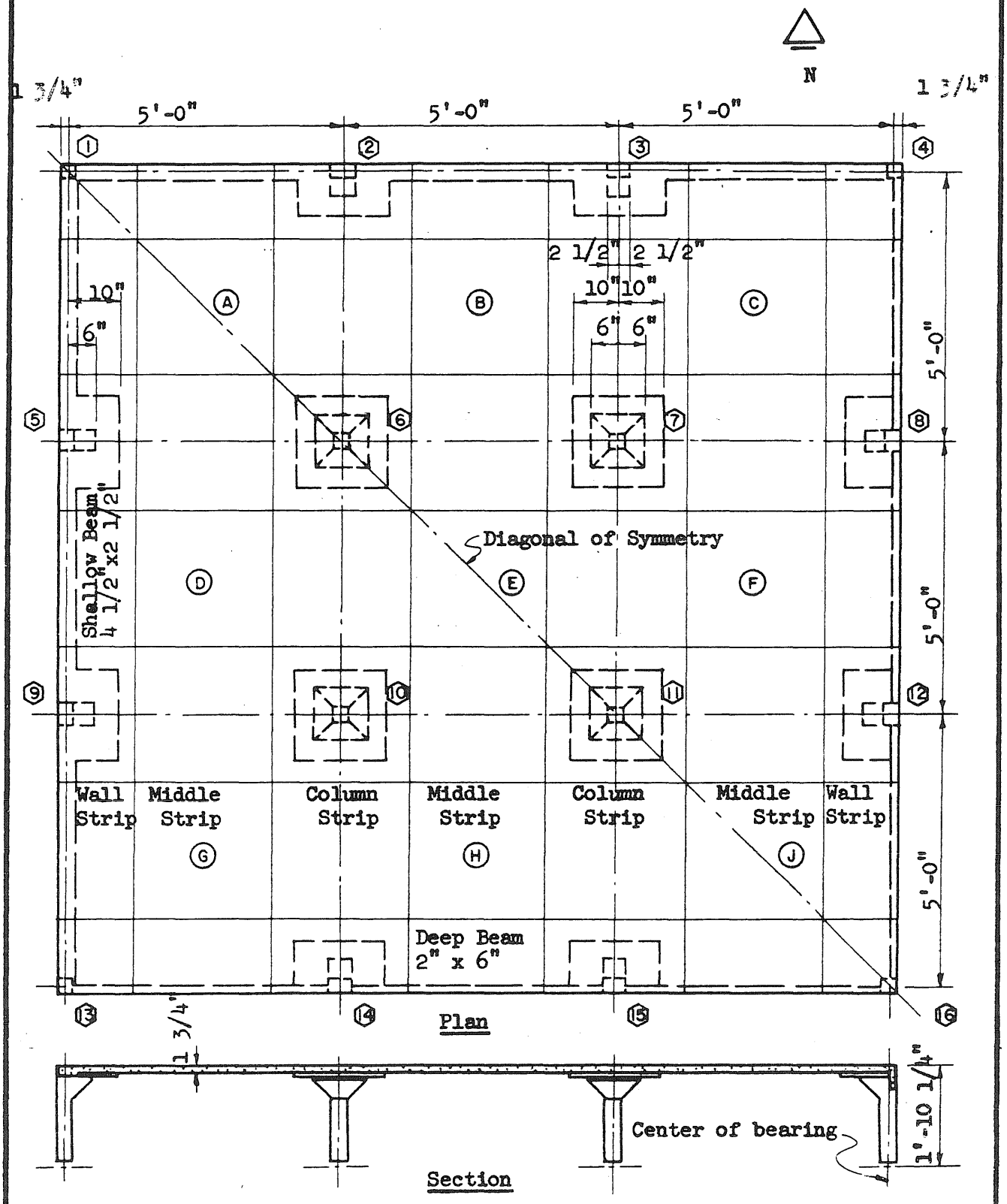

FIG. 2.4 LAYOUT OF TEST STRUCTURE

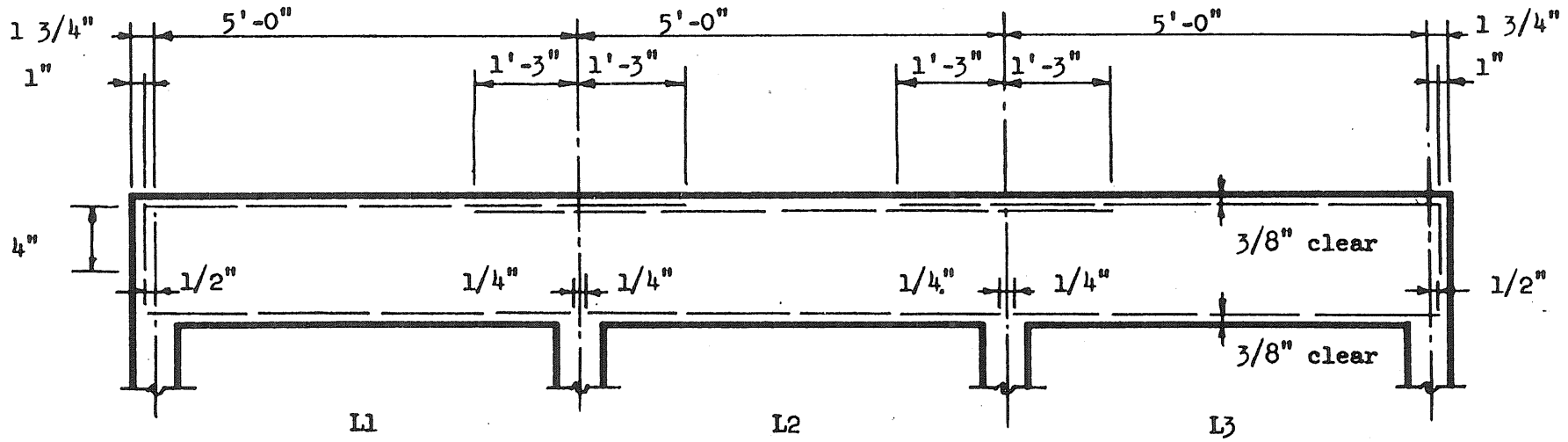

Shallow Beam

L1	L2	L3
5 - #2 x 6' - 7 1/2" top	2 - #2 x 7' - 6" top	5 - #2 x 6' - 7 1/2" top
5 - #2 x 5' - 0 1/4" bottom	2 - #2 x 9' - 11 1/2" bottom	5 - #2 x 5' - 0 1/4" bottom

Deep Beam

L1	L2	L3
3 - #2 x 6' - 7 1/2" top	1 - #2 x 7' - 6" top	3 - #2 x 6' - 7 1/2" top
3 - #2 x 5' - 0 1/4" bottom	3 - #2 x 4' - 11 1/2" bottom	3 - #2 x 5' - 0 1/4" bottom

Stirrups

	Beam	No. Stirrups	Size	Spacing Each End From Face of Support
Shallow	L1	28	1/8" Sq. Bars	10@ 1", 1@ 2", 3@ 4 3/4"
	L2	28	1/8" Sq. Bars	10@ 1", 1@ 2", 3@ 4 3/4"
Deep	L1	18	1/8" Sq. Bars	8@ 2 5/8", 1@ 4 1/2"
	L2	18	1/8" Sq. Bars	8@ 2 5/8", 1@ 4 1/2"

FIG. 2.5 ARRANGEMENT OF BEAM REINFORCEMENT

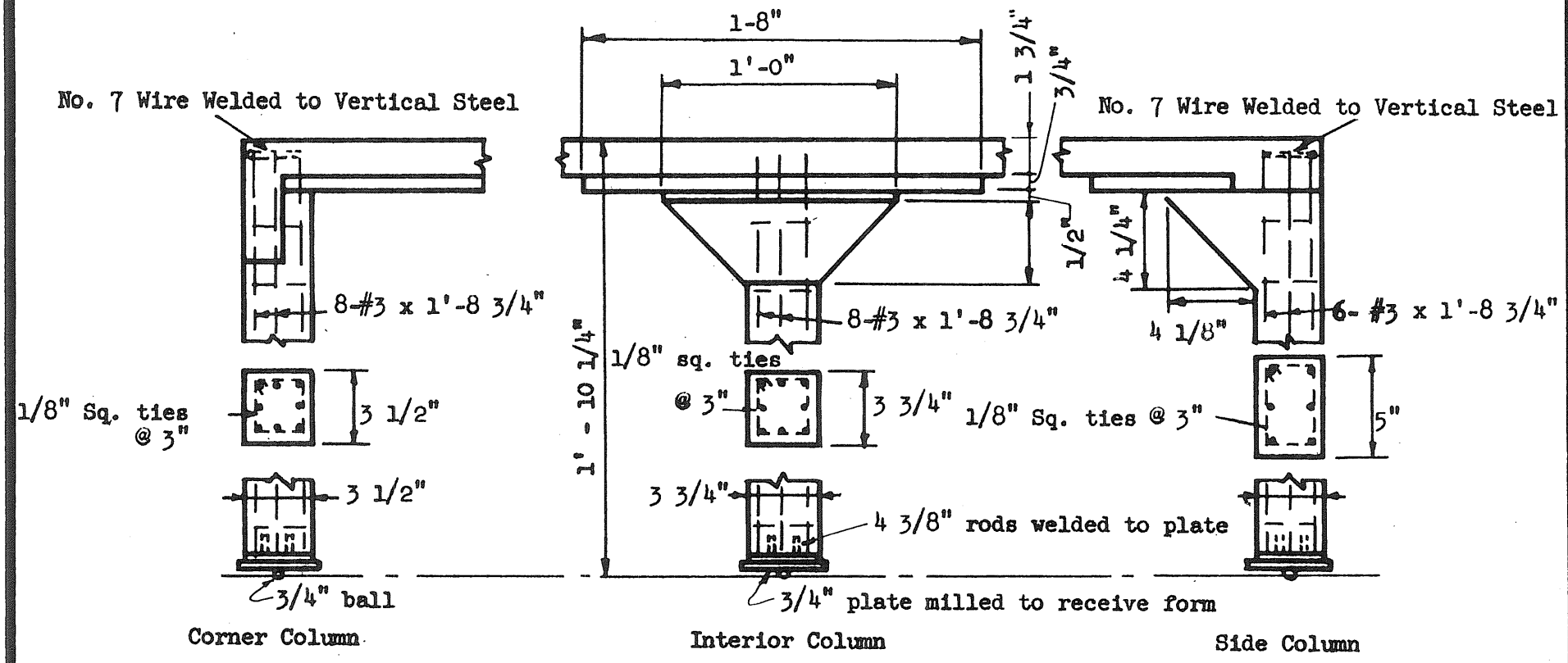

FIG. 2.6 ARRANGEMENT OF COLUMN REINFORCEMENT

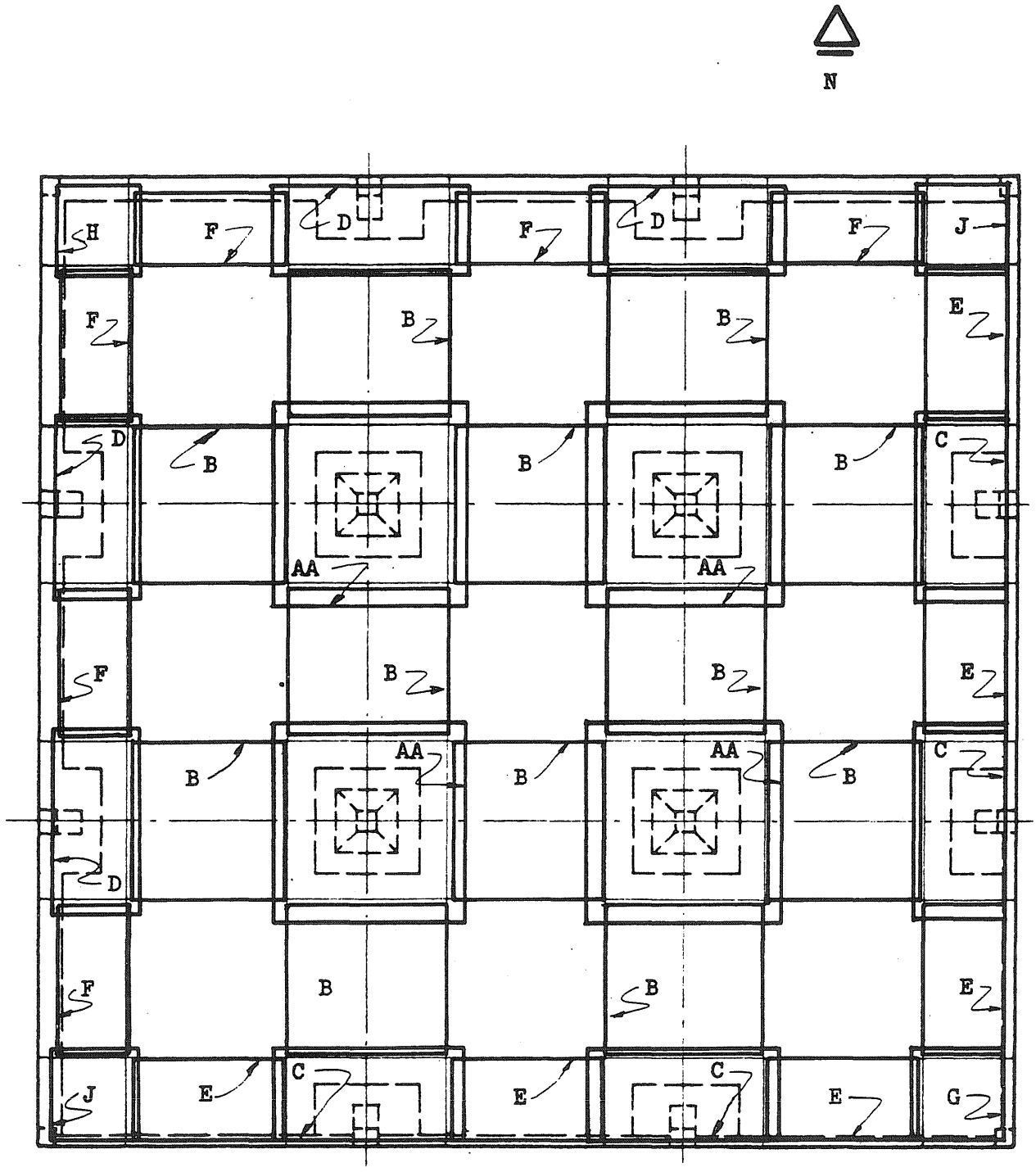

FIG. 2.7(a) ARRANGEMENT OF WELDED WIRE FABRIC TOP REINFORCEMENT

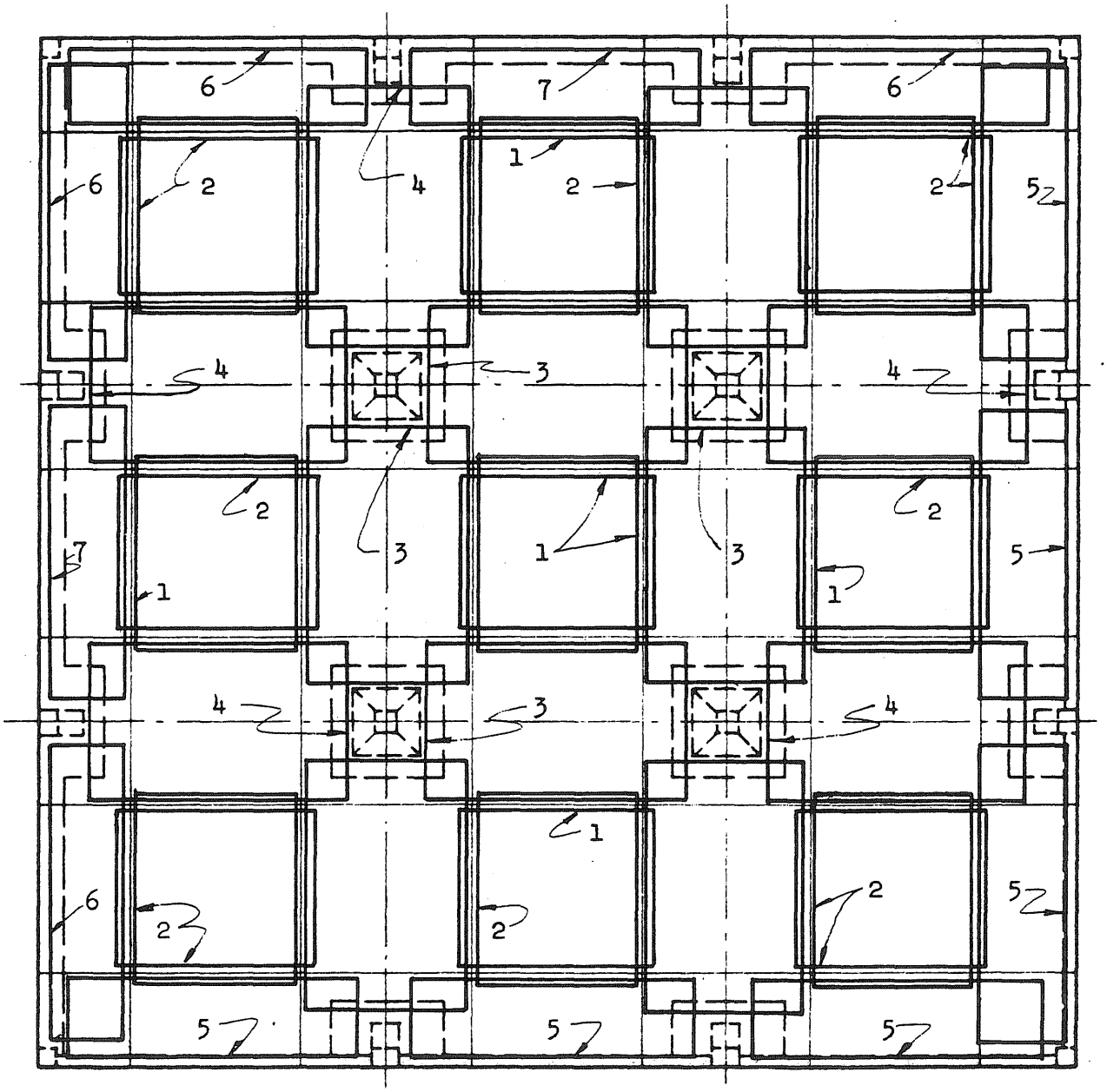

FIG. 2.7(b) ARRANGEMENT OF WELDED WIRE FABRIC BOTTOM REINFORCEMENT

BOTTOM REINFORCEMENT

Designation	Wire Spacing (in.)		Wire Size (Gage No.)	
	Main	Transverse	Main	Transverse
1	1	3	14	16
2	1	3	13	15
3	1	2	12.5	12.5
4	1	2	12	12.5
5	1	2	14	12.5
6	1	2	11.5	12.5
7	1	2	12	12.5

TOP REINFORCEMENT

Designation	Wire Spacing (in.)		Wire Size (Gage No.)	
	Main	Transverse	Main	Transverse
AA	1	1	10	10
B	1	3	13	16
C	1	1	12.5	12
D	1	3	11.5	10
E	1	3	12.5	16
F	1	1	14.5	16
G	1	1	13	13
H	1	1	10	10
J	1	1	9.5	12

SECTIONAL AREAS OF WELDED WIRE FABRIC

Gage No.	Diameter (in.)	Area (sq. in.)
9.5	0.142	0.0157
10	0.135	0.0143
11.5	0.115	0.0102
12	0.106	0.0087
12.5	0.099	0.0076
13	0.092	0.0066
14	0.080	0.0050
14.5	0.077	0.0046
15	0.072	0.0041
16	0.063	0.0031

FIG. 2.7(c) GUIDE TO DESIGNATION OF SLAB REINFORCEMENT

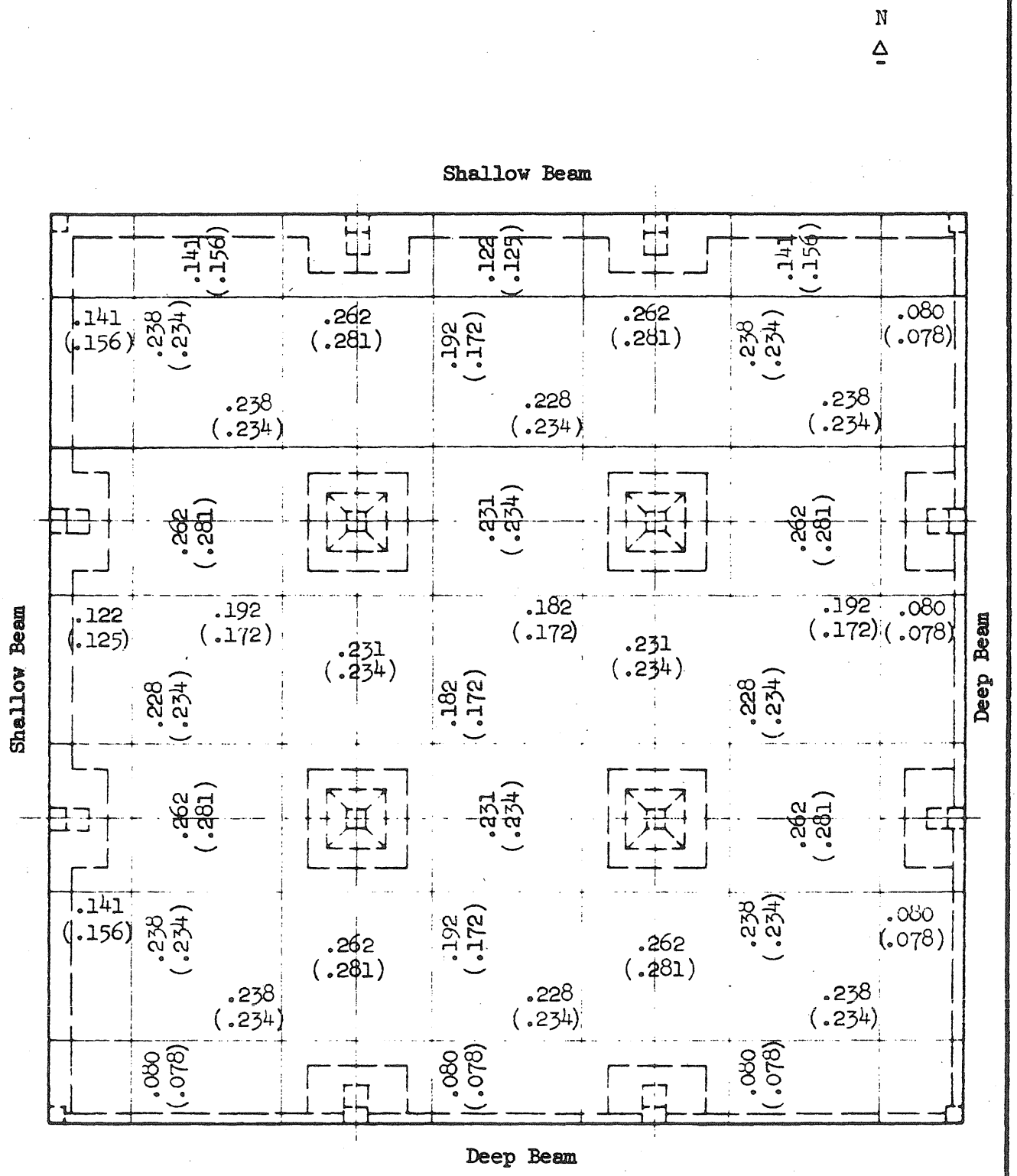

FIG.2.8 COMPARISON OF CROSS-SECTIONAL AREAS OF SLAB POSITIVE REINFORCEMENT PROVIDED IN TEST STRUCTURES NO. 2 AND NO. 5

Values in parentheses refer to Test Structure No. 2
All values are given in square inches.

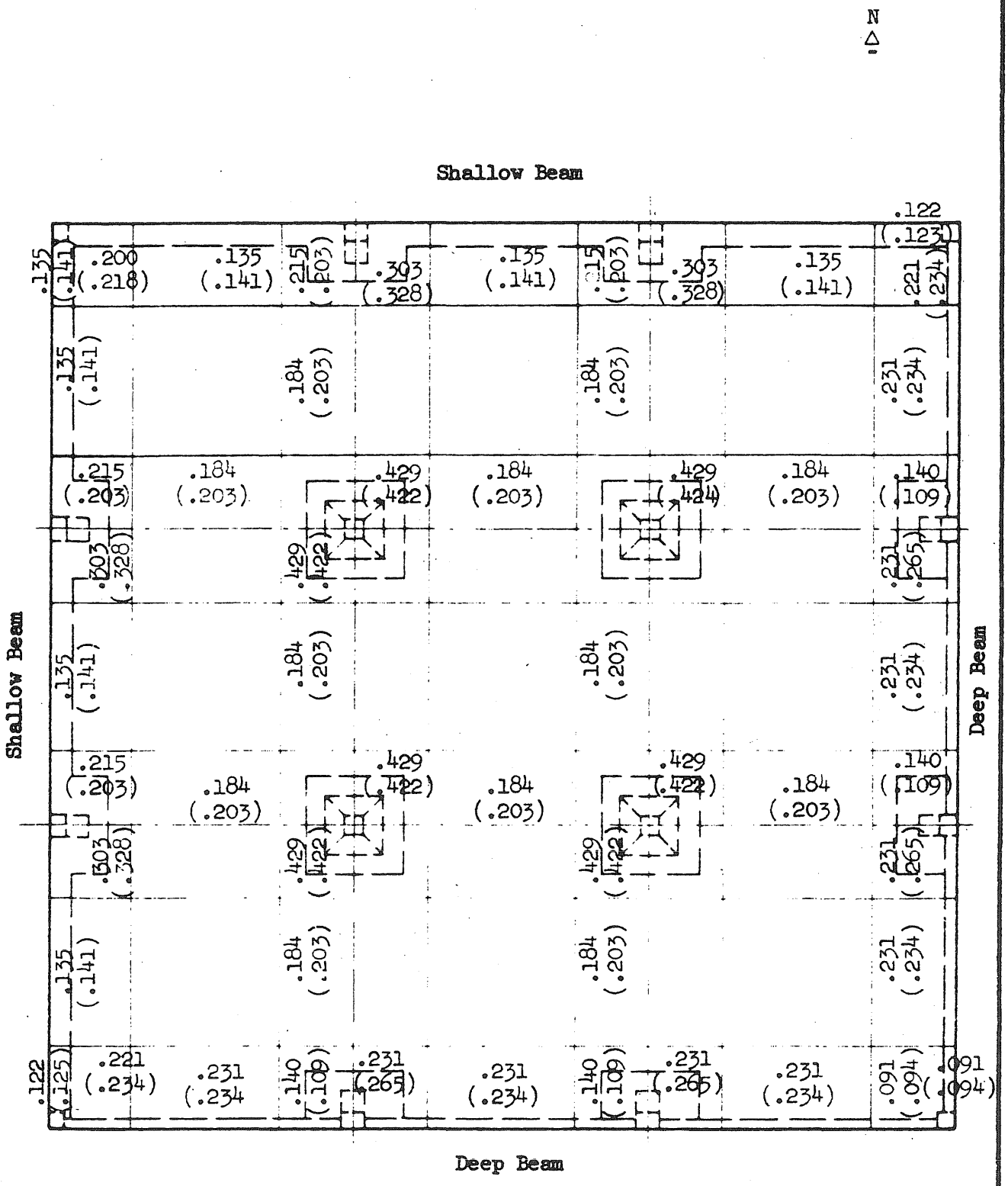

FIG.2.9 COMPARISON OF CROSS-SECTIONAL AREAS OF SLAB NEGATIVE REINFORCEMENT PROVIDED IN TEST STRUCTURES NO. 2 AND NO. 5

Values in parentheses refer to Test Structure No. 2
All values are given in square inches.

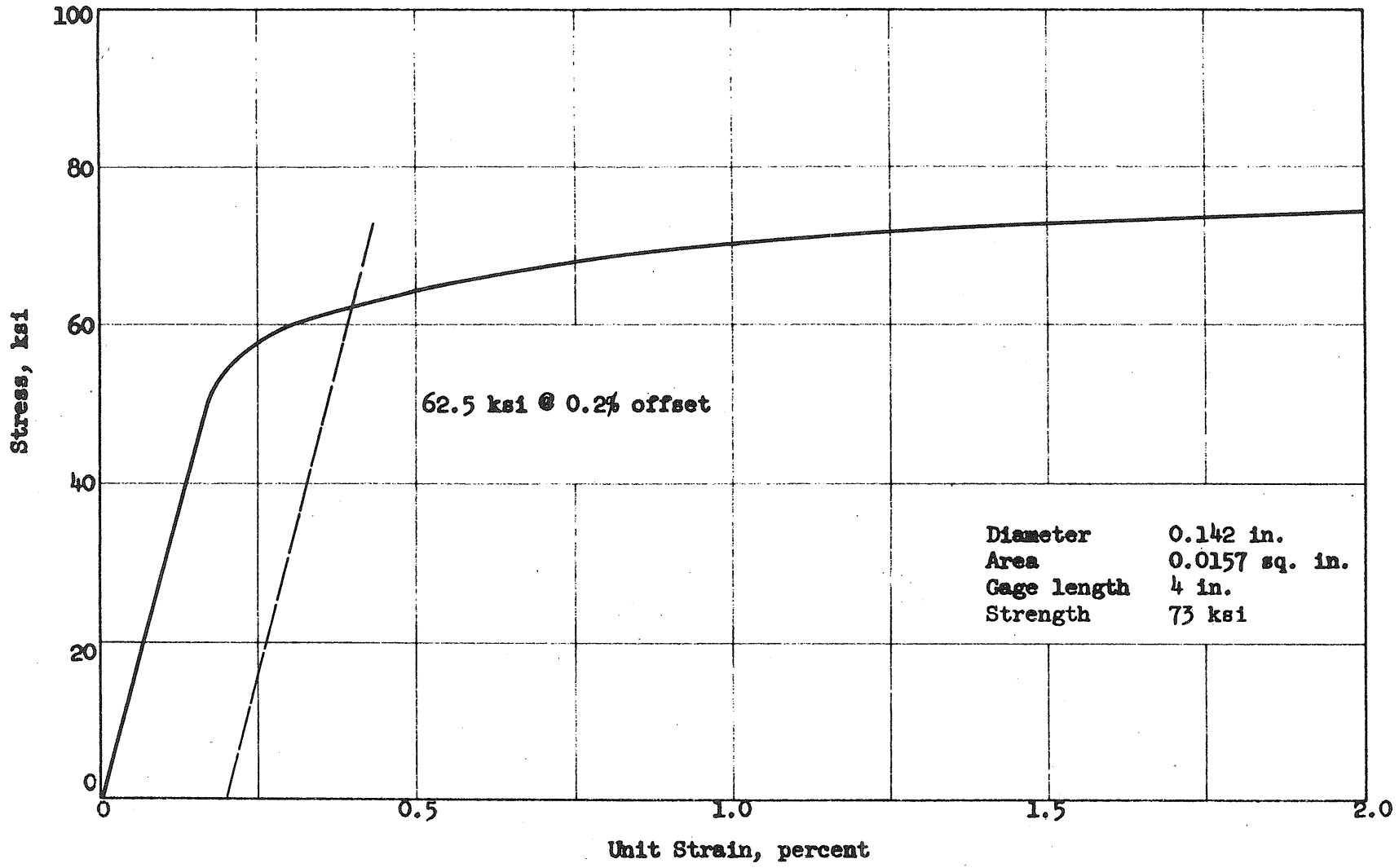

FIG. 3.1 TYPICAL STRESS-STRAIN RELATIONSHIP FOR #9 1/2 GAGE WELDED WIRE REINFORCEMENT

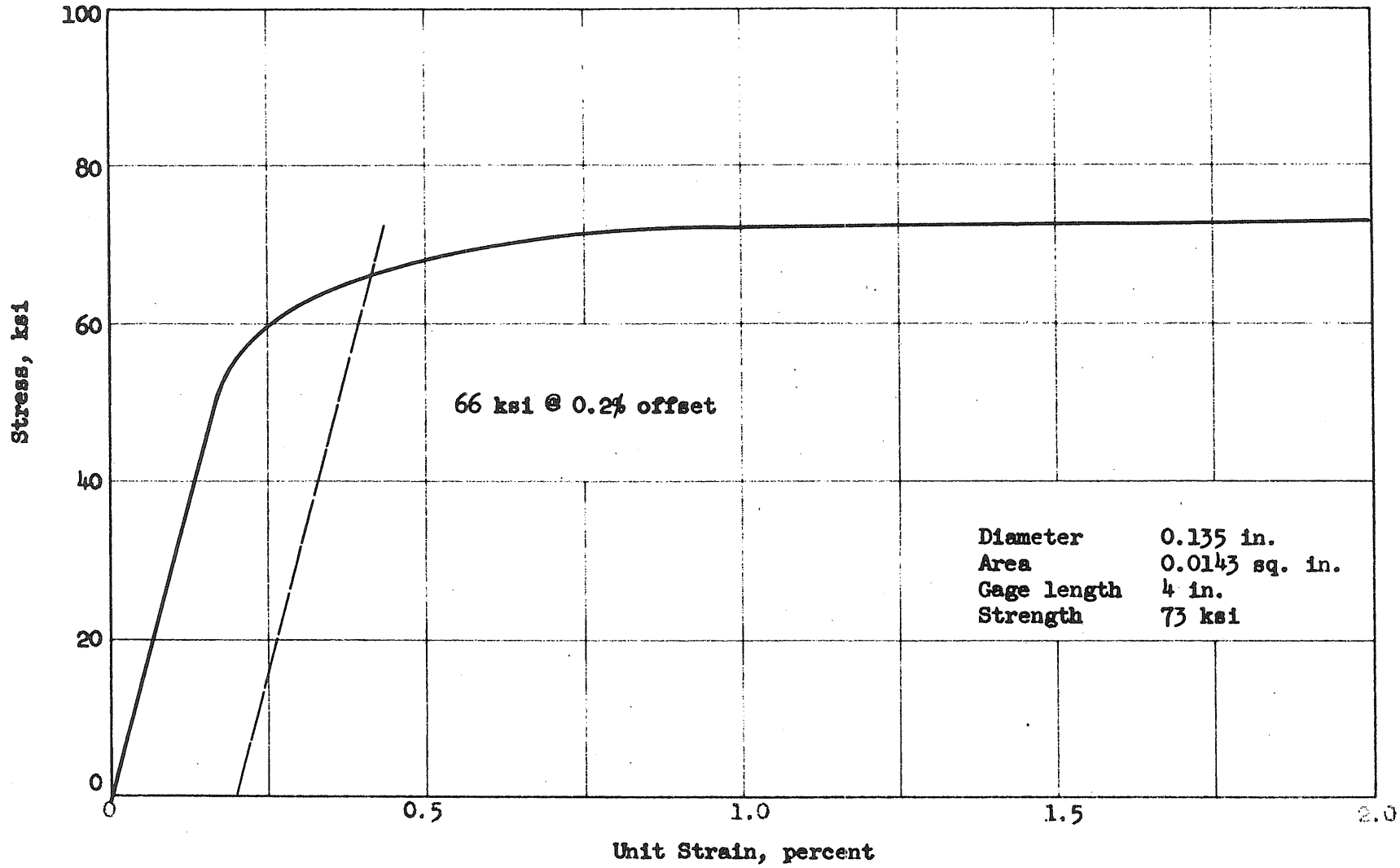

FIG. 3.2 TYPICAL STRESS-STRAIN RELATIONSHIP FOR #10 GAGE WELDED WIRE REINFORCEMENT

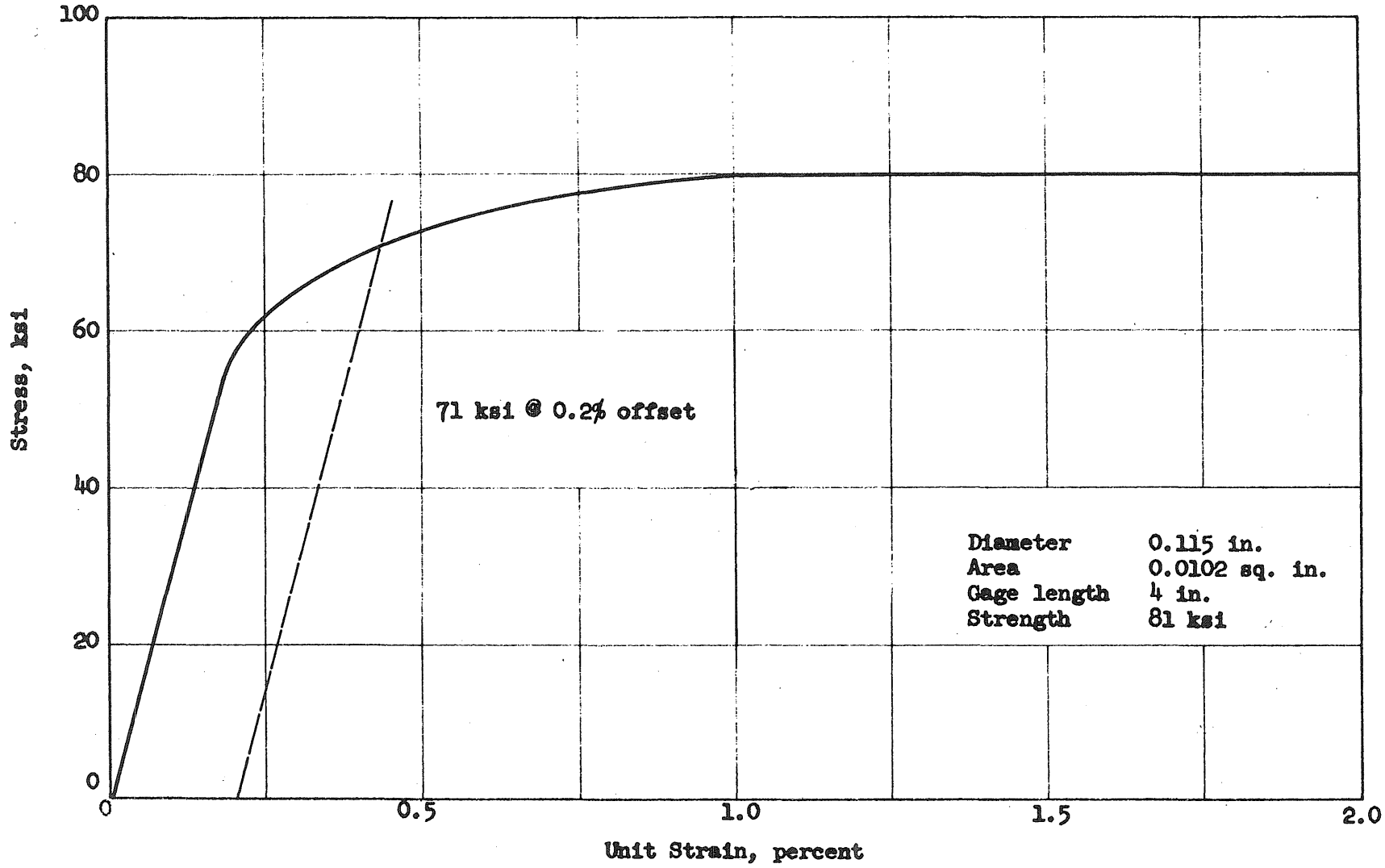

FIG. 3.3 TYPICAL STRESS-STRAIN RELATIONSHIP FOR #11 1/2 GAGE WELDED WIRE REINFORCEMENT

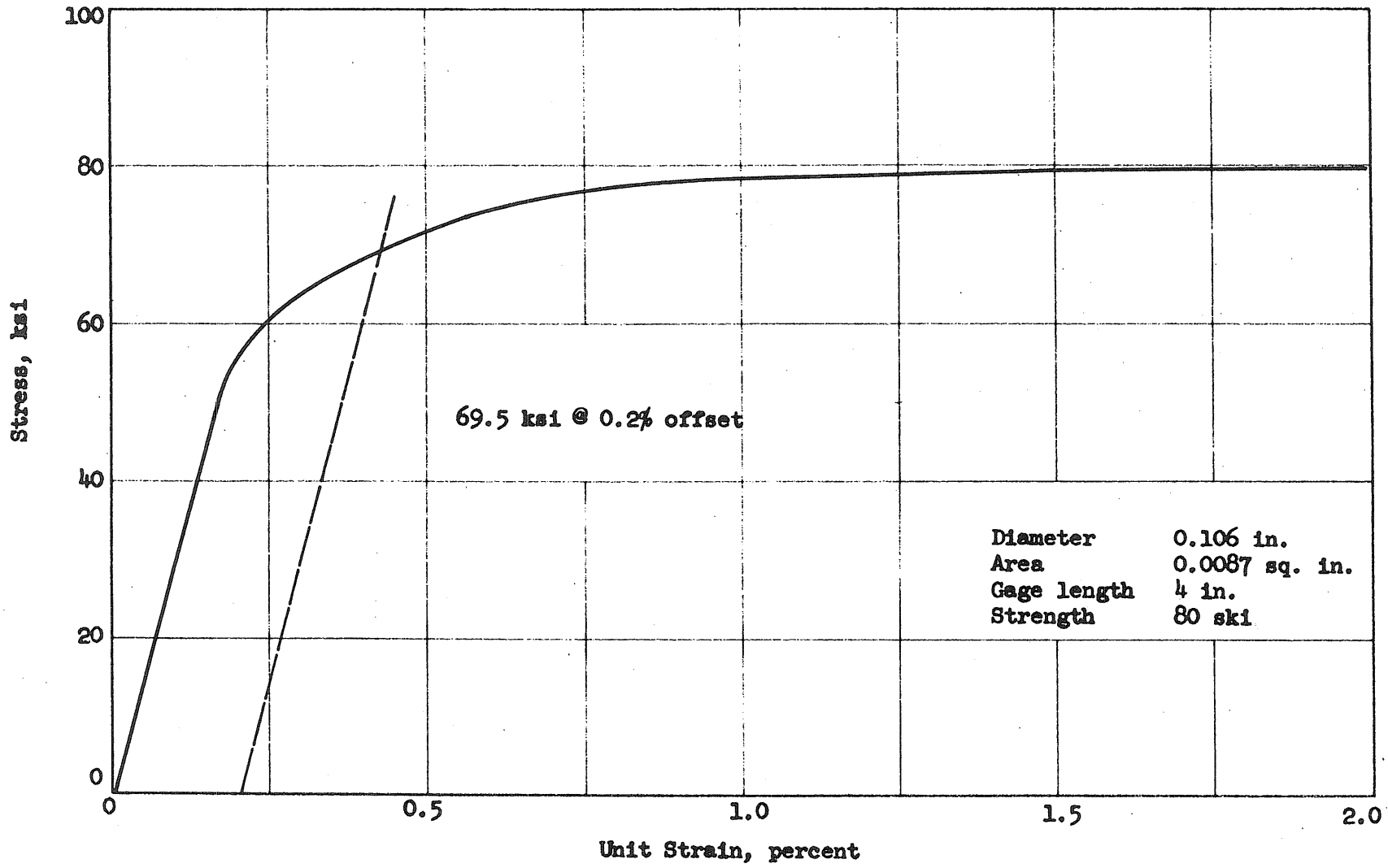

FIG. 3.4 TYPICAL STRESS-STRAIN RELATIONSHIP FOR #12 GAGE WELDED WIRE REINFORCEMENT

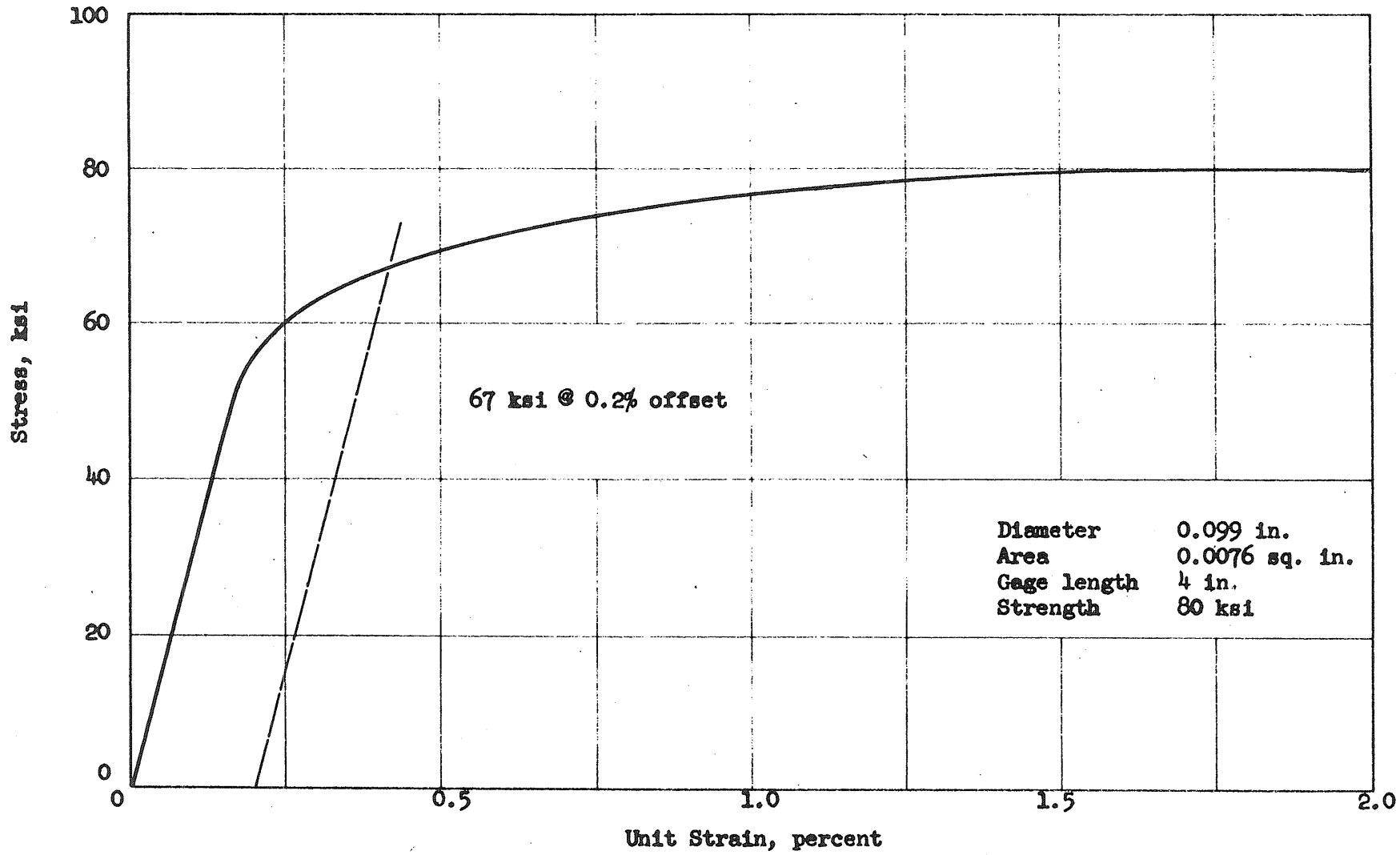

FIG. 3.5 TYPICAL STRESS-STRAIN RELATIONSHIP FOR #12 1/2 AND #14 GAGE WELDED WIRE REINFORCEMENT

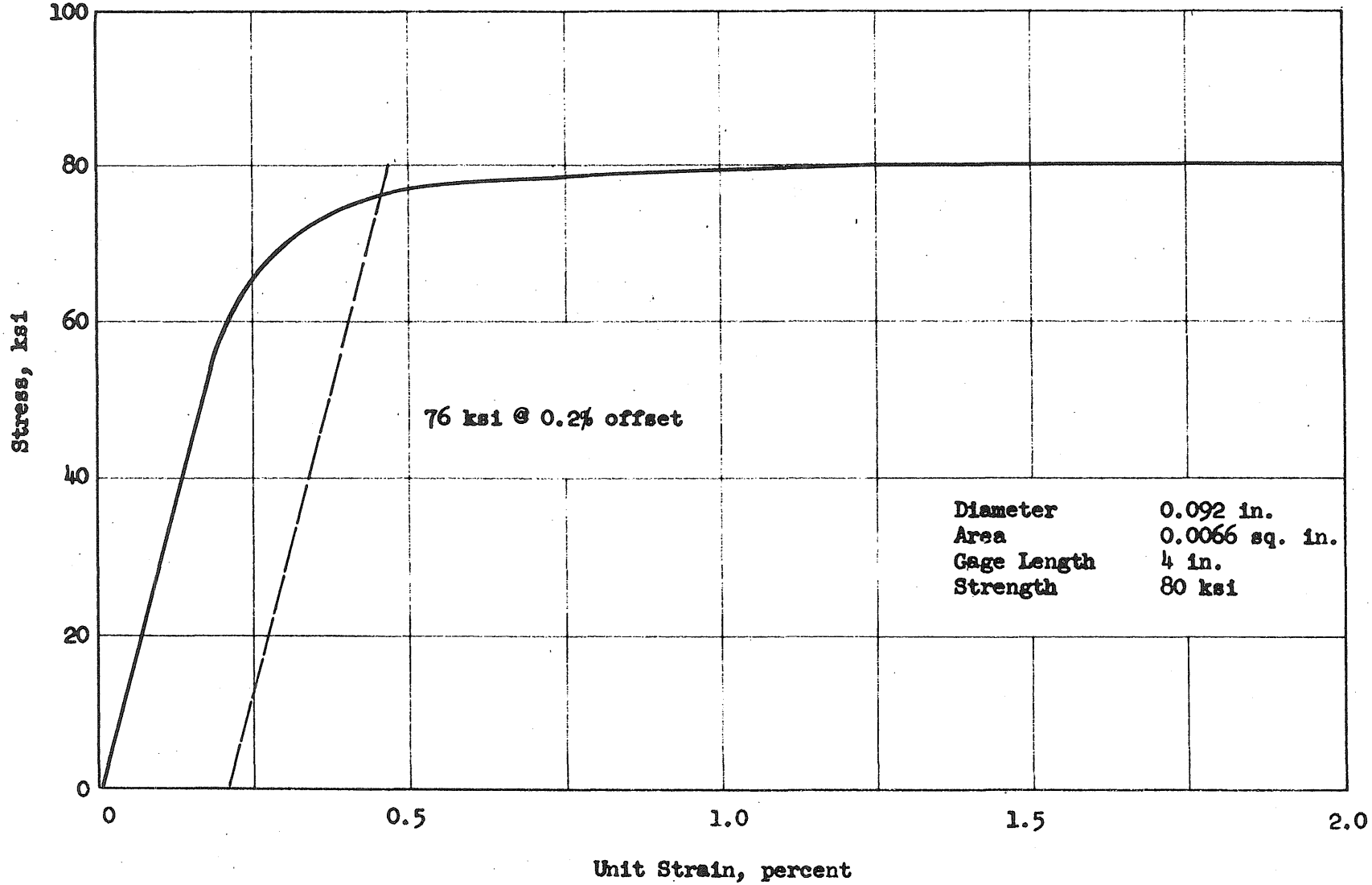

FIG. 3.6 TYPICAL STRESS-STRAIN RELATIONSHIP FOR #13 GAGE WELDED WIRE REINFORCEMENT

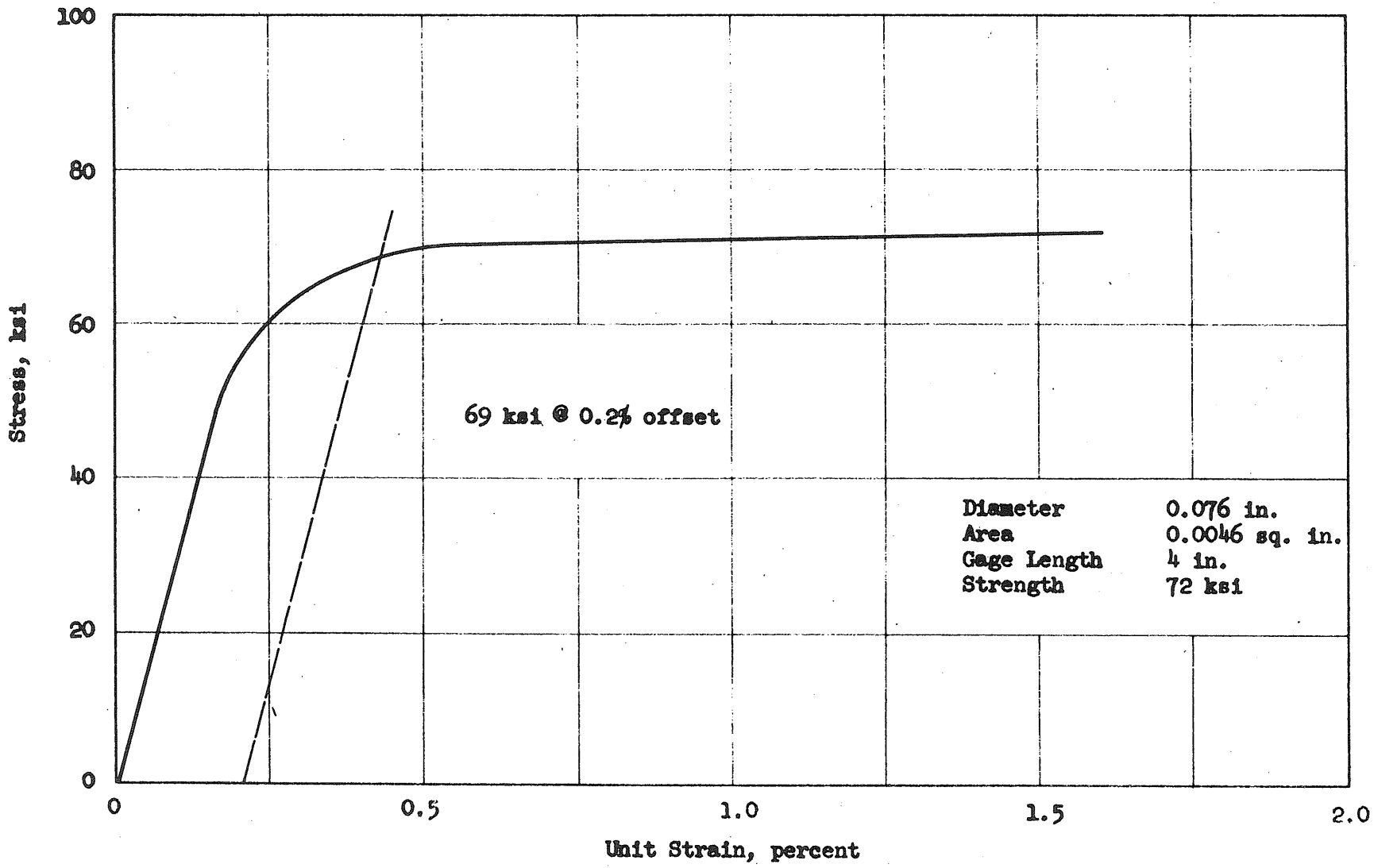

FIG. 3.7 TYPICAL STRESS-STRAIN RELATIONSHIP FOR #14 1/2 GAGE WELDED WIRE REINFORCEMENT

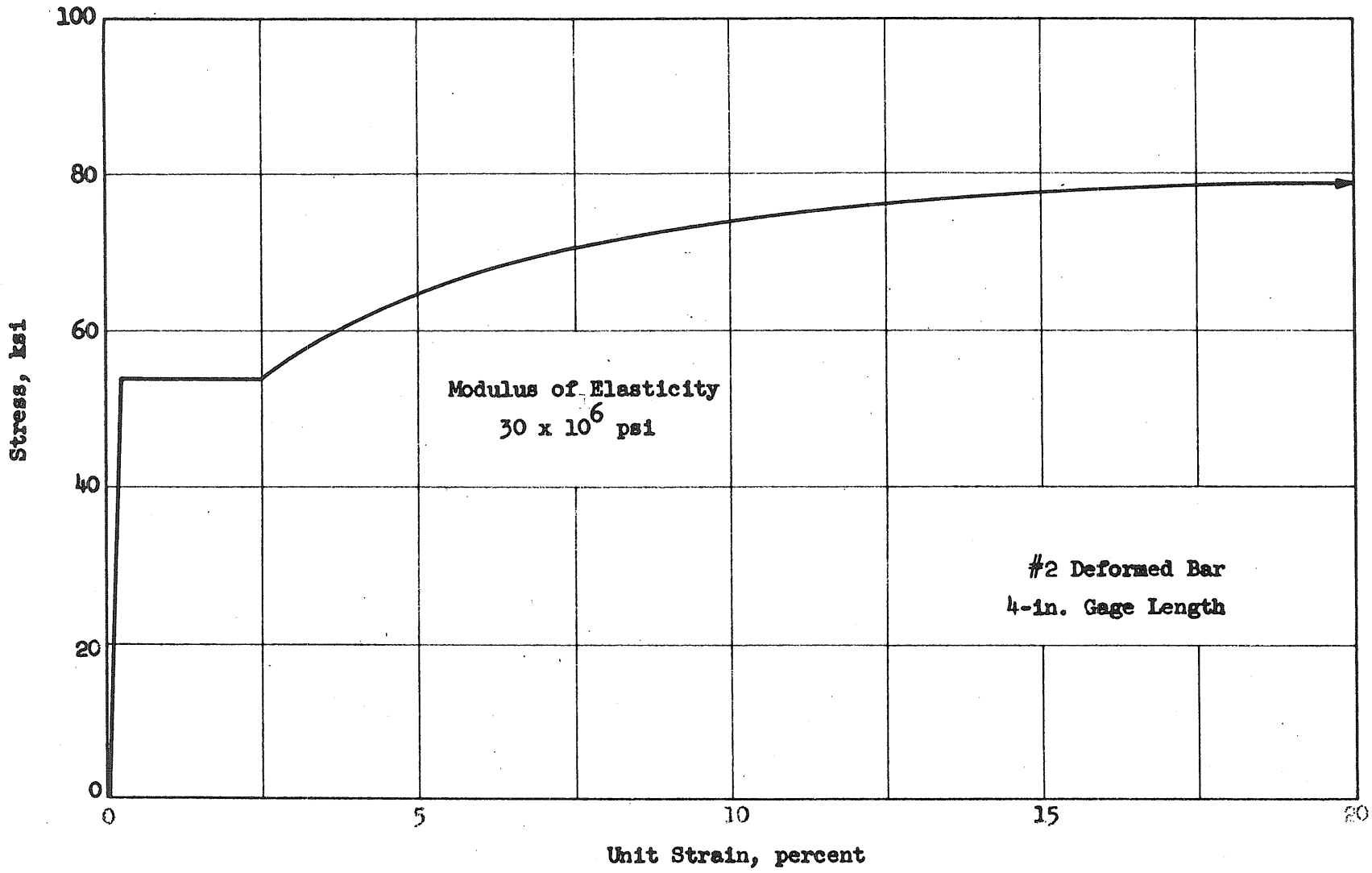

FIG. 3.8 TYPICAL STRESS-STRAIN RELATIONSHIP FOR BEAM STEEL

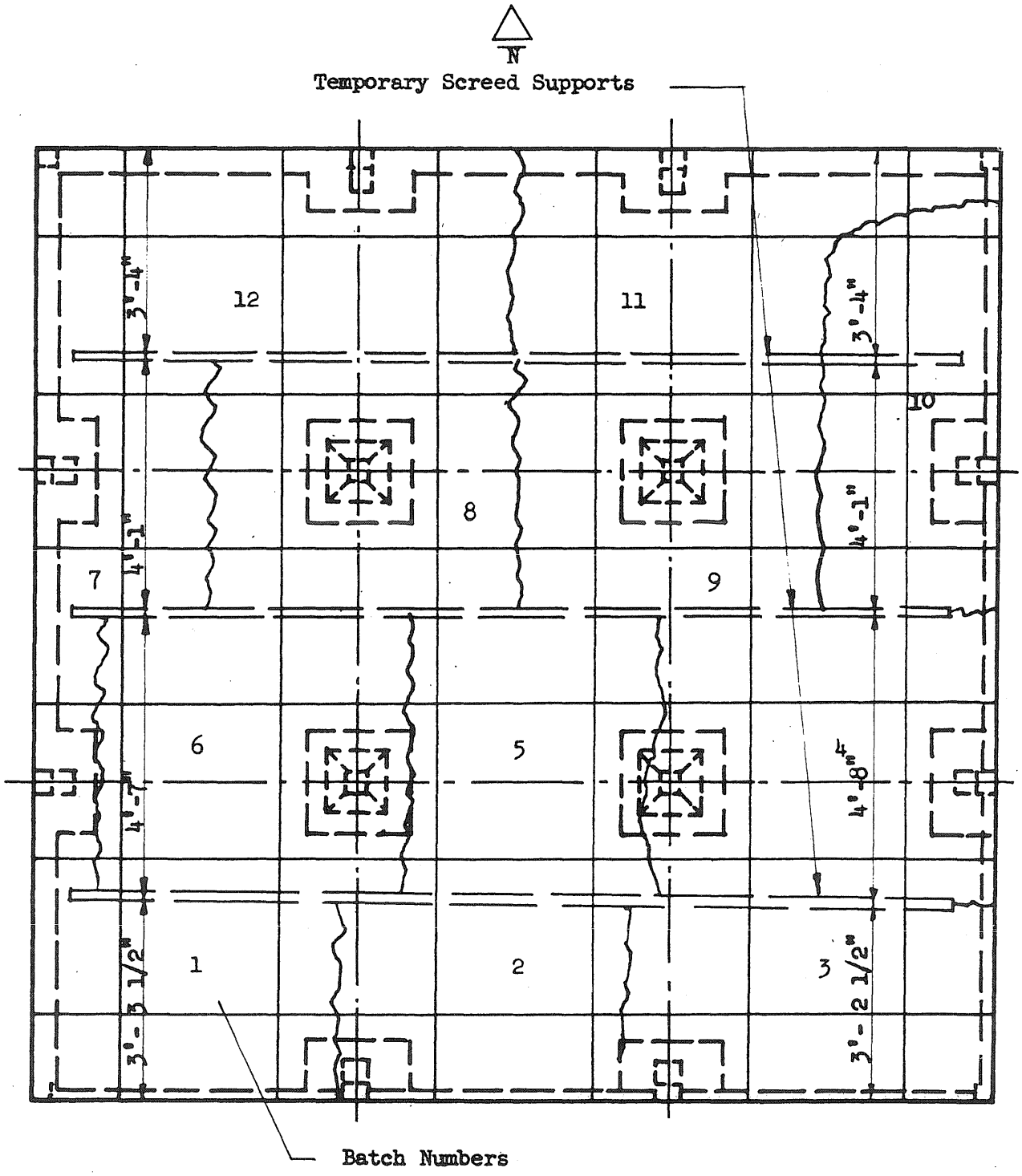

FIG. 3.9 LOCATION OF CONCRETE BATCHES

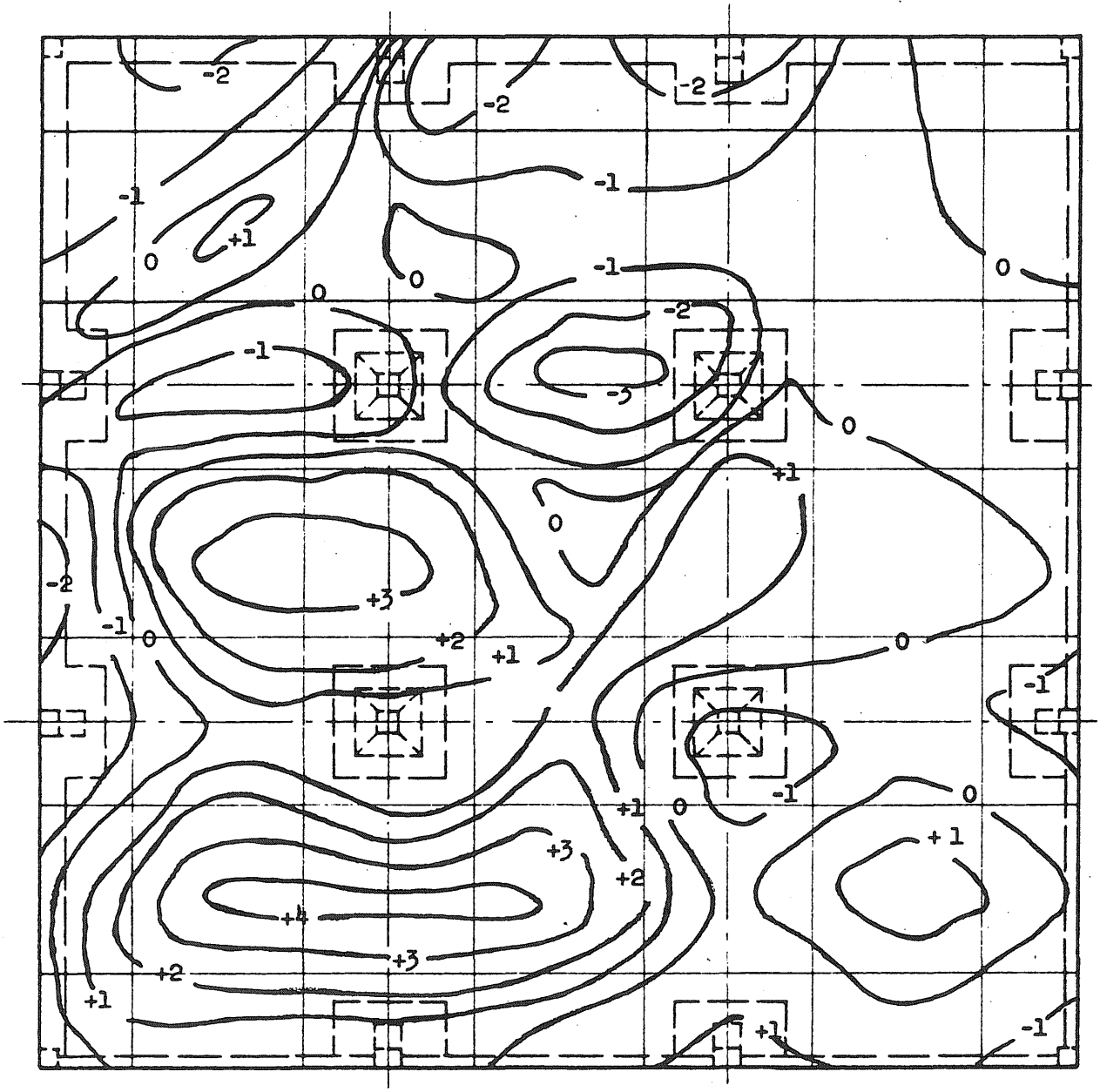

FIG. 3.10 DEVIATION OF SLAB THICKNESS

Note: Dimensions in 1/32-in. intervals.

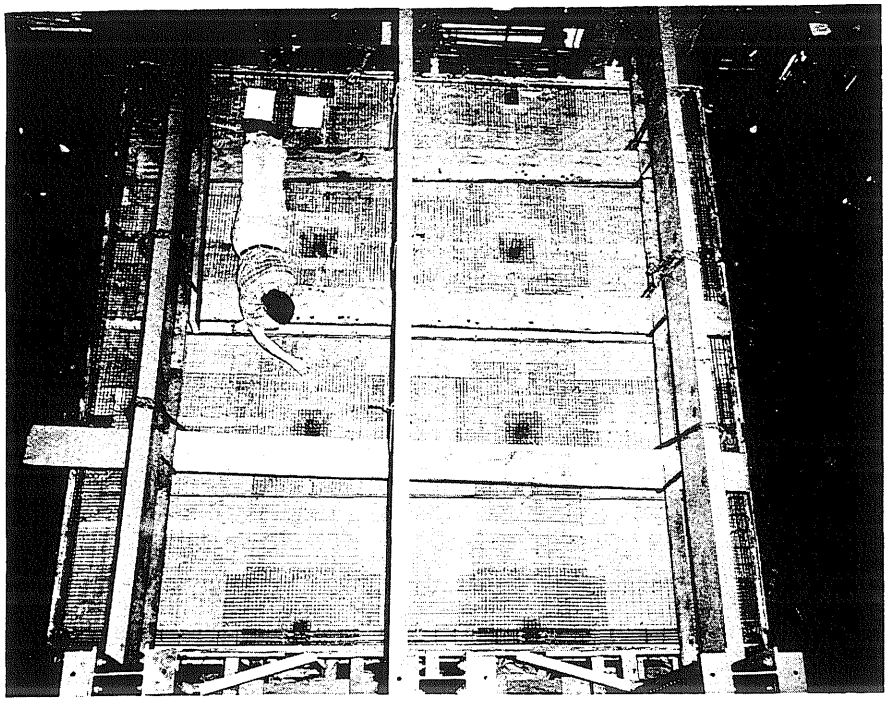

(a) Over-All View

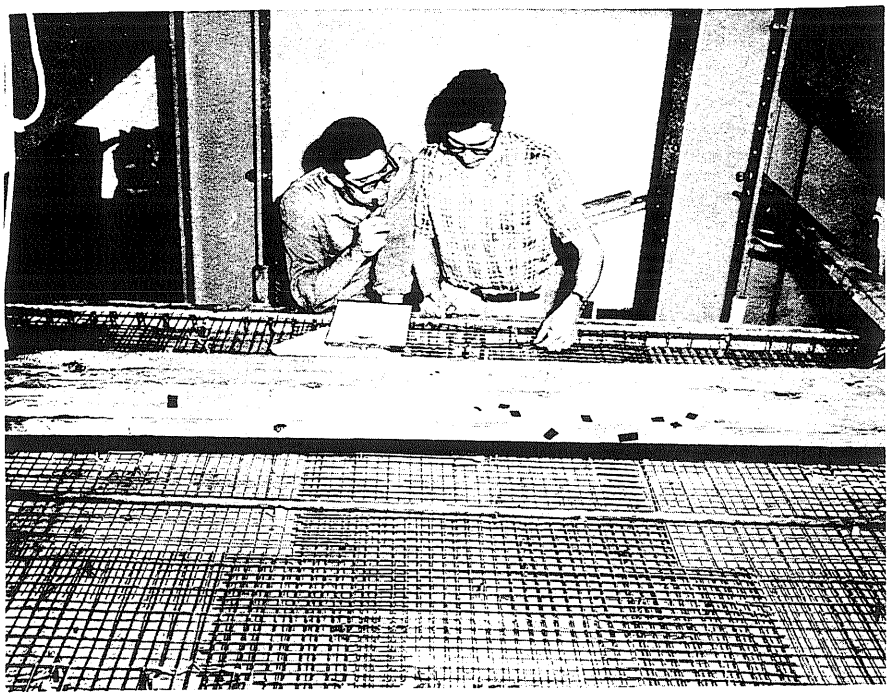

(b) Close-Up View Showing Wire Reinforcement

NOTE: Pipe seen in figure is a temporary screed support.

FIG. 3.11 PHOTOGRAPHS OF REINFORCEMENT IN PLACE

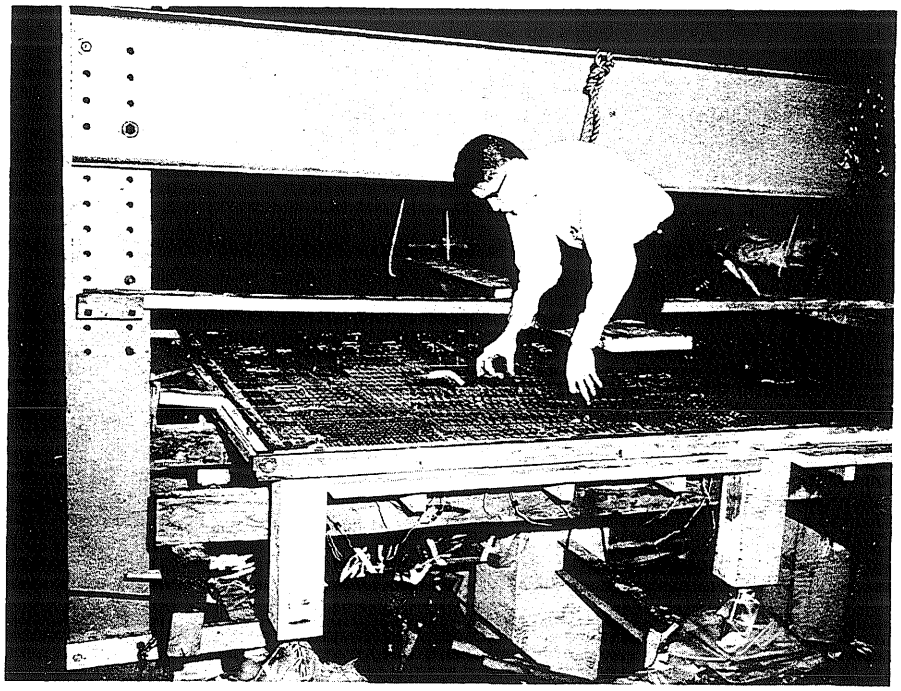

(a) Placement of Wire Reinforcement

(b) Casting Operation

FIG. 3.12 PHOTOGRAPHS OF REINFORCEMENT AND CONCRETE PLACEMENT

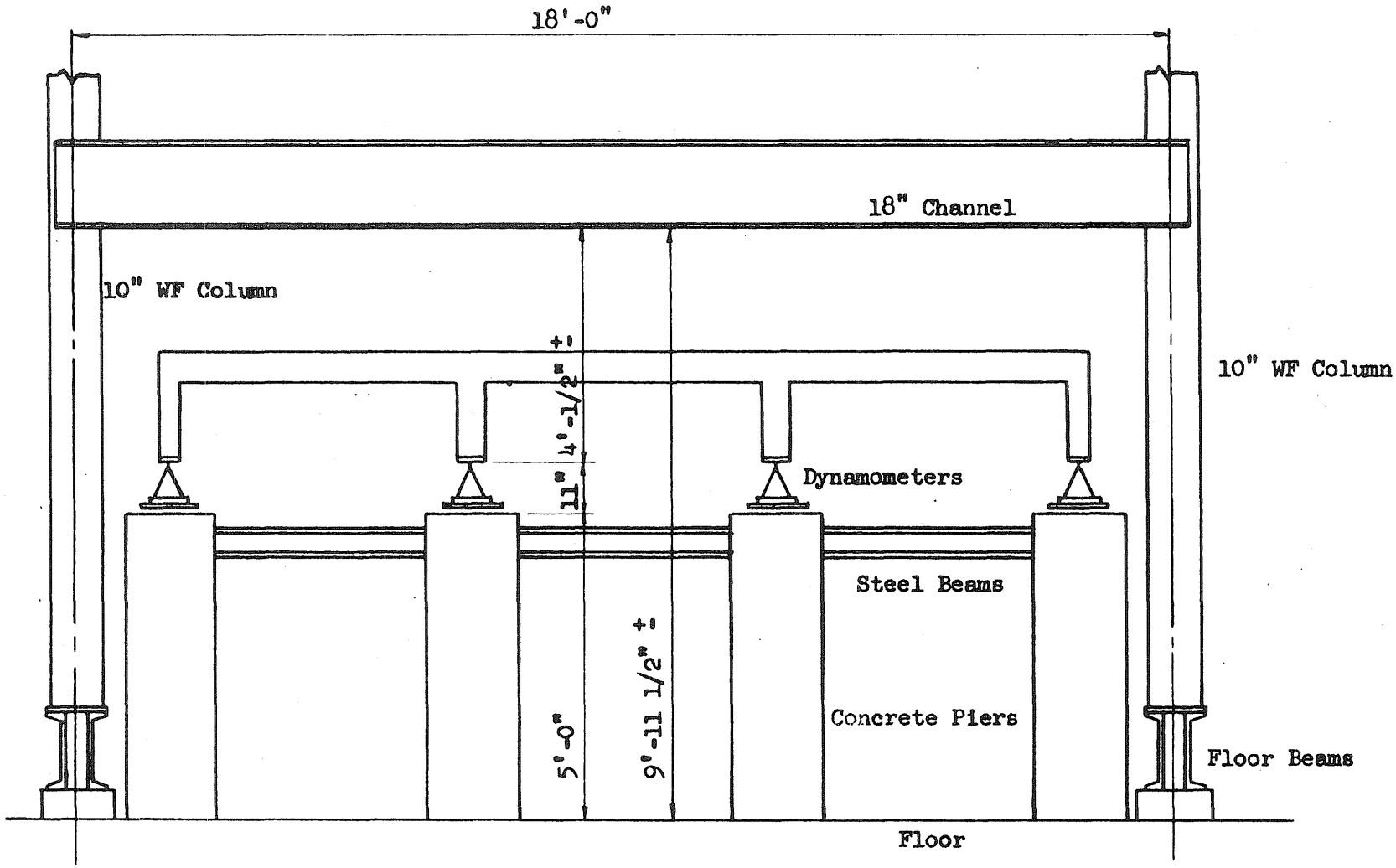

FIG. 4.1 ELEVATION OF REACTION FRAME AND LOADING FRAME

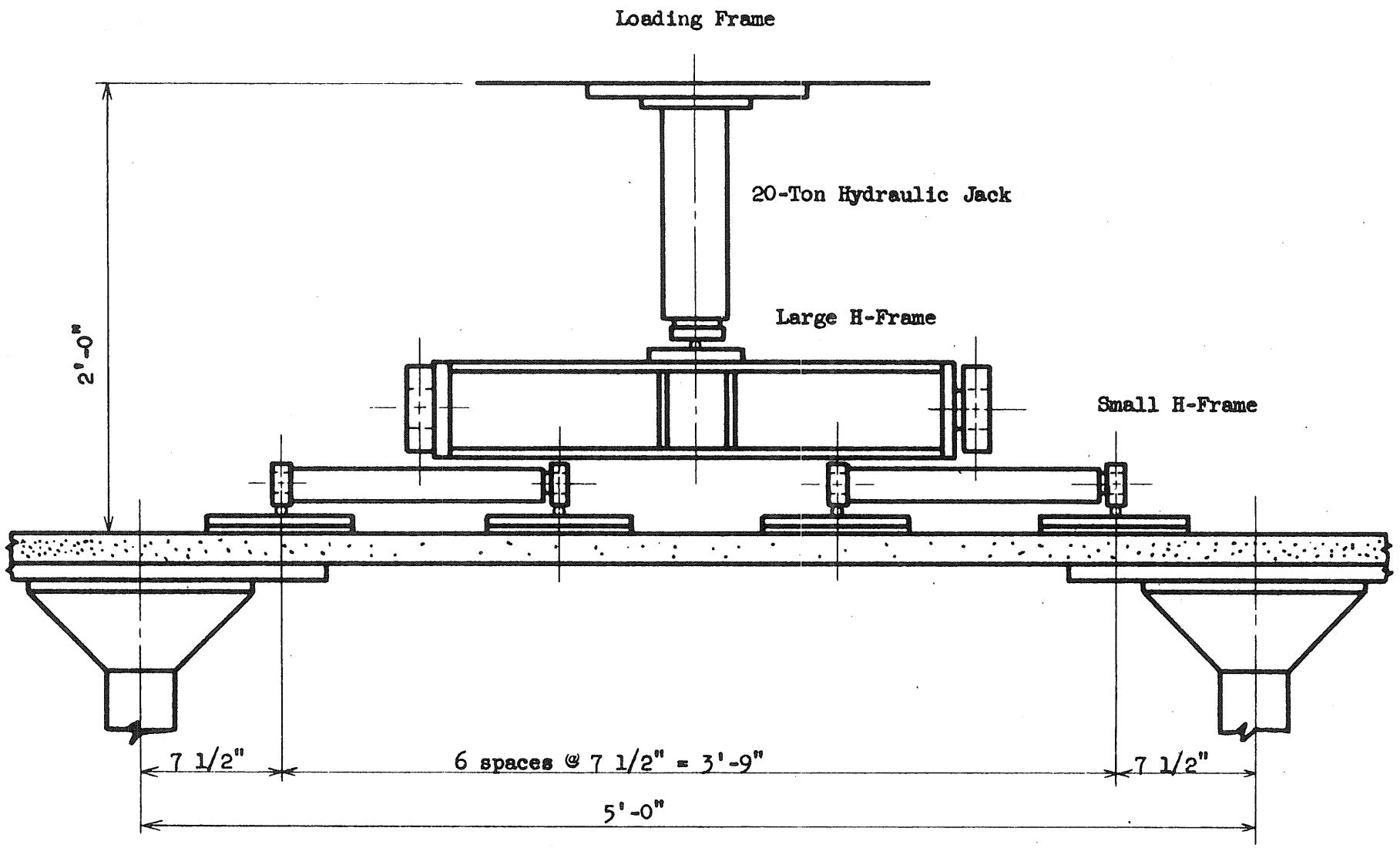

FIG. 4.2 ELEVATION OF LOAD DISTRIBUTING SYSTEM

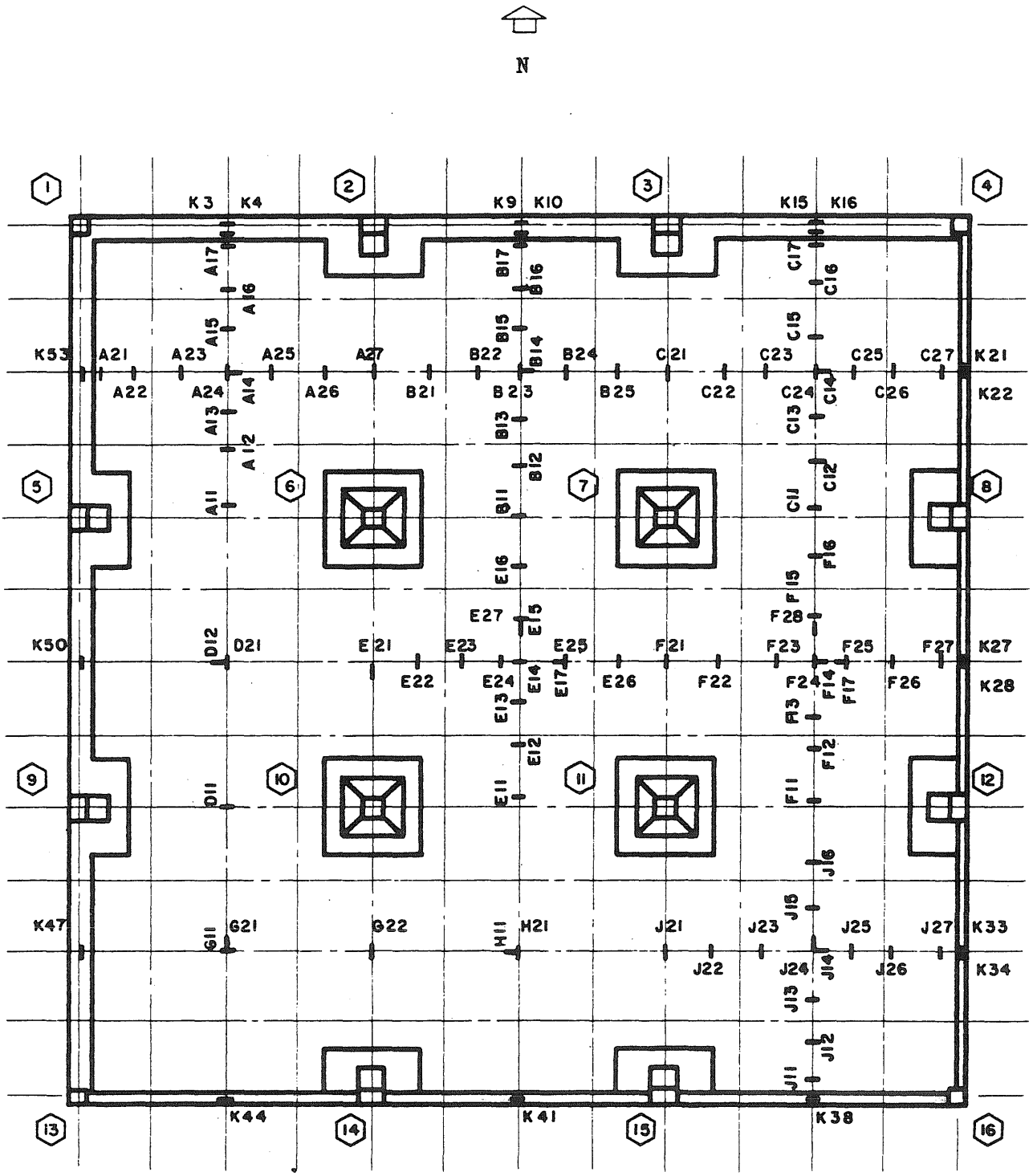

FIG. 5.1 LOCATION AND DESIGNATION OF BOTTOM STRAIN GAGES

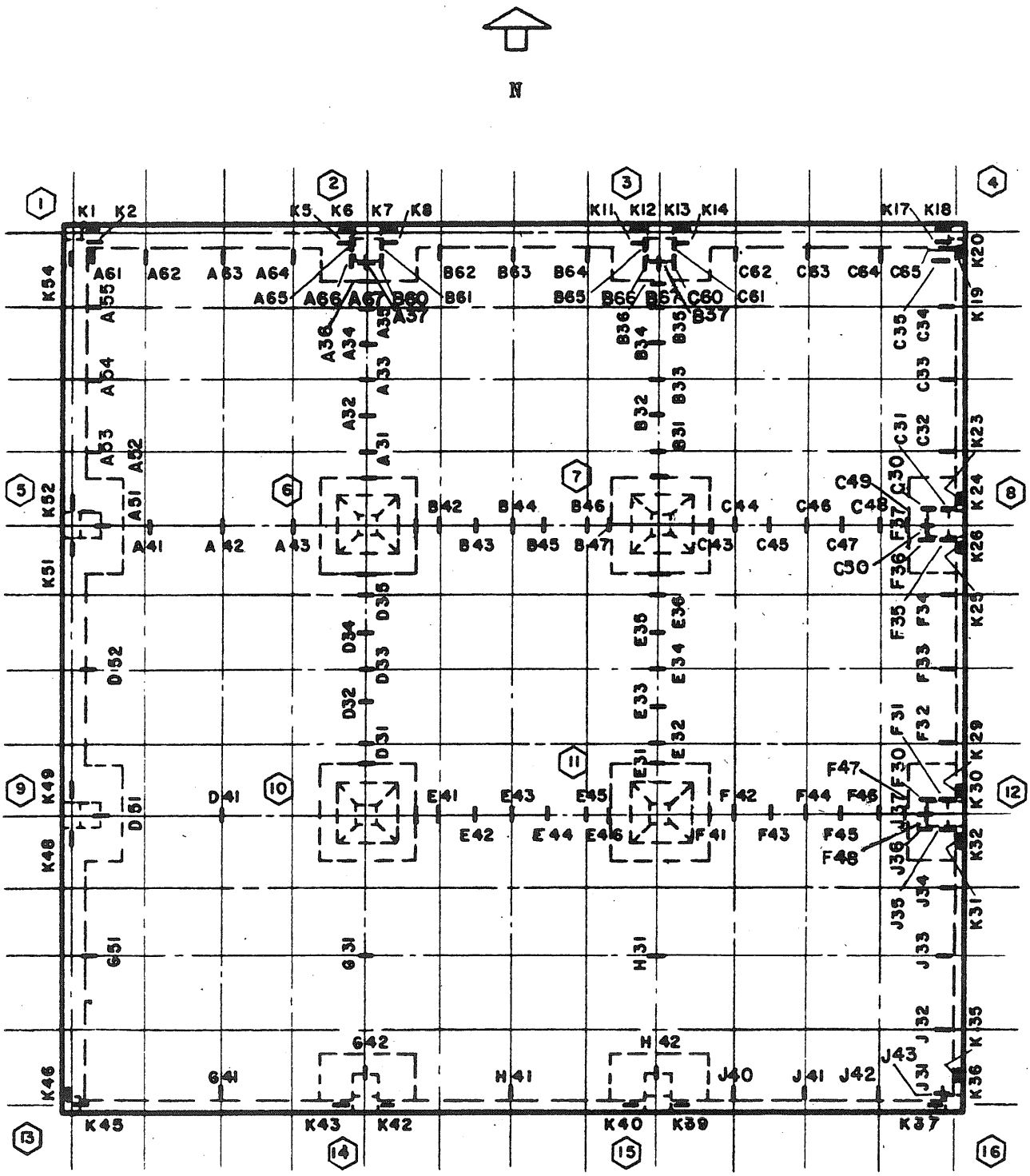

FIG. 5.2 LOCATION AND DESIGNATION OF TOP STRAIN GAGES

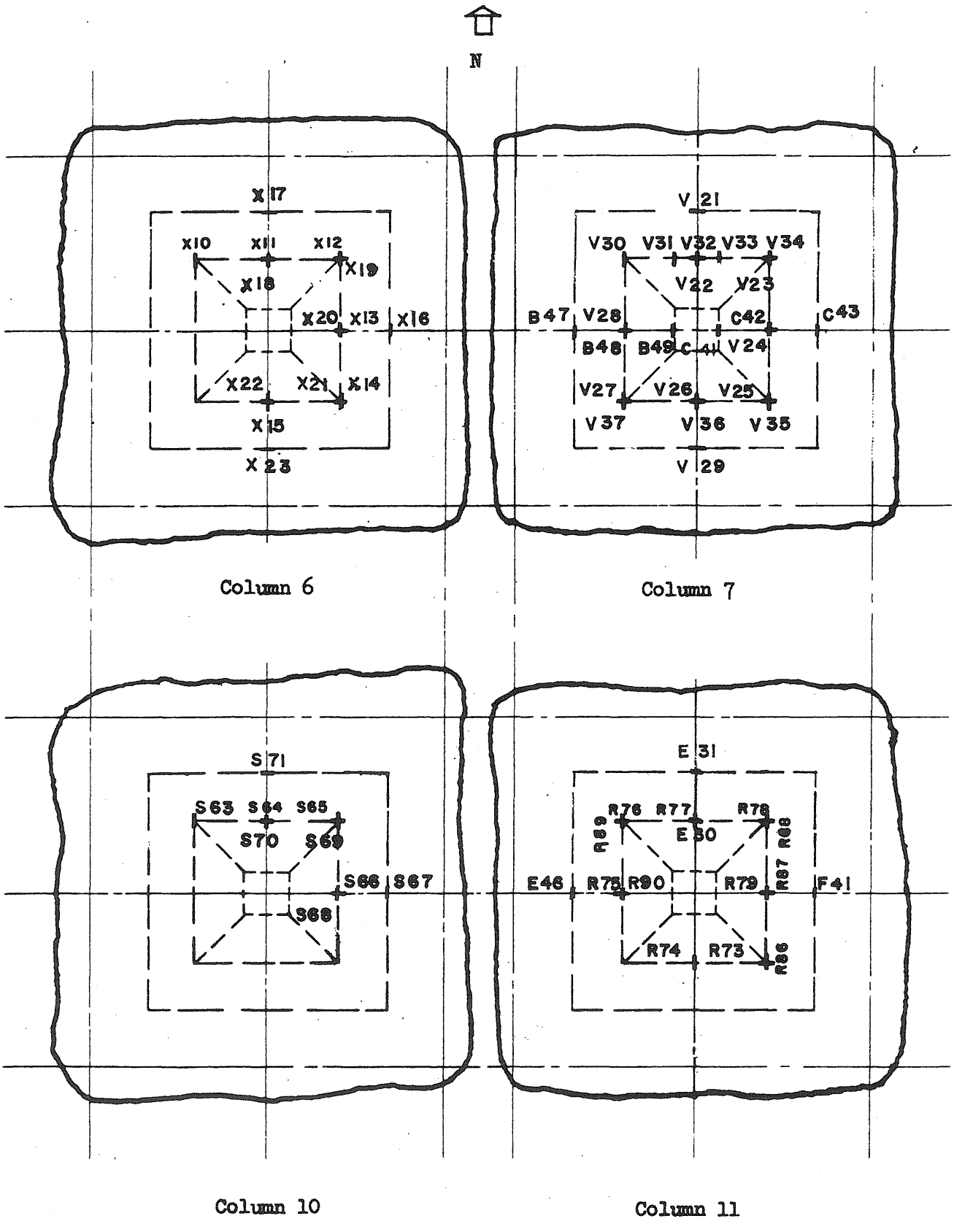

FIG. 5.3 LOCATION AND DESIGNATION OF STRAIN GAGES AT INTERIOR COLUMNS

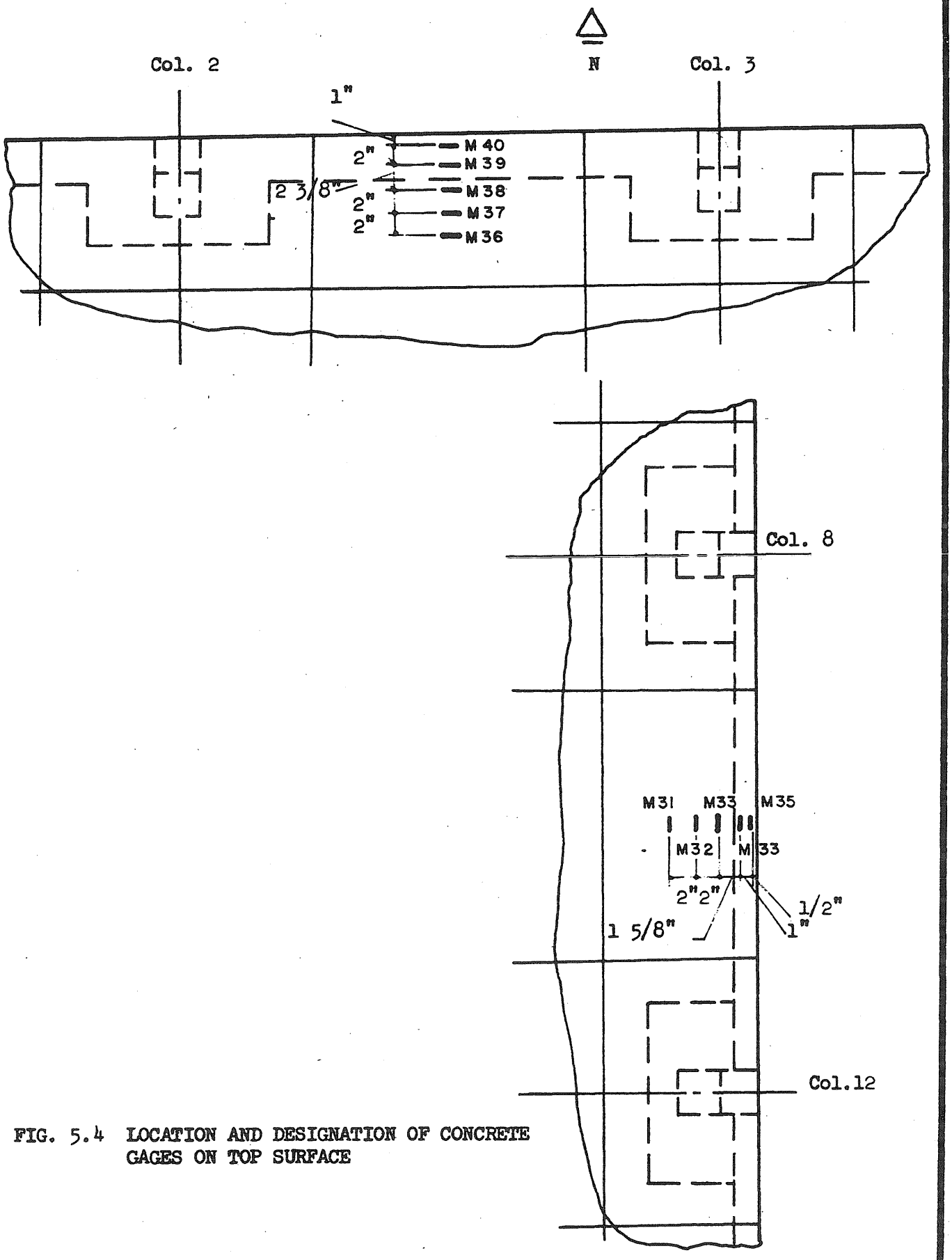

FIG. 5.4 LOCATION AND DESIGNATION OF CONCRETE GAGES ON TOP SURFACE

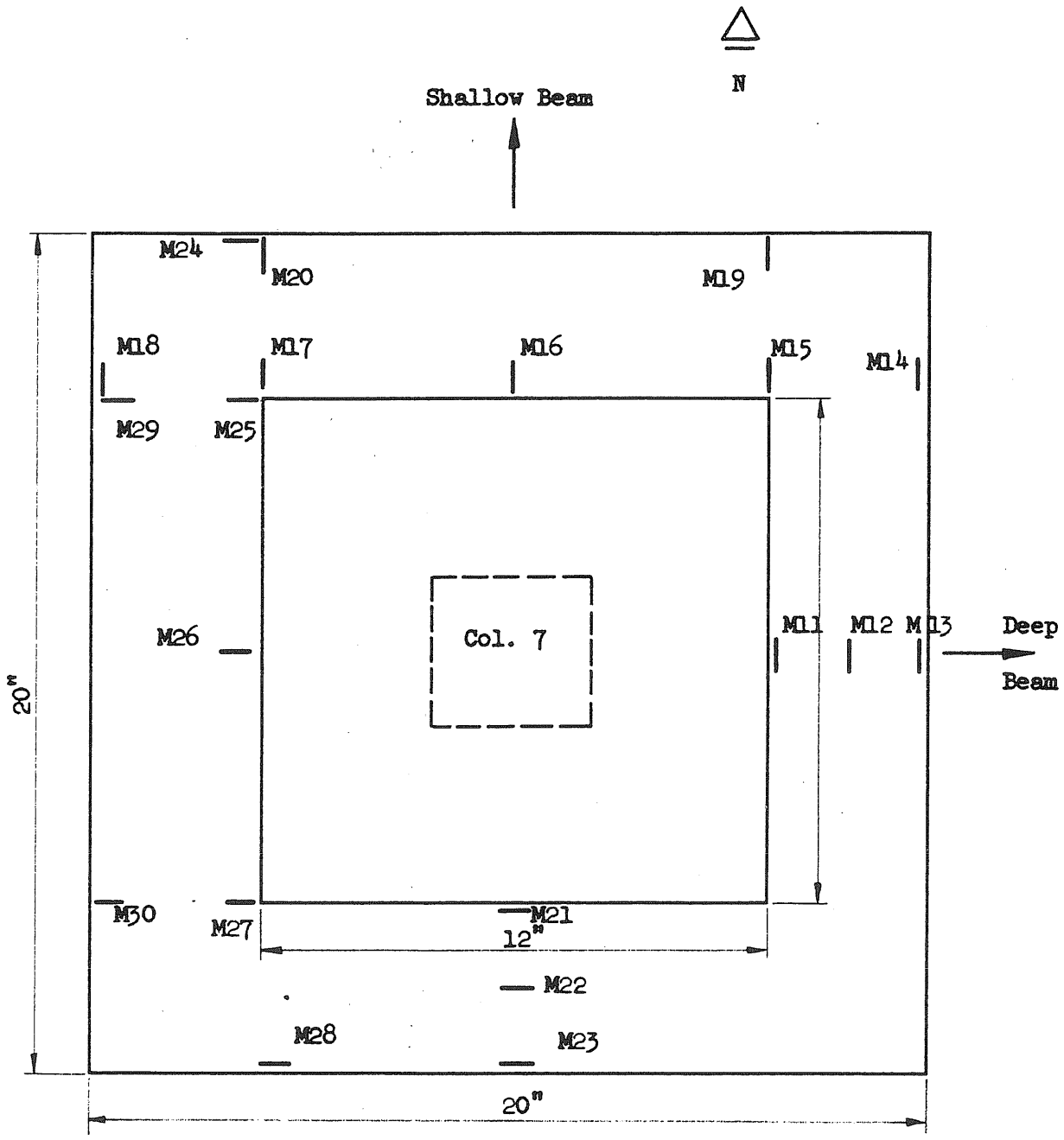

FIG. 5.5 LOCATION AND DESIGNATION OF CONCRETE STRAIN GAGES ON DROP PANEL AT COLUMN 7

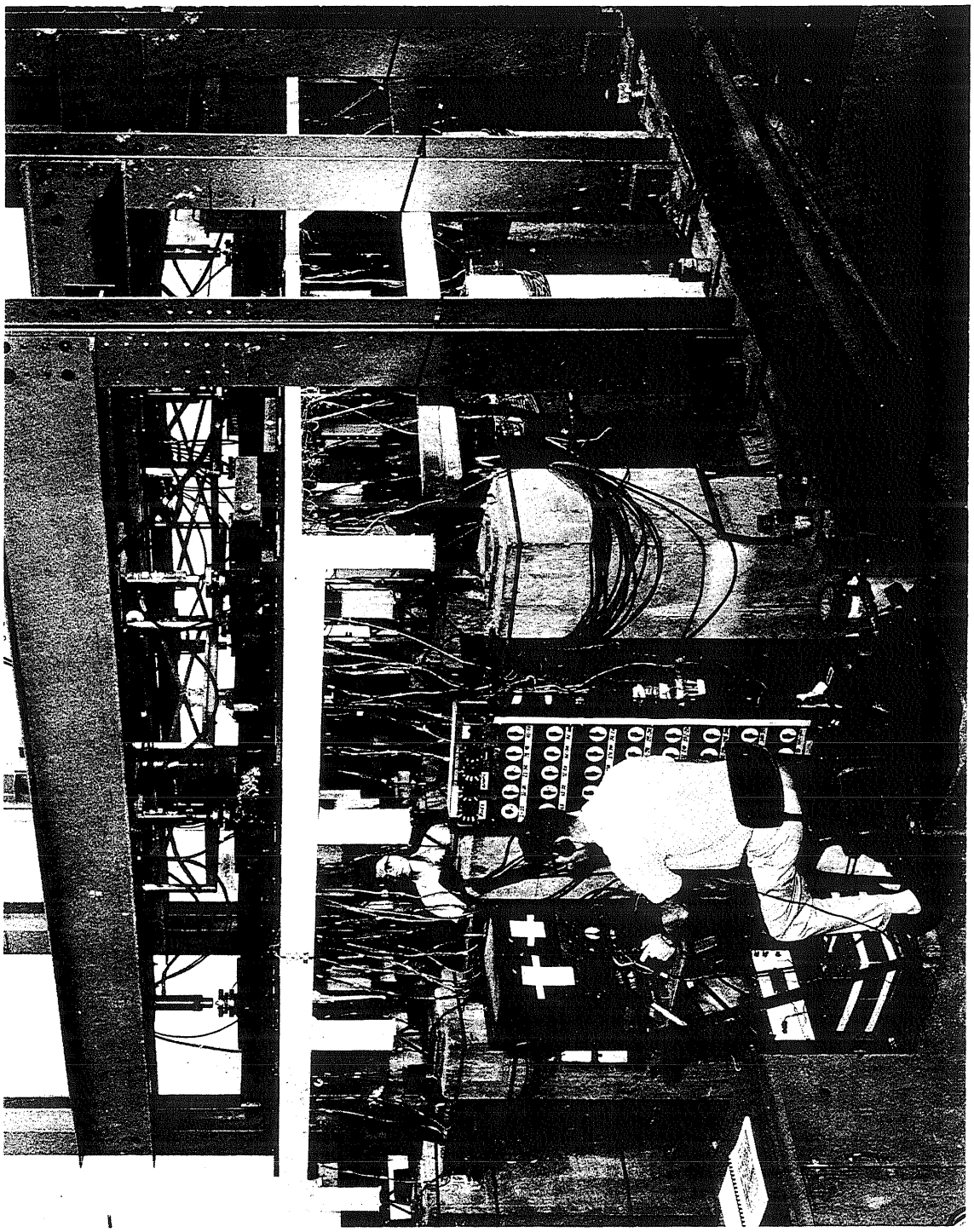

FIG. 5.6 VIEW OF TEST STRUCTURE SHOWING INTRUMENT PANELS

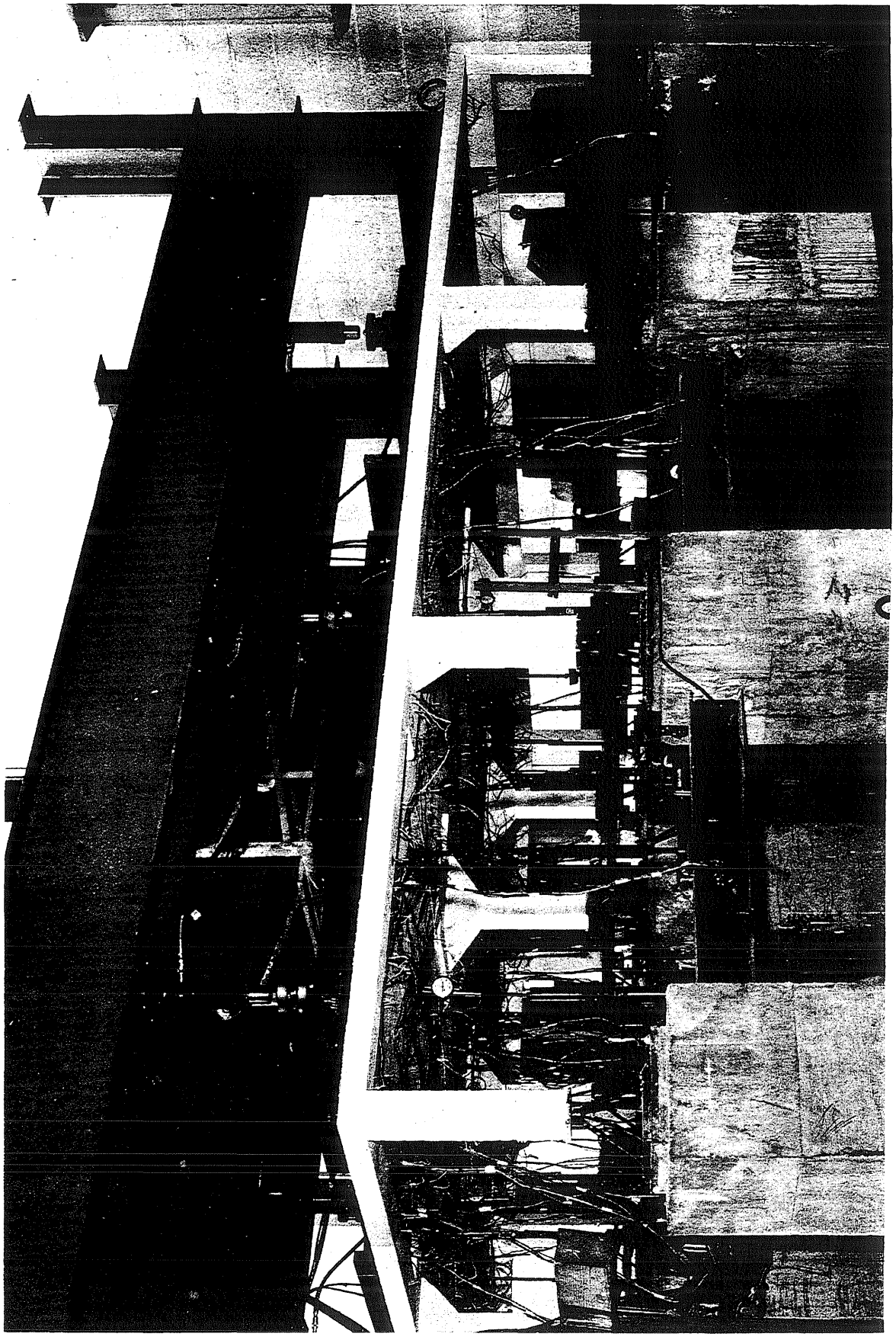

FIG. 5.7 VIEW OF UNDERSIDE OF TEST STRUCTURE

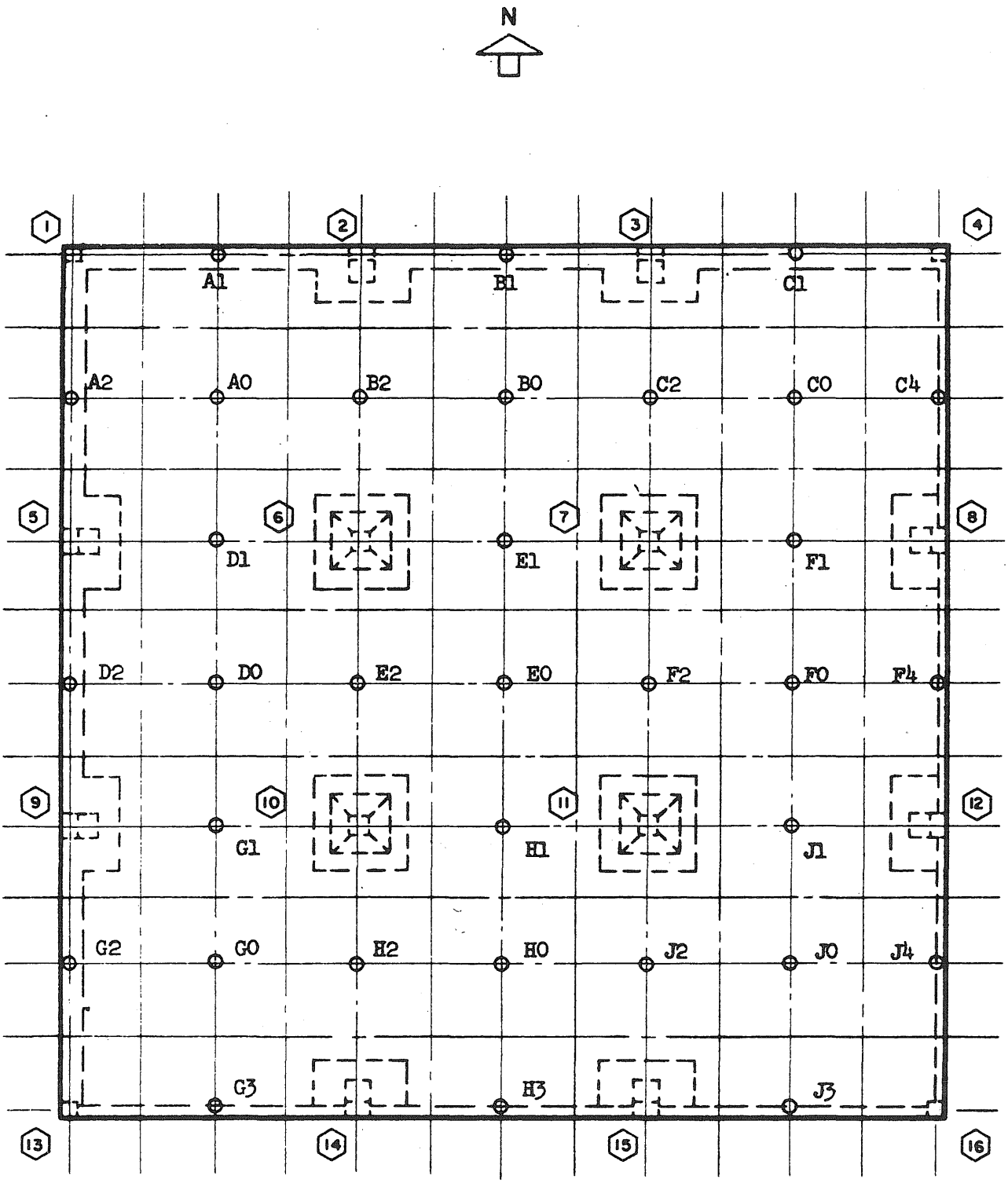

FIG. 5.8 LOCATION AND DESIGNATION OF THE DEFLECTION DIAL GAGES

Location of deflection measurements is shown in Fig. 5.6

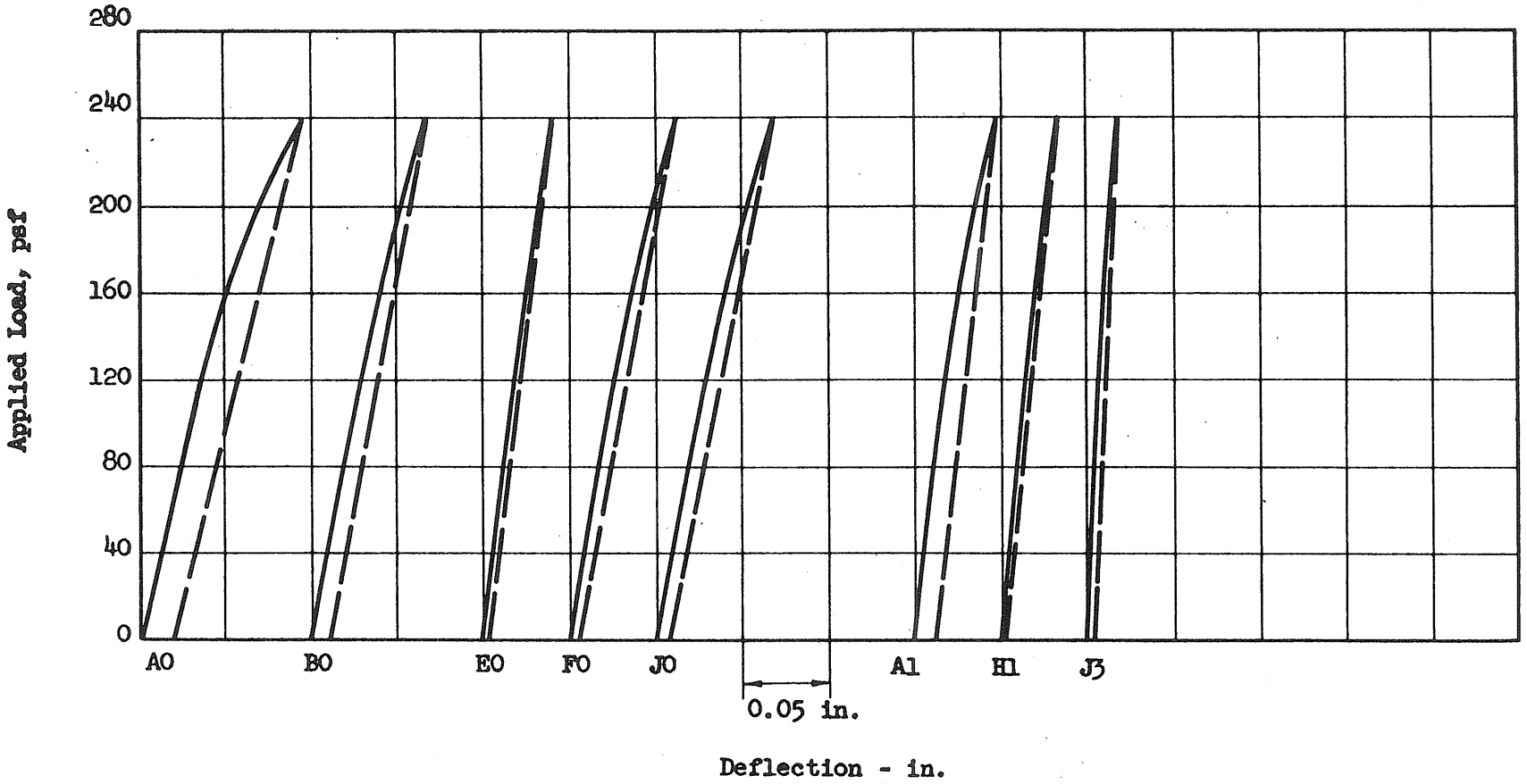

FIG. 7.1 LOAD-DEFLECTION CURVES, TEST 502

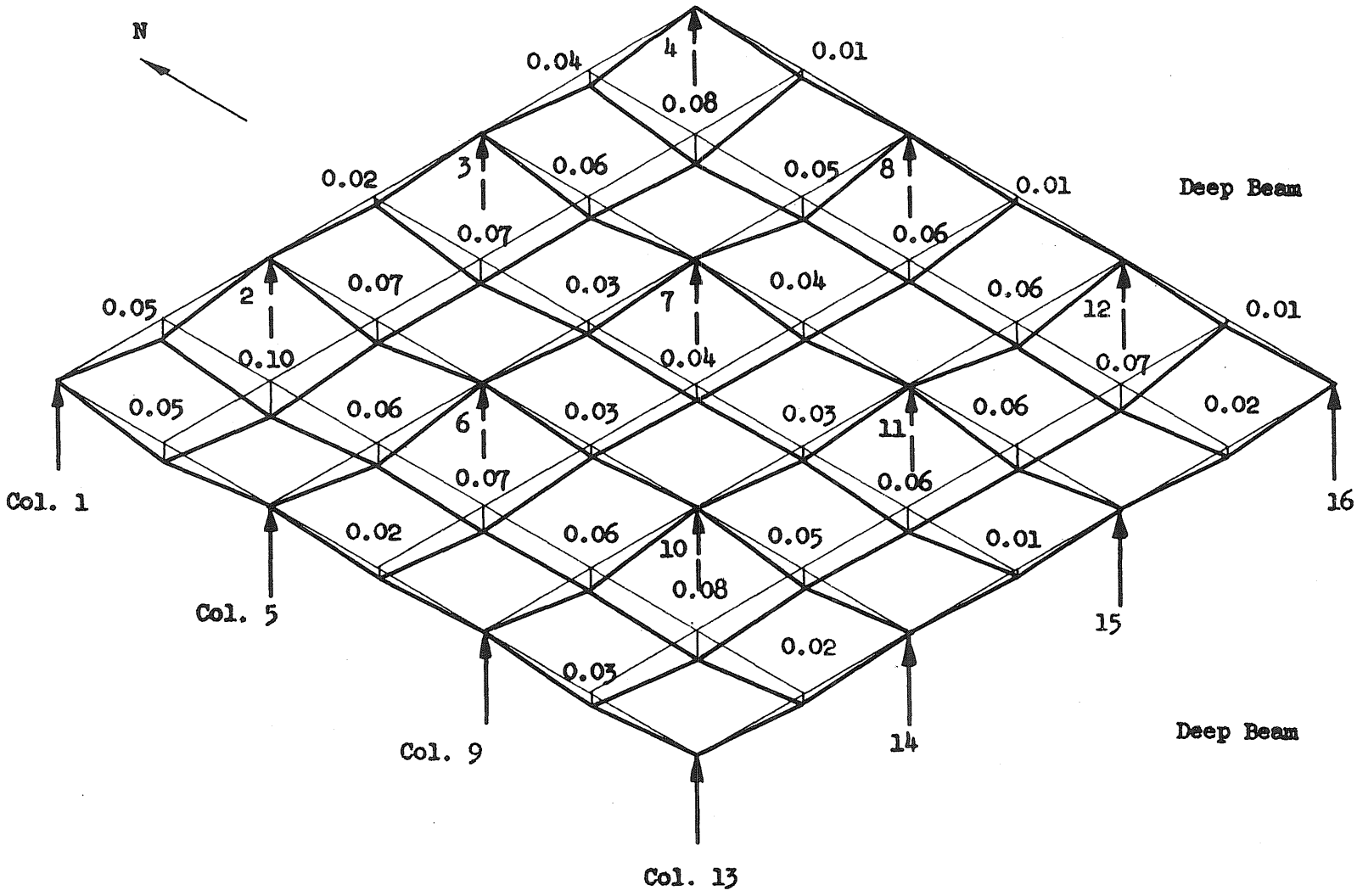

FIG. 7.2 SCHEMATIC DEFLECTION DIAGRAM, TEST 502

Location of strain gages is shown in Fig. 5.1

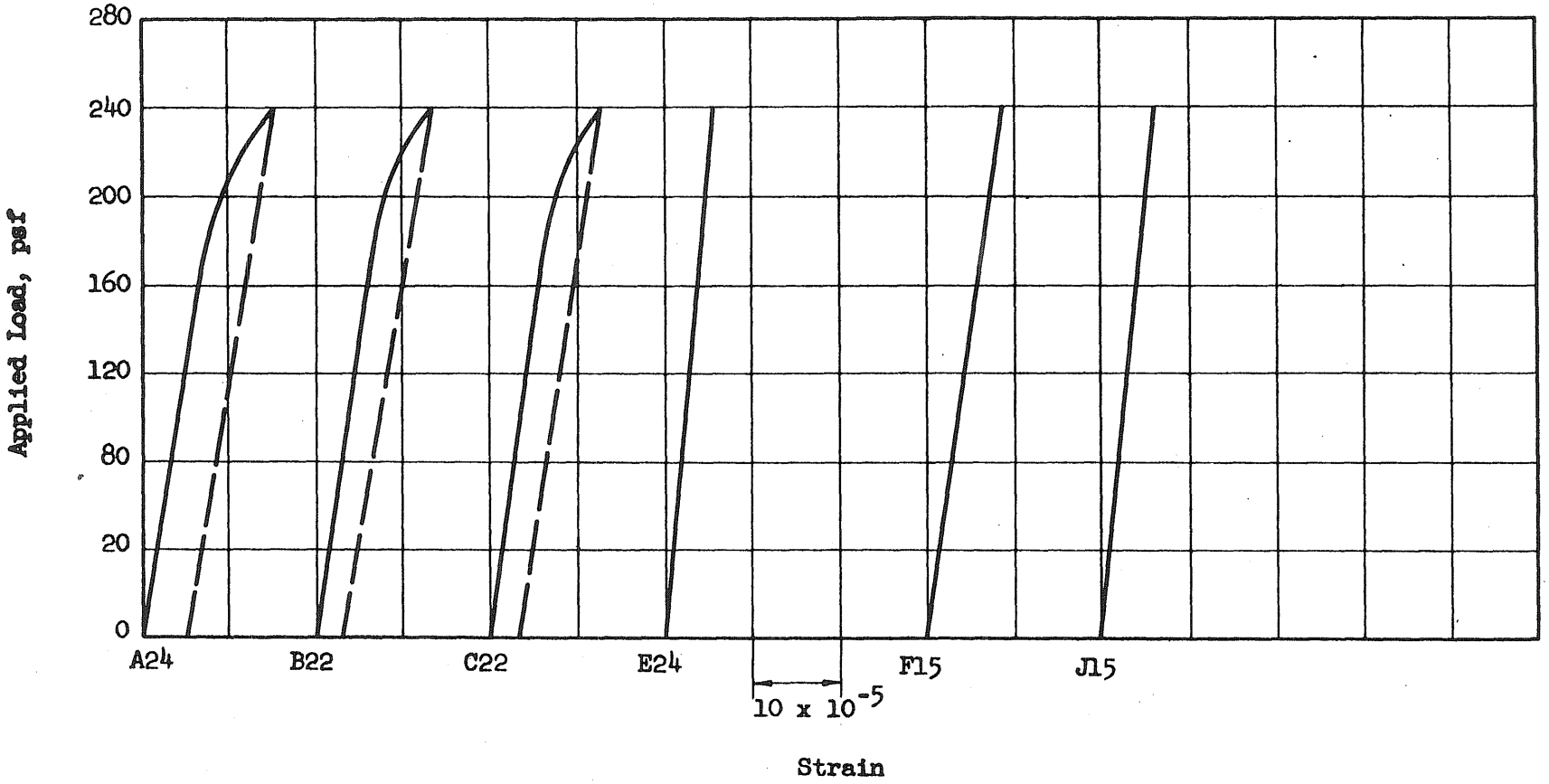

FIG. 7.3 LOAD-STRAIN CURVES FOR BOTTOM REINFORCEMENT, TEST 502

Location of strain gages is shown in Figs. 5.2 and 5.3

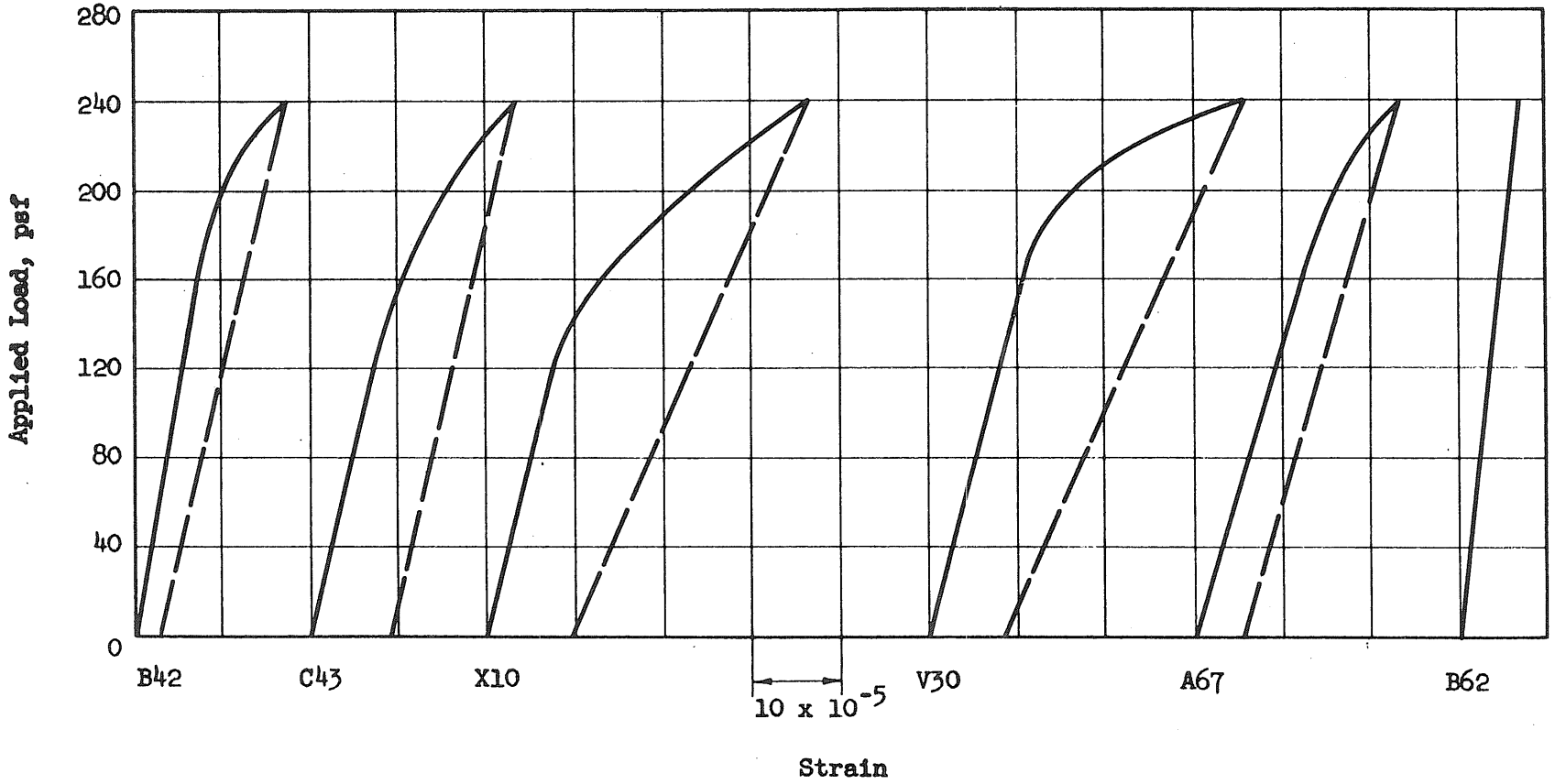

FIG. 7.4 LOAD-STRAIN CURVES FOR TOP REINFORCEMENT, TEST 502

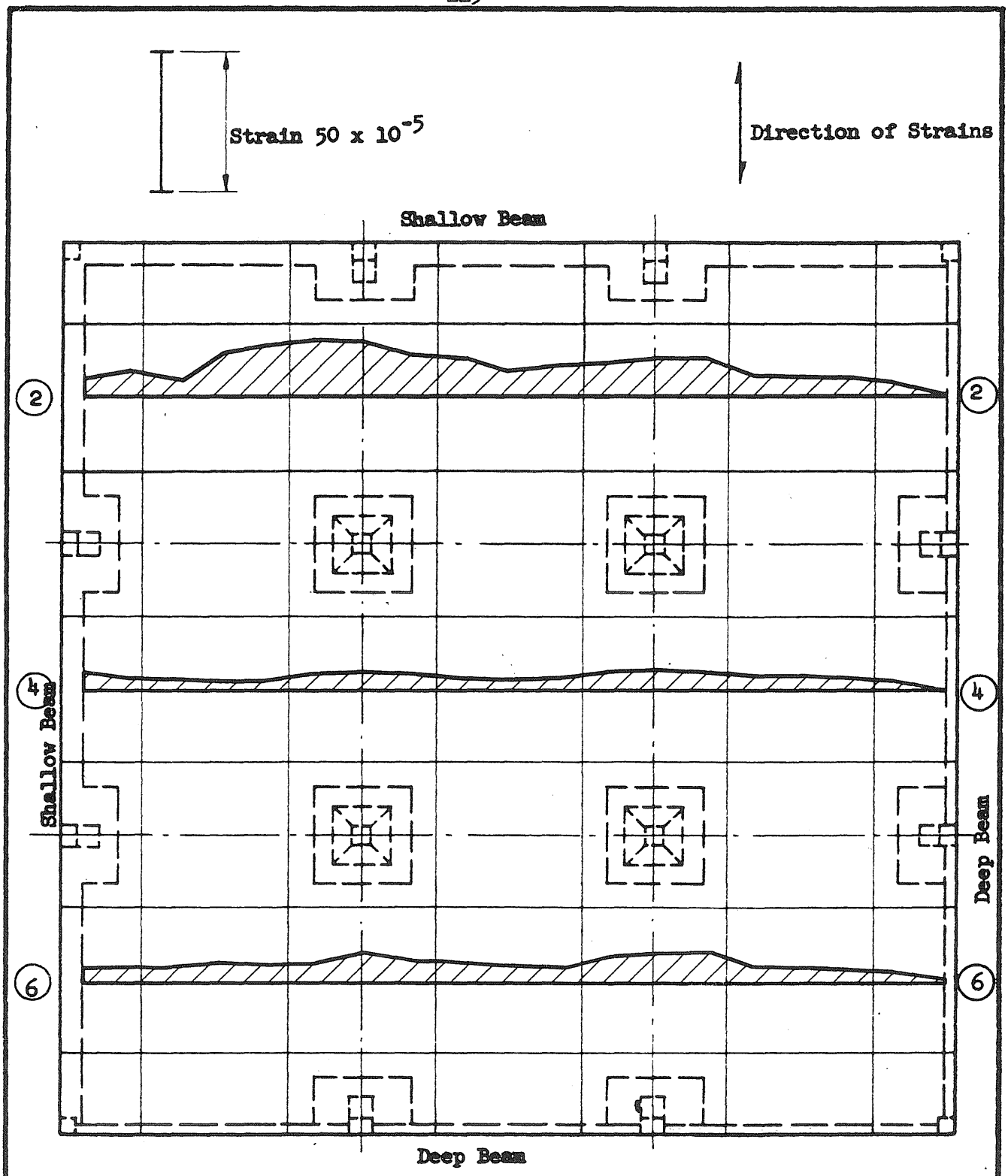

FIG. 7.5 DISTRIBUTION OF STRAINS, POSITIVE MOMENT SECTIONS, TEST 502

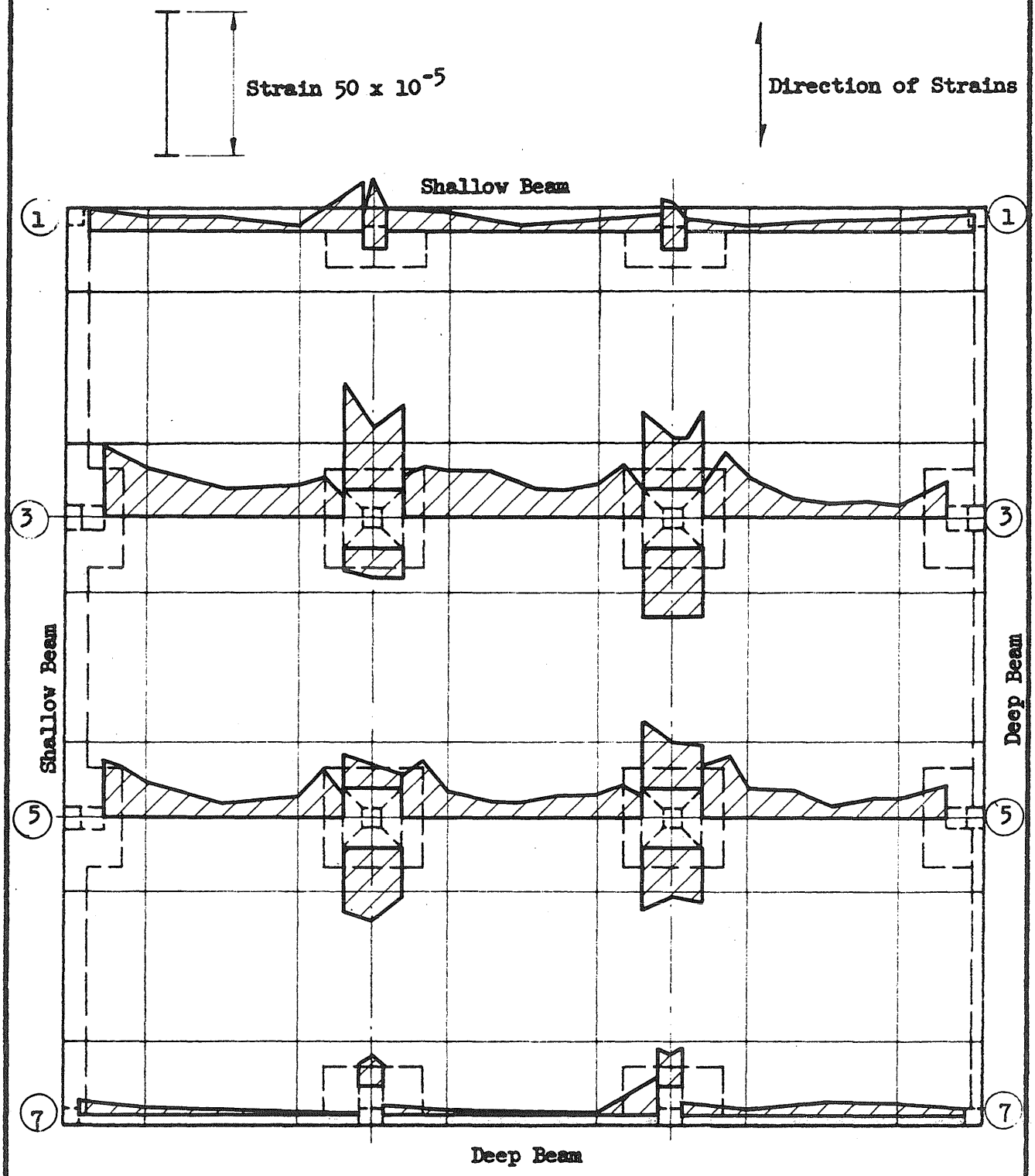

FIG. 7.6 DISTRIBUTION OF STRAINS, NEGATIVE MOMENT SECTIONS, TEST 502

Note: Strains across the column capitals are plotted with the edge of the capital as a base line

Location of deflection measurements is shown in Fig. 5.6

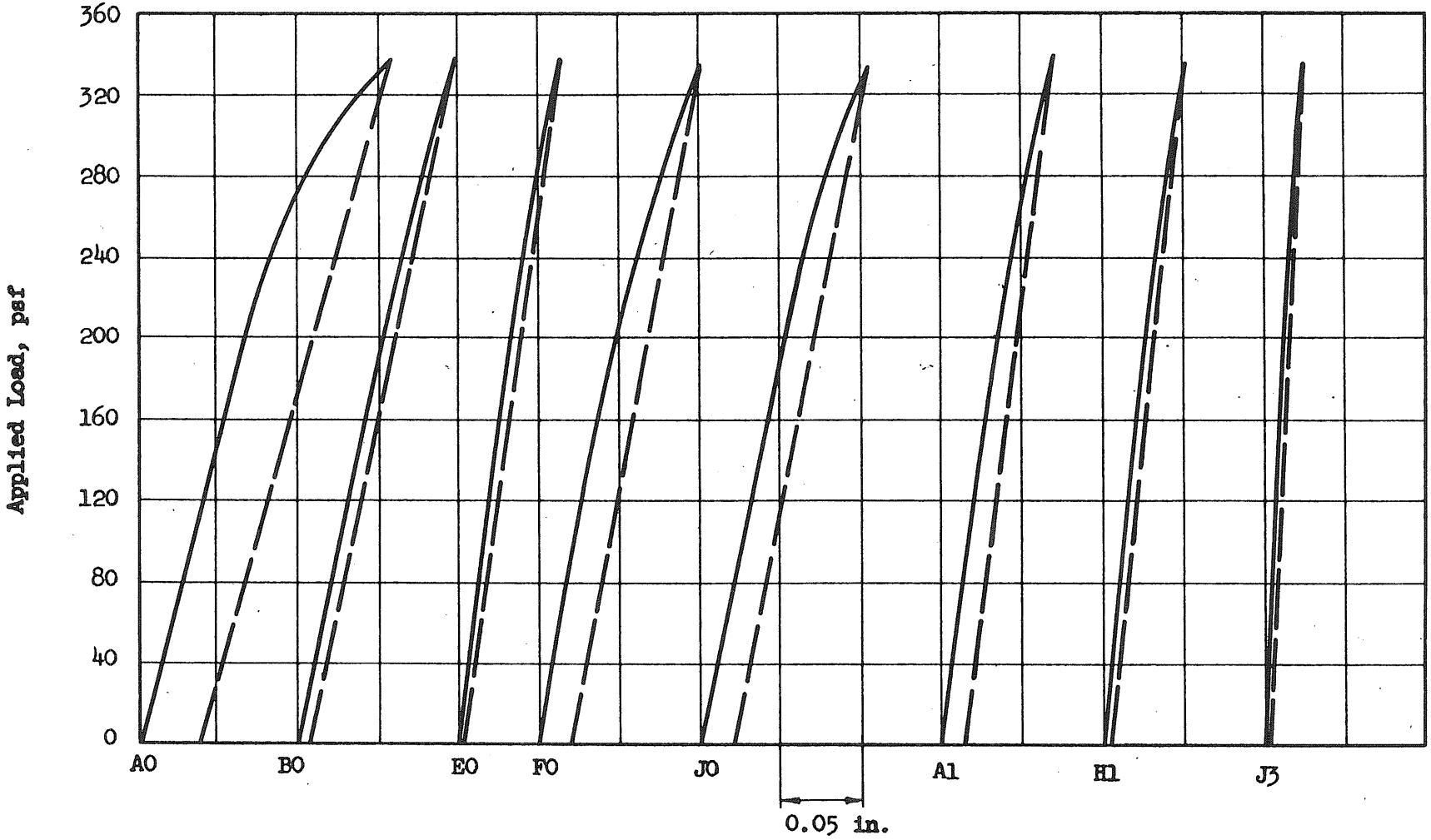

FIG. 7.7 LOAD-DEFLECTION CURVES, TEST 503

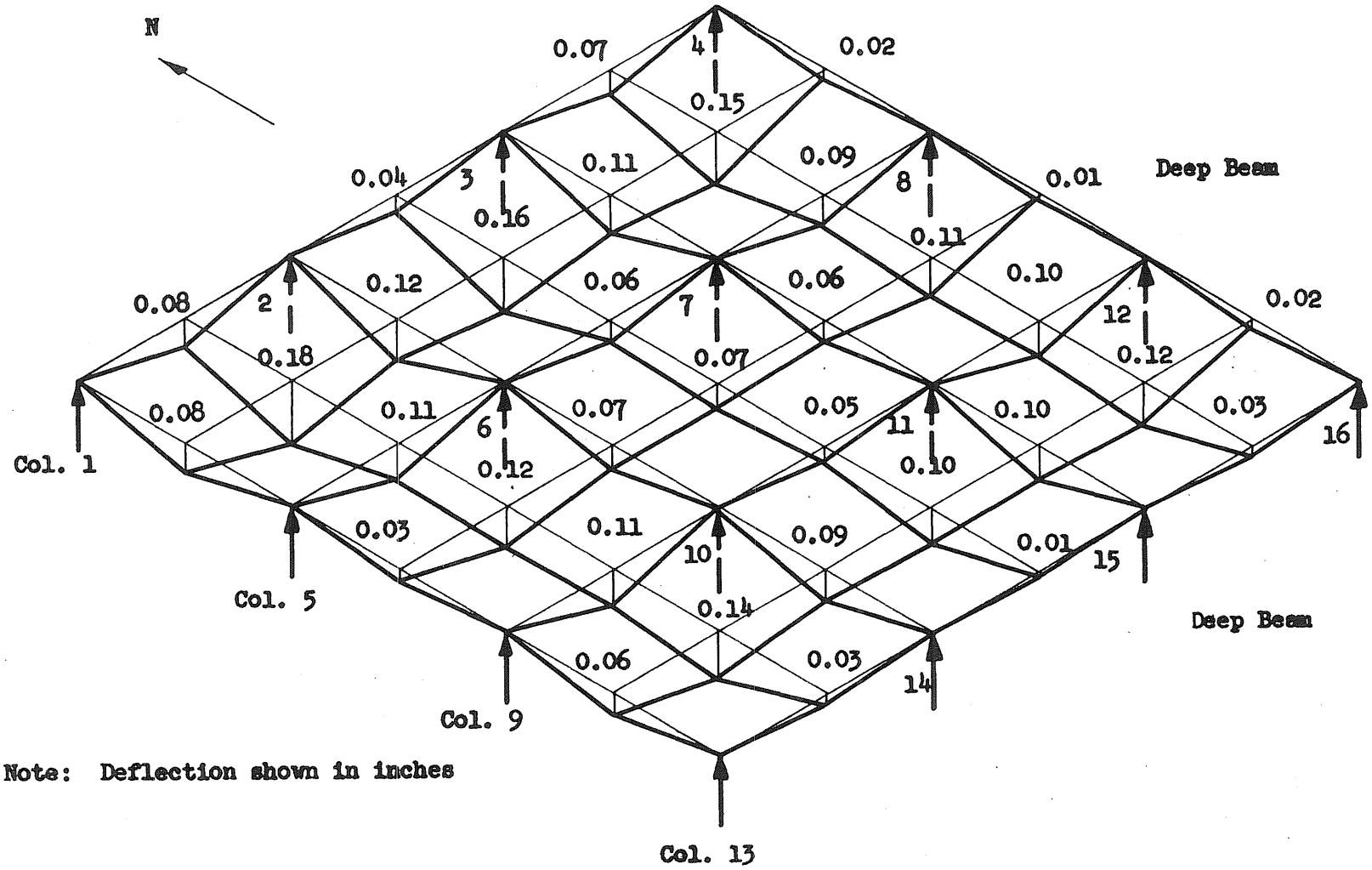

Note: Deflection shown in inches

FIG. 7.8 SCHEMATIC DEFLECTION DIAGRAM, TEST 503

Location of strain gages is shown in Fig. 5.1

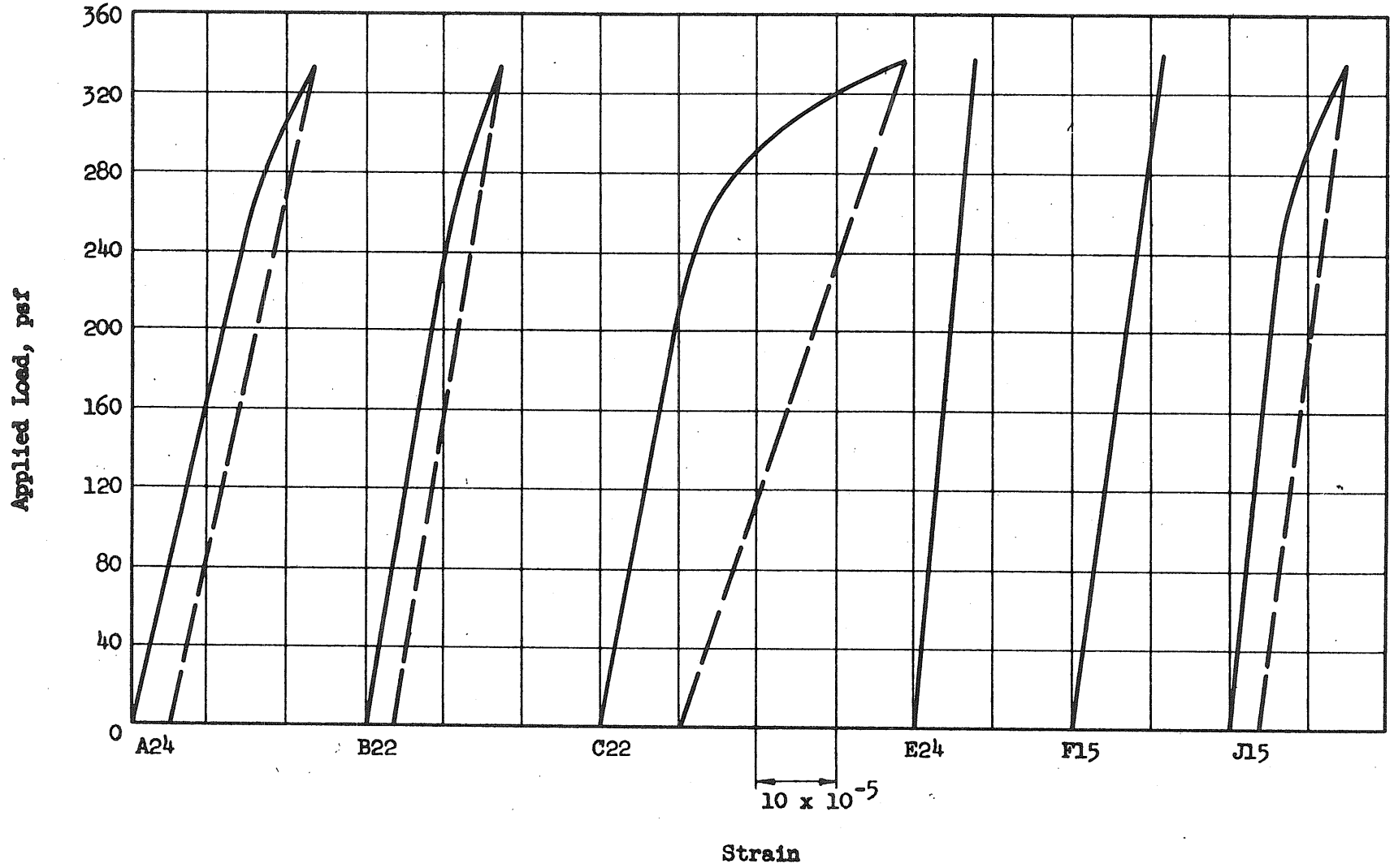

FIG. 7.9 LOAD-STRAIN CURVES FOR BOTTOM REINFORCEMENT, TEST 503

Location of strain gages is shown in Figs. 5.2 and 5.3

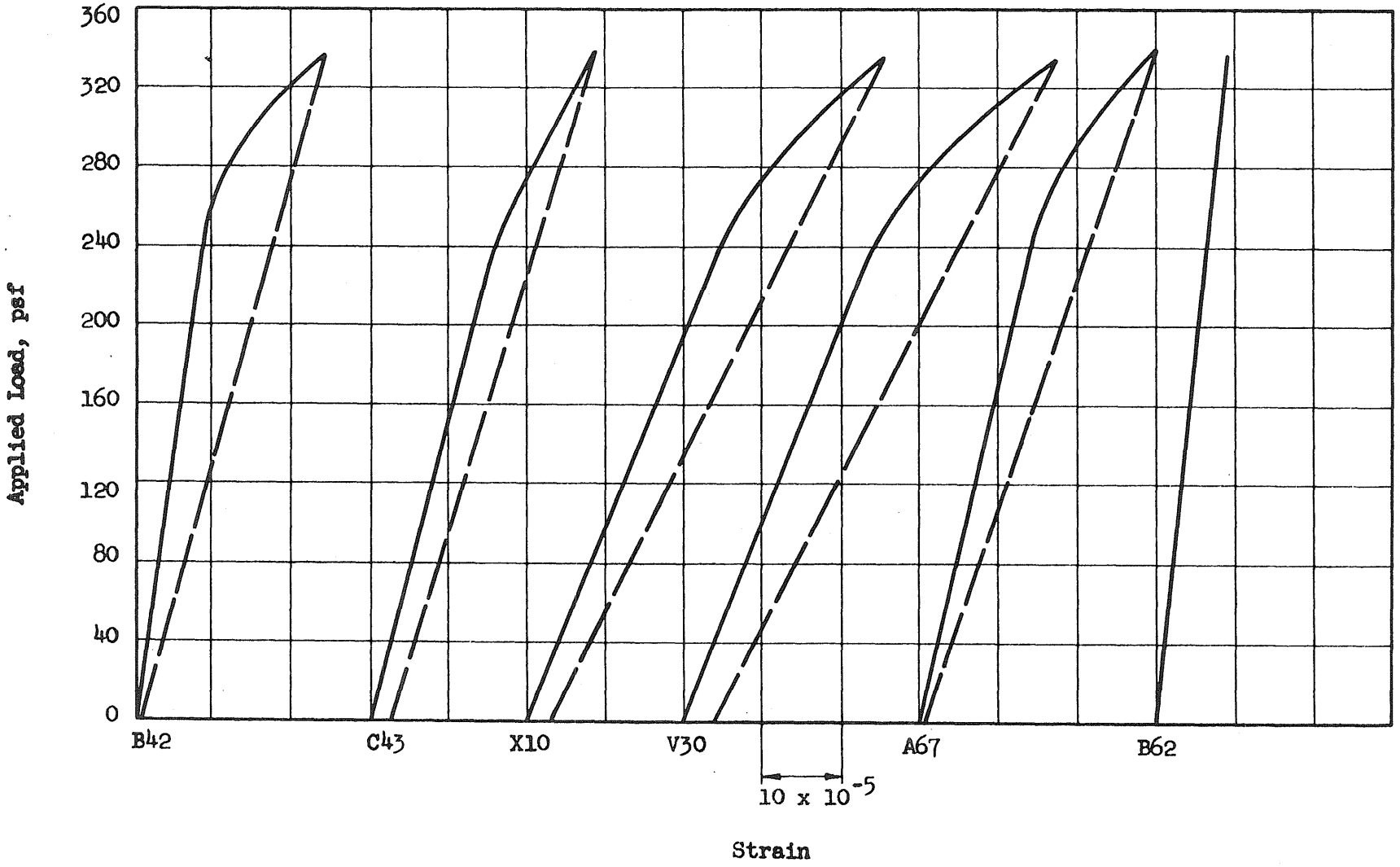

FIG. 7.10 LOAD-STRAIN CURVES FOR TOP REINFORCEMENT, TEST 503

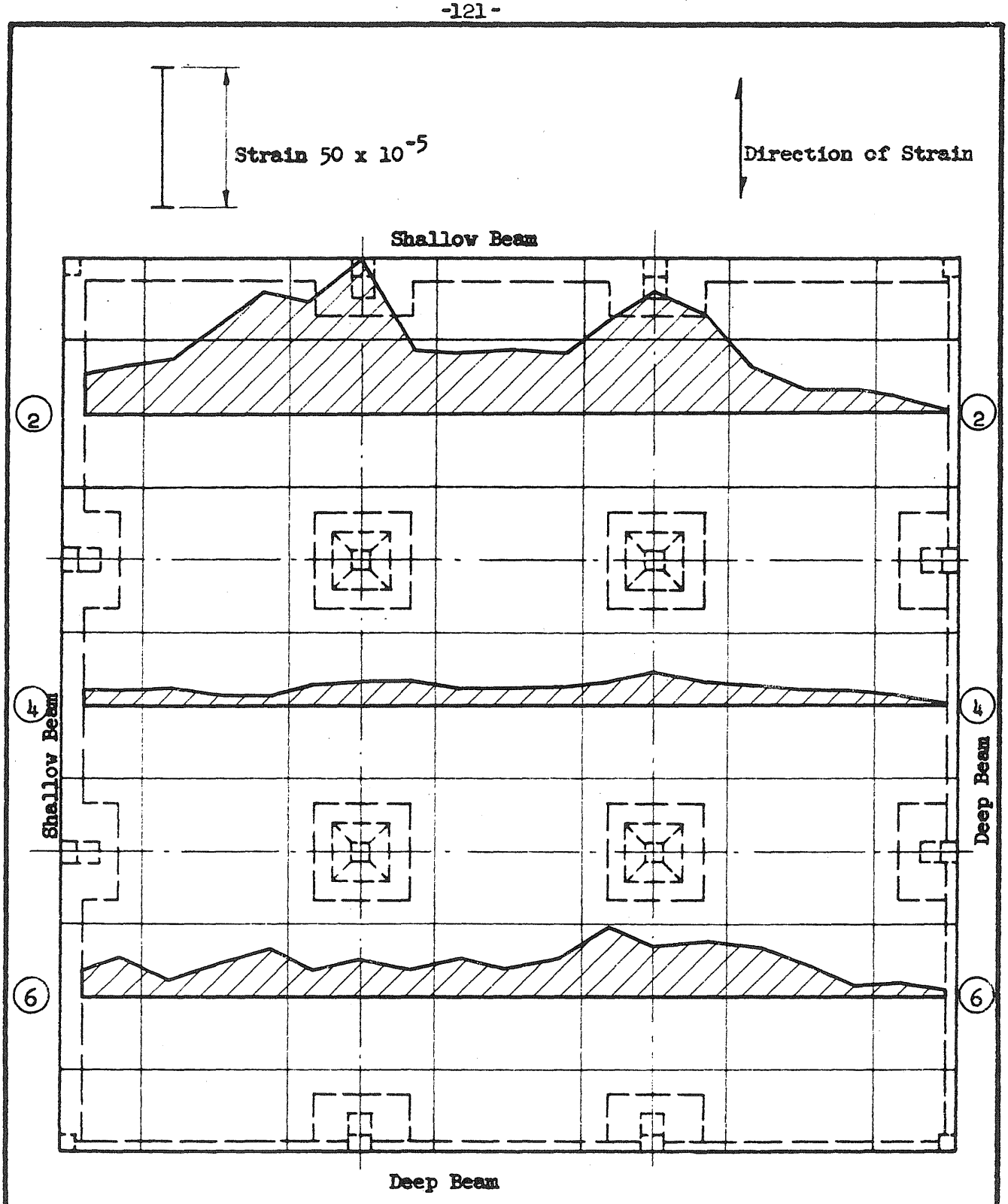

FIG. 7.11 DISTRIBUTION OF STRAINS, POSITIVE MOMENT SECTIONS, TEST 503

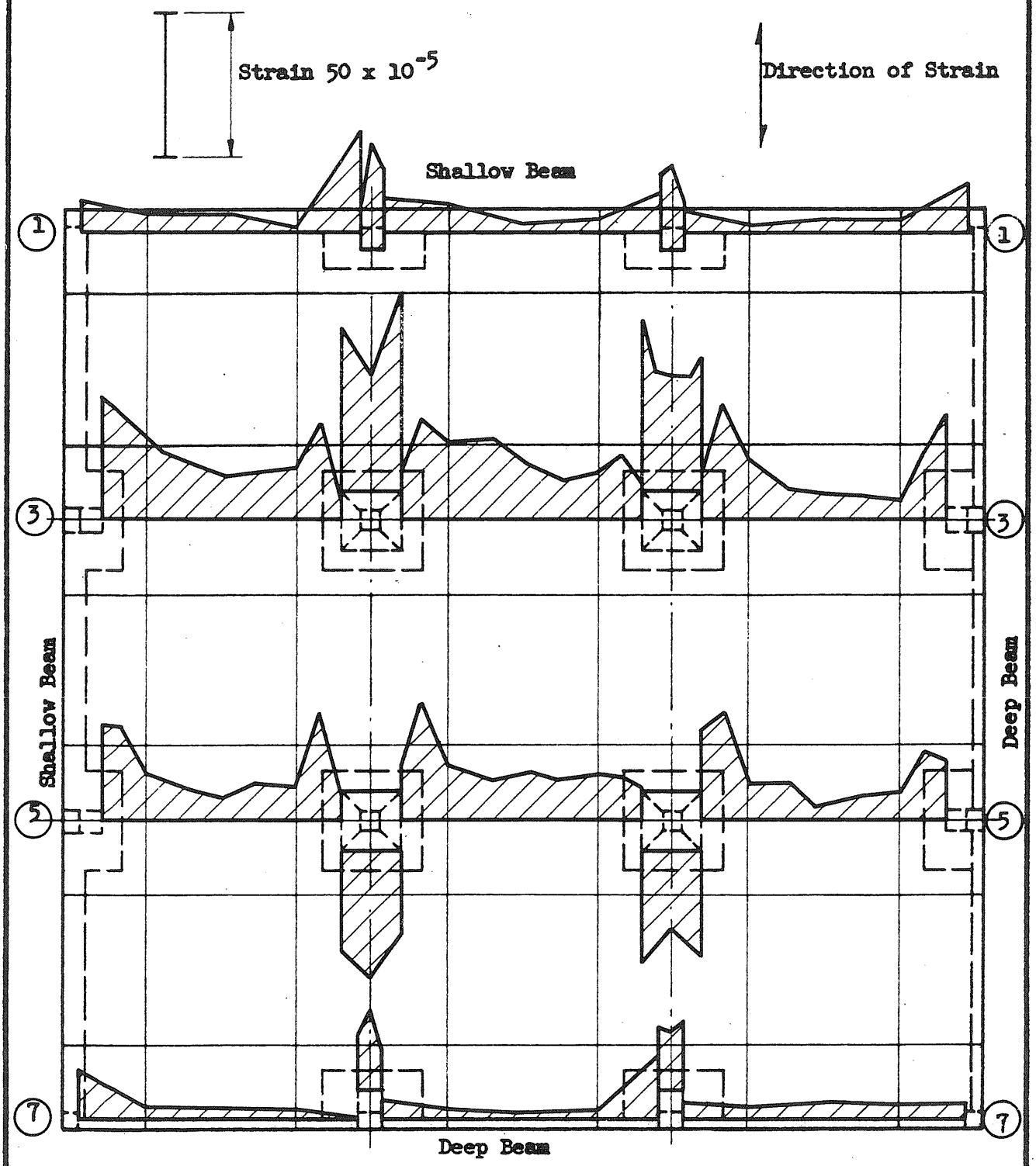

FIG. 7.12 DISTRIBUTION OF STRAINS, NEGATIVE MOMENT SECTIONS, TEST 503

Note: Strains across the column capitals are plotted with the edge of the capital as a base line

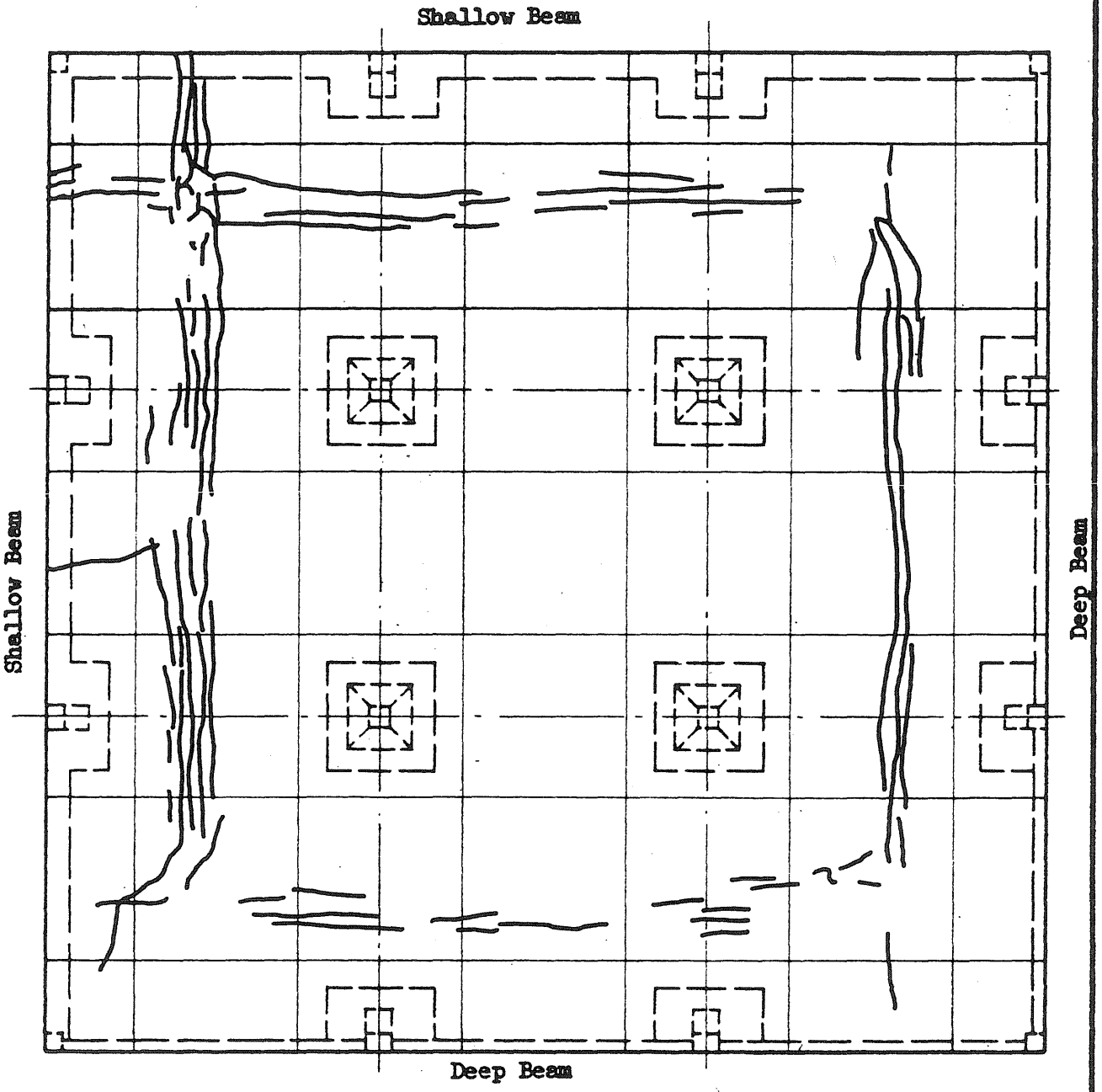

FIG. 7.13 CRACK PATTERN ON BOTTOM OF SLAB, TEST 503

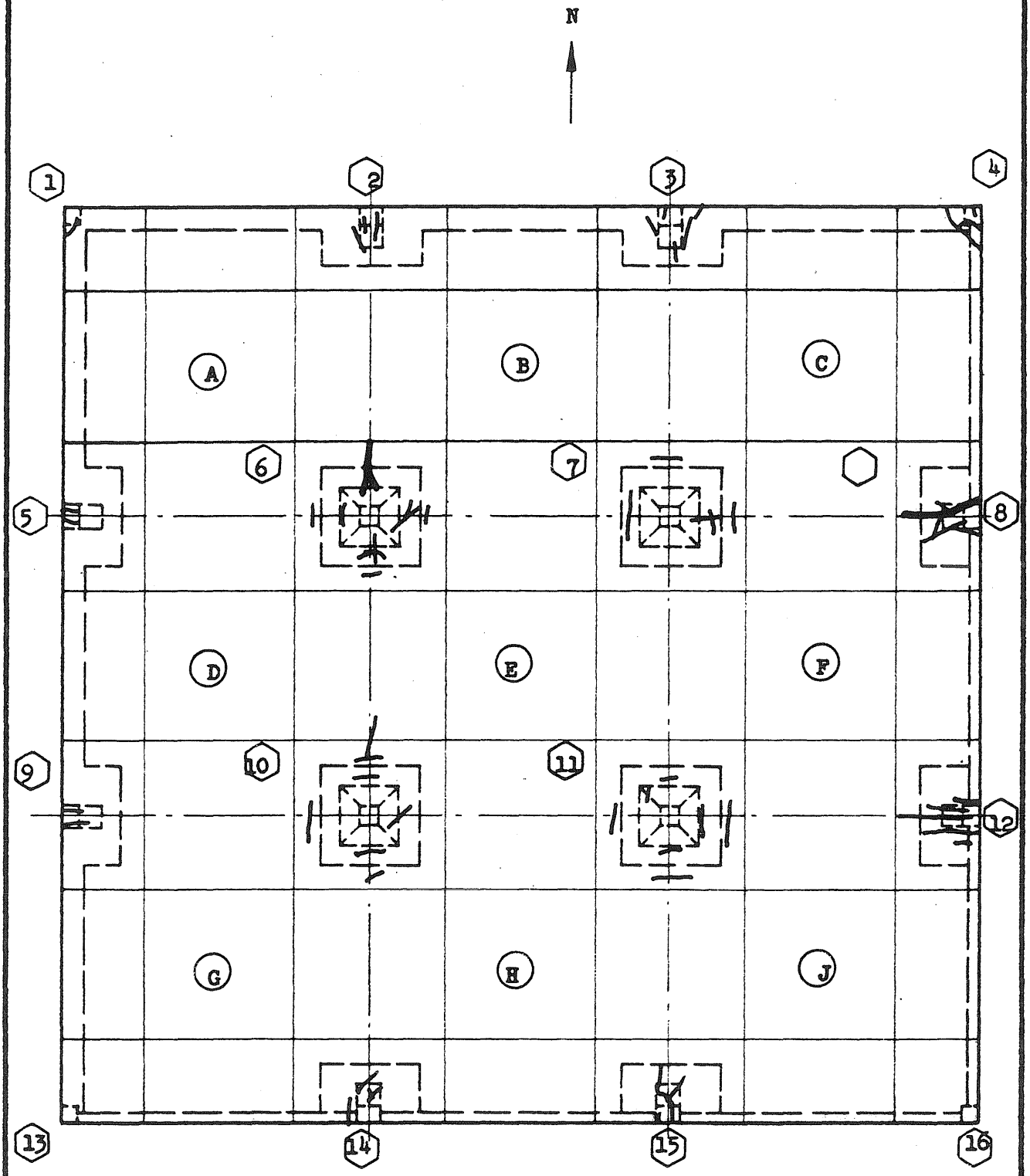

FIG. 7.14 CRACK PATTERN ON TOP OF SLAB, TEST 503

Location of deflection measurements is shown in Fig. 5.6

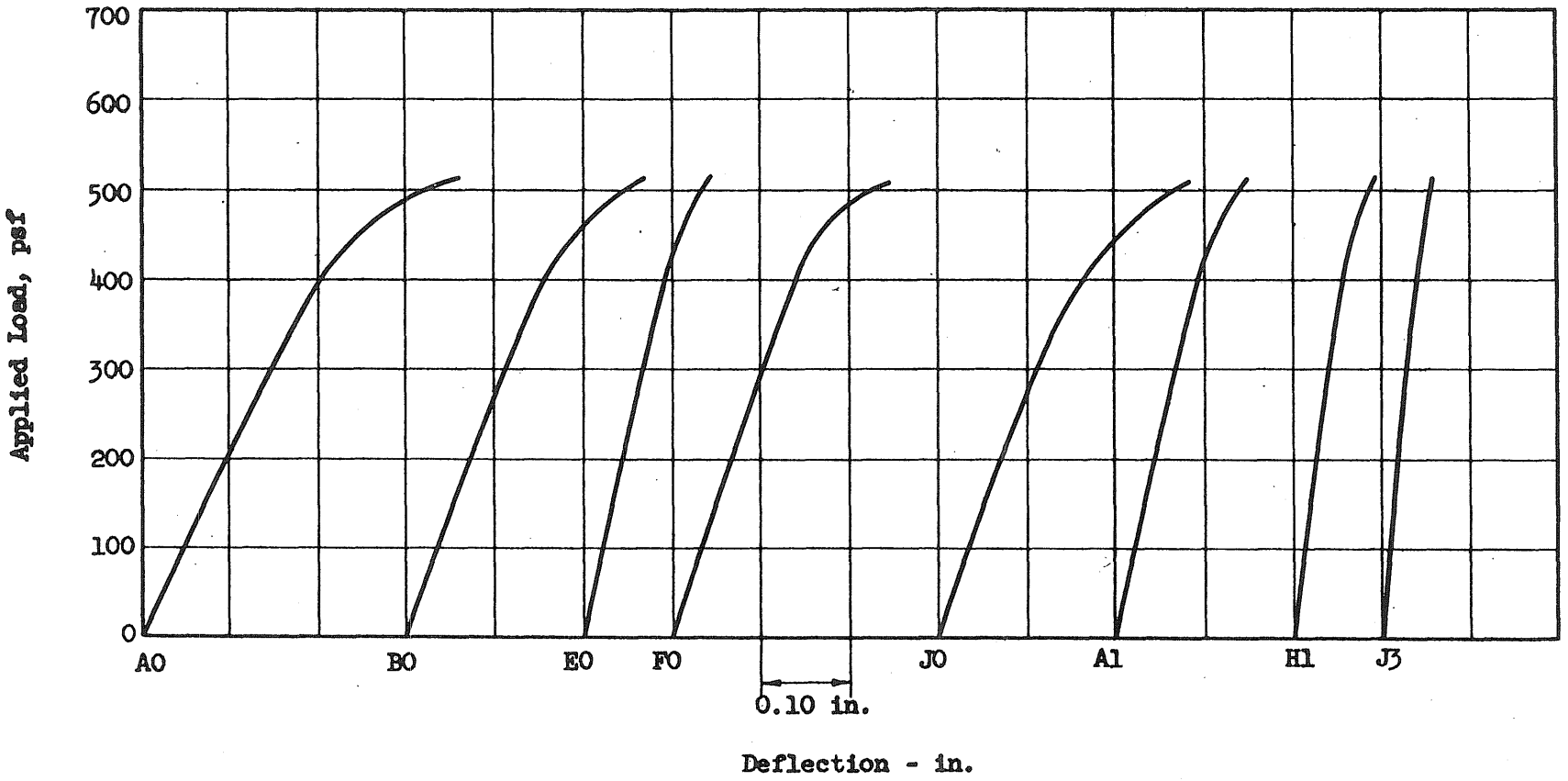

FIG. 7.15 LOAD-DEFLECTION CURVES, TEST 512

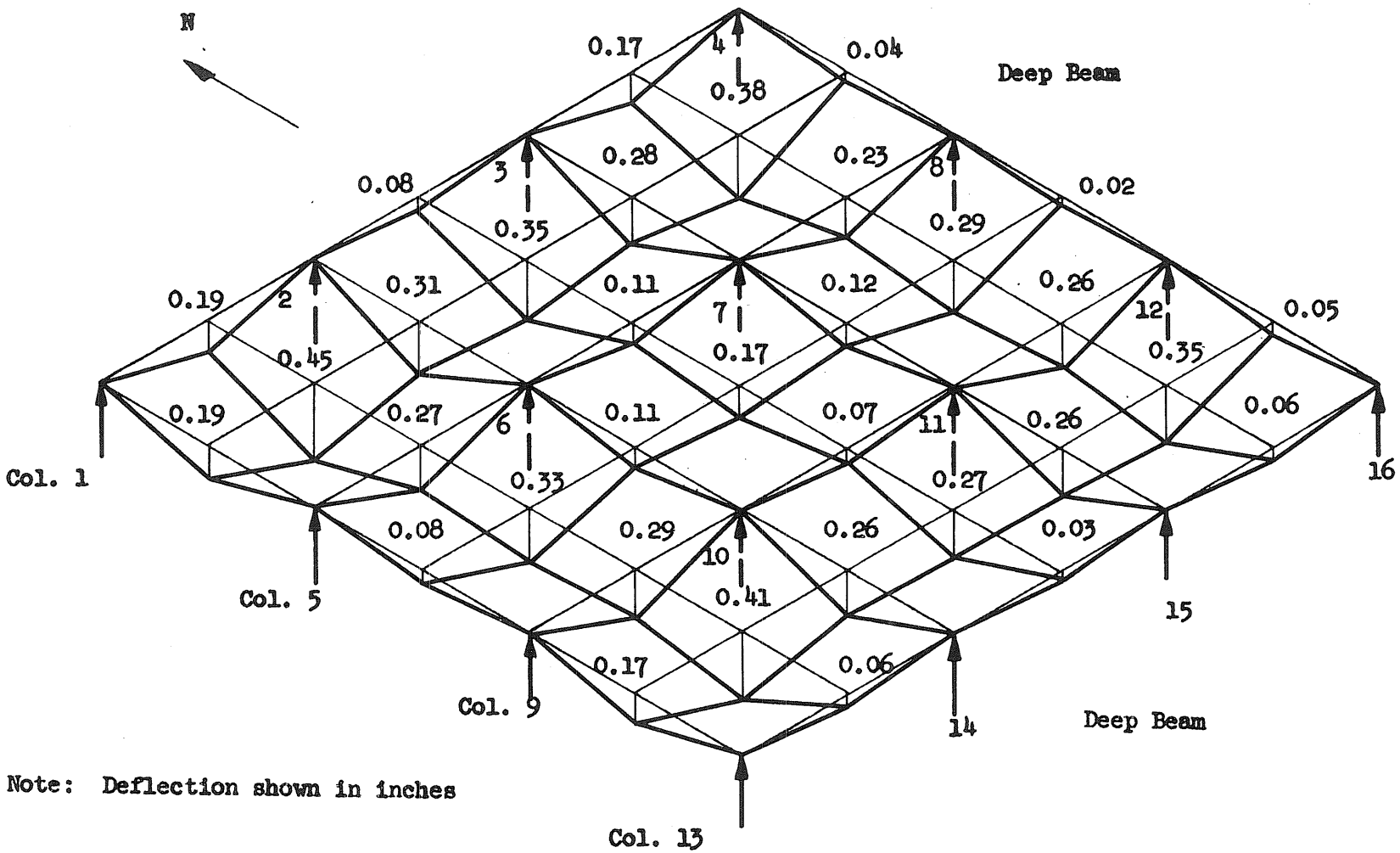

Note: Deflection shown in inches

FIG. 7.16 SCHEMATIC DEFLECTION DIAGRAM, TEST 512

Location of strain gages is shown in Fig. 5.1

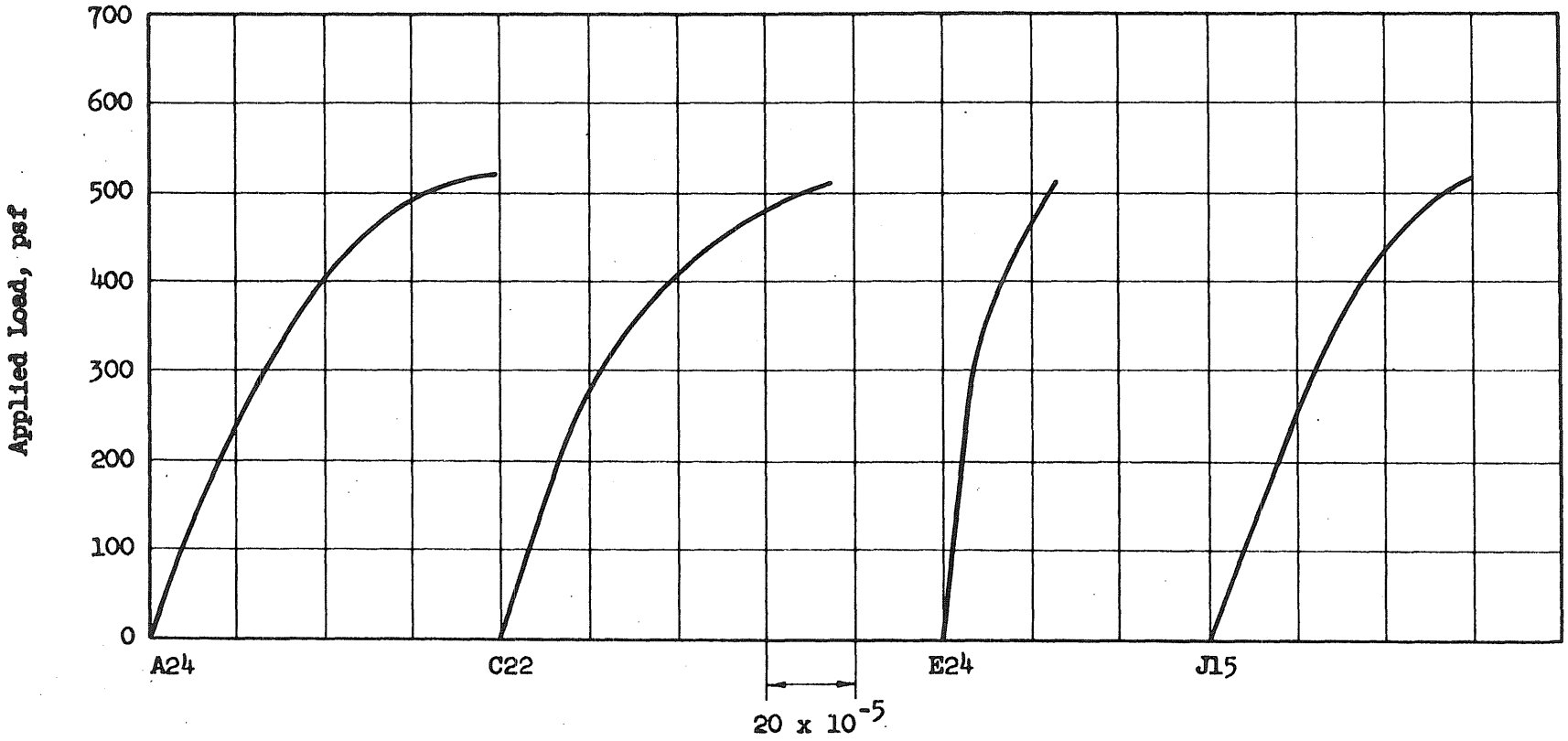

FIG. 7.17 LOAD-STRAIN CURVES FOR BOTTOM REINFORCEMENT, TEST 512

Location of strain gages is shown in Figs. 5.2 and 5.3

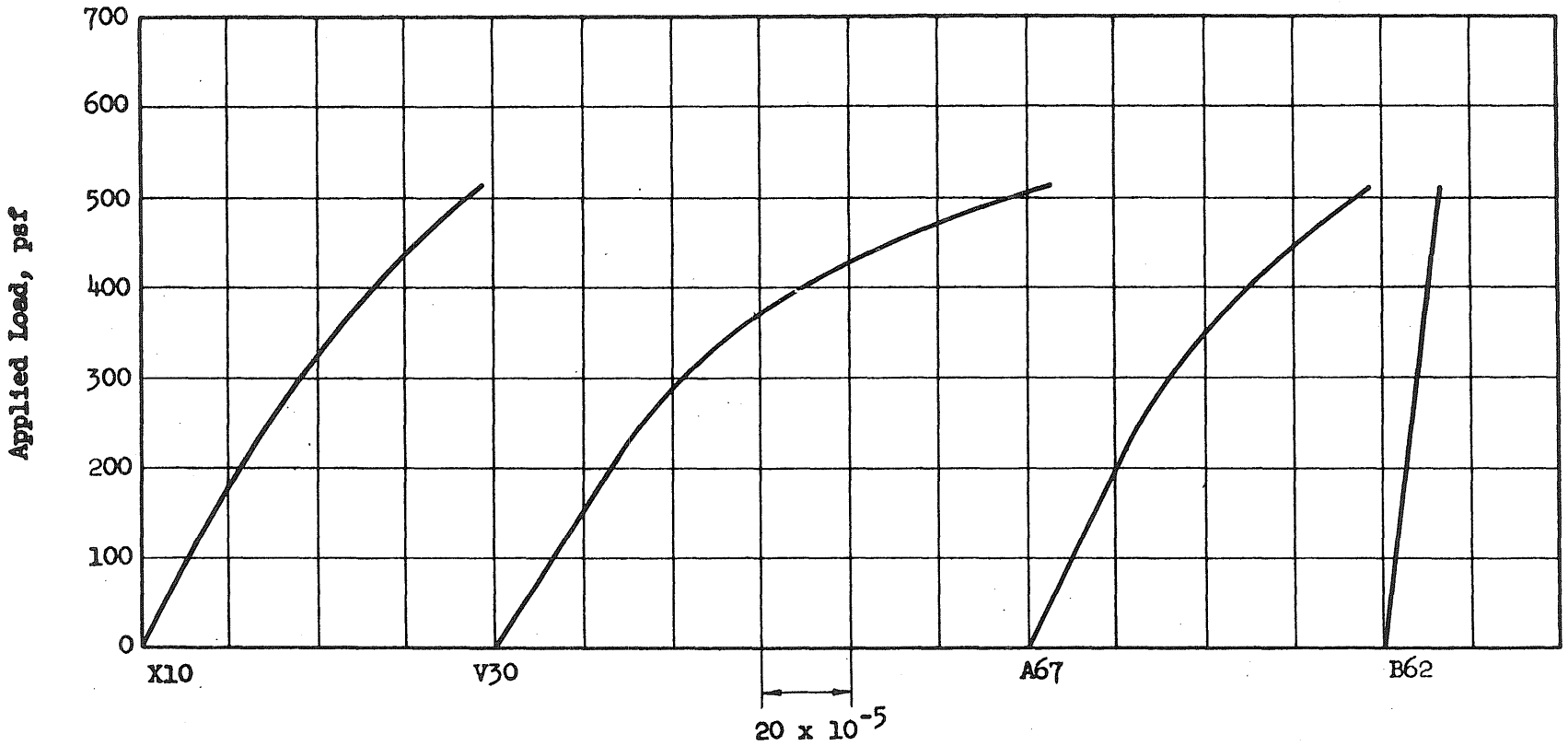

FIG. 7.18 LOAD-STRAIN CURVES FOR TOP REINFORCEMENT, TEST 512

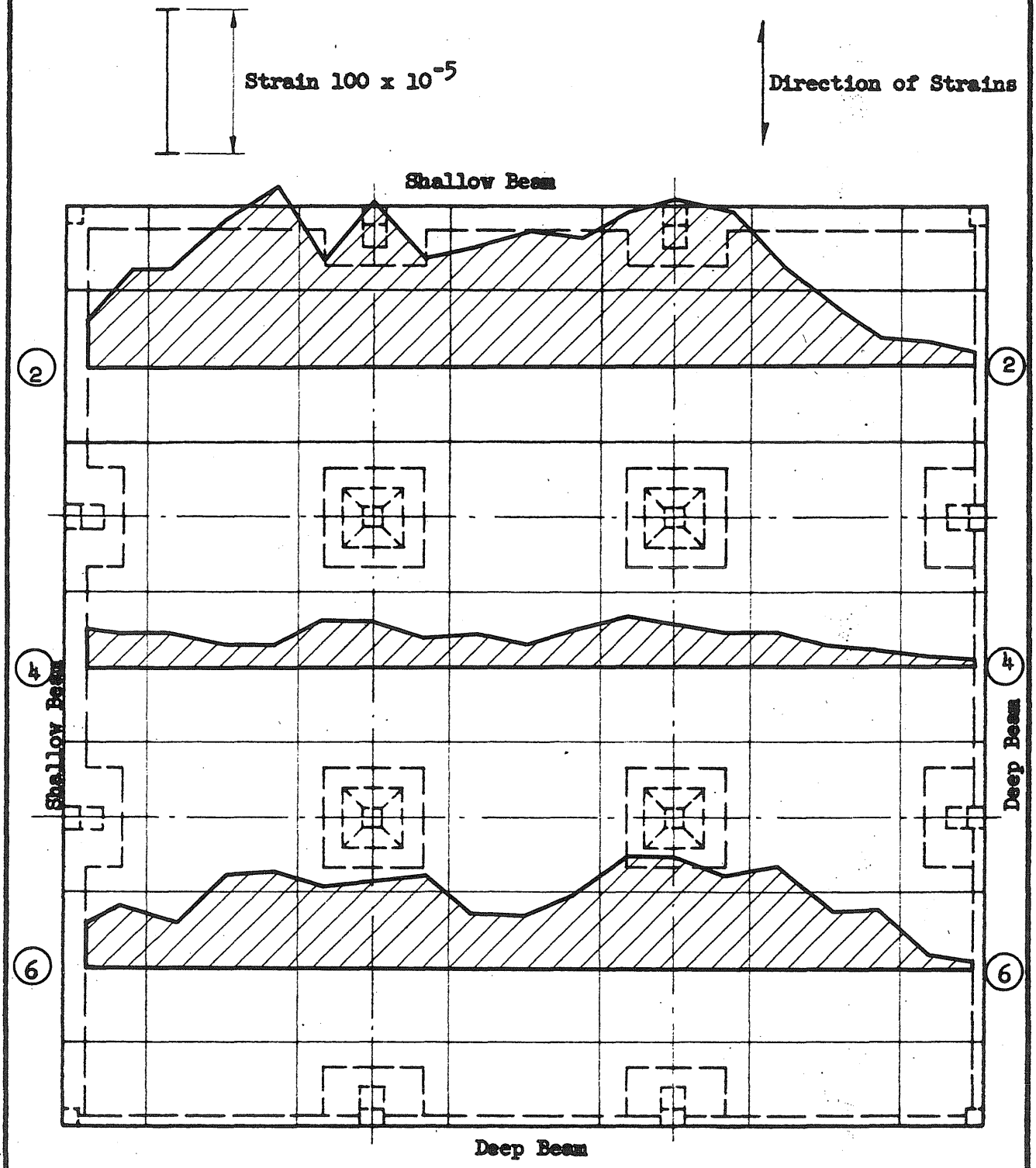

FIG. 7.19 DISTRIBUTION OF STRAINS, POSITIVE MOMENT SECTIONS, TEST 512

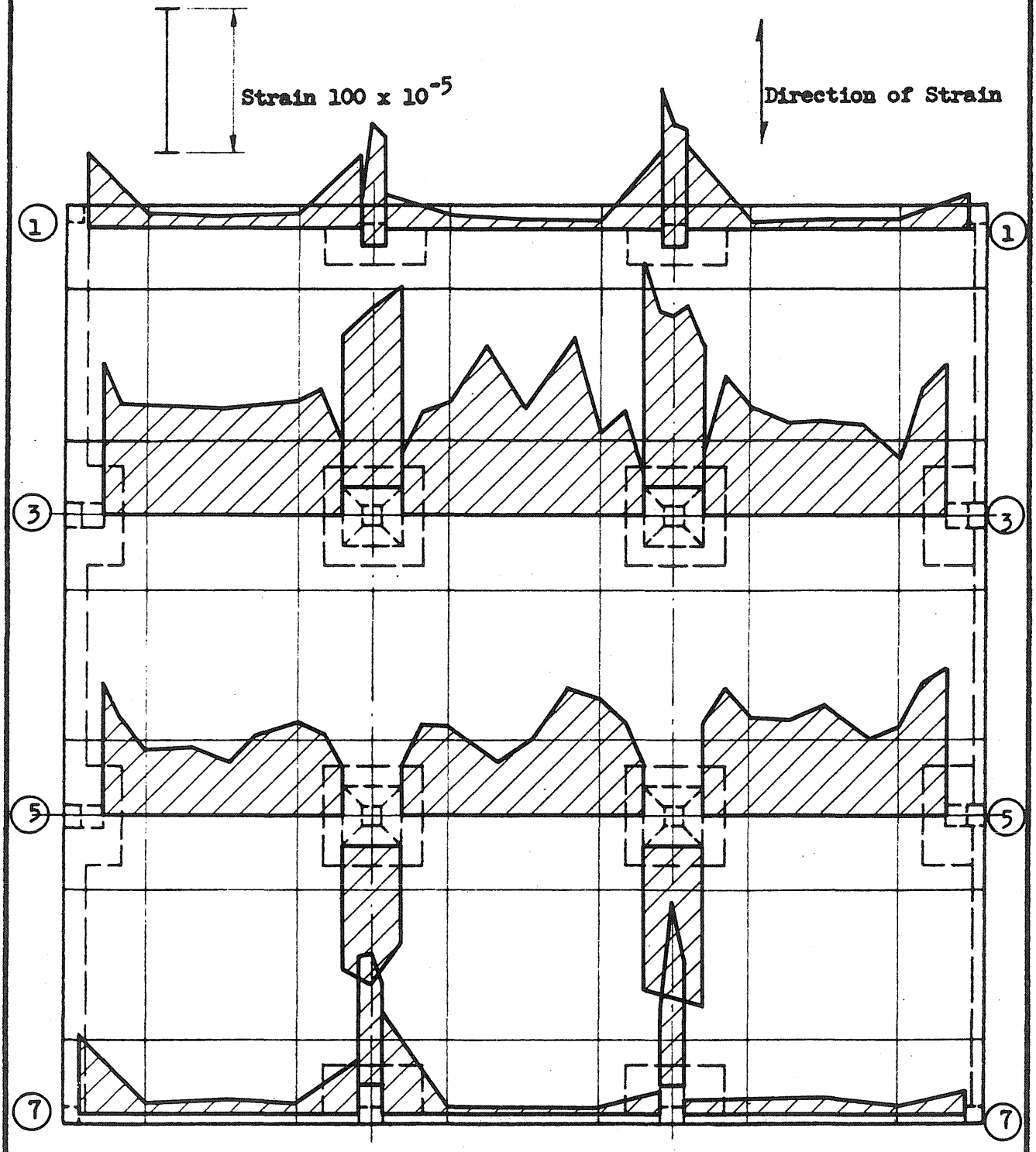

FIG. 7.20 DISTRIBUTION OF STRAINS, NEGATIVE MOMENT SECTIONS, TEST 512

Note: Strains across the column capitals are plotted with the edge of the capital as a base line

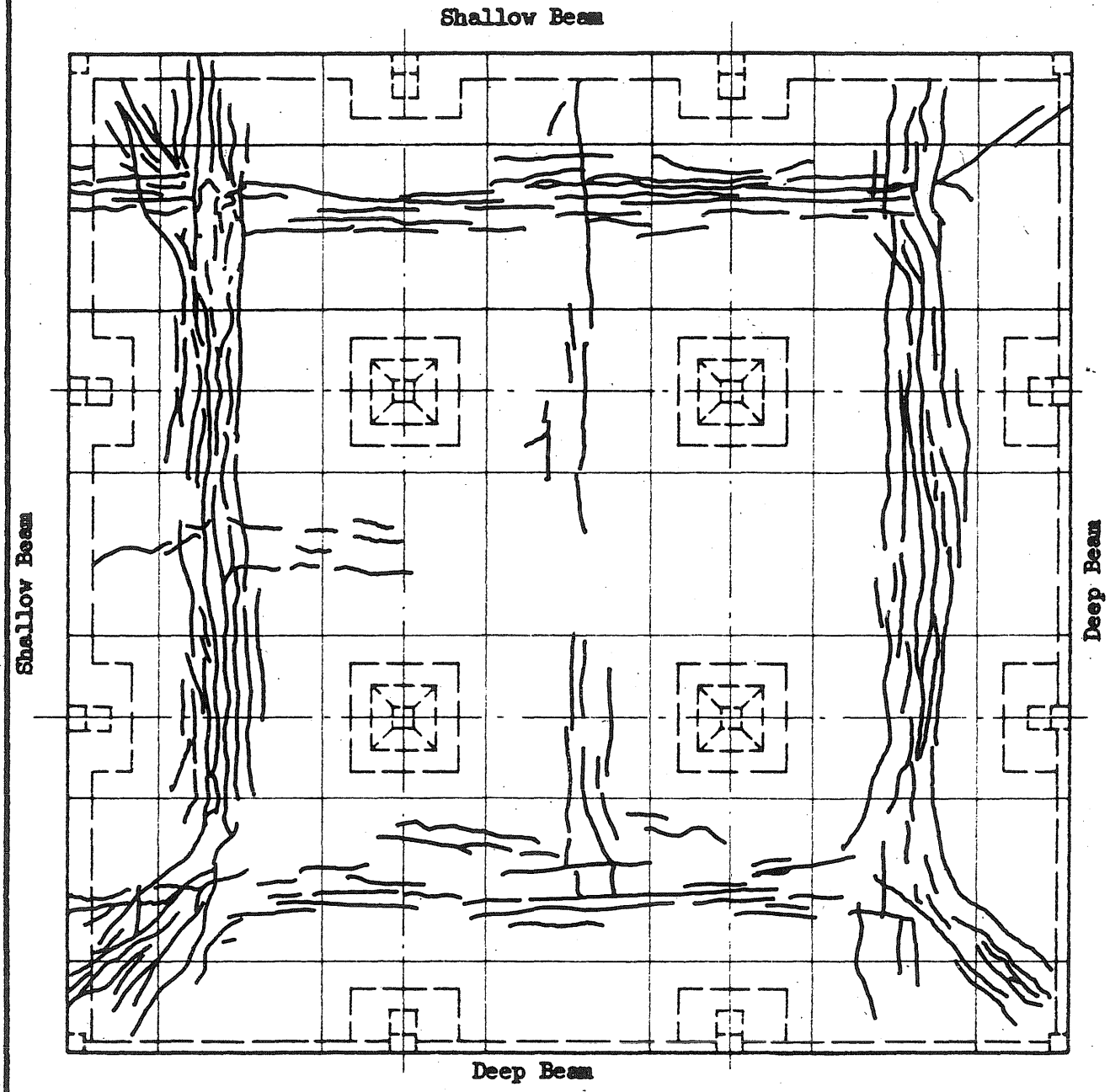

FIG. 7.21 CRACK PATTERN ON BOTTOM OF SLAB, TEST 512

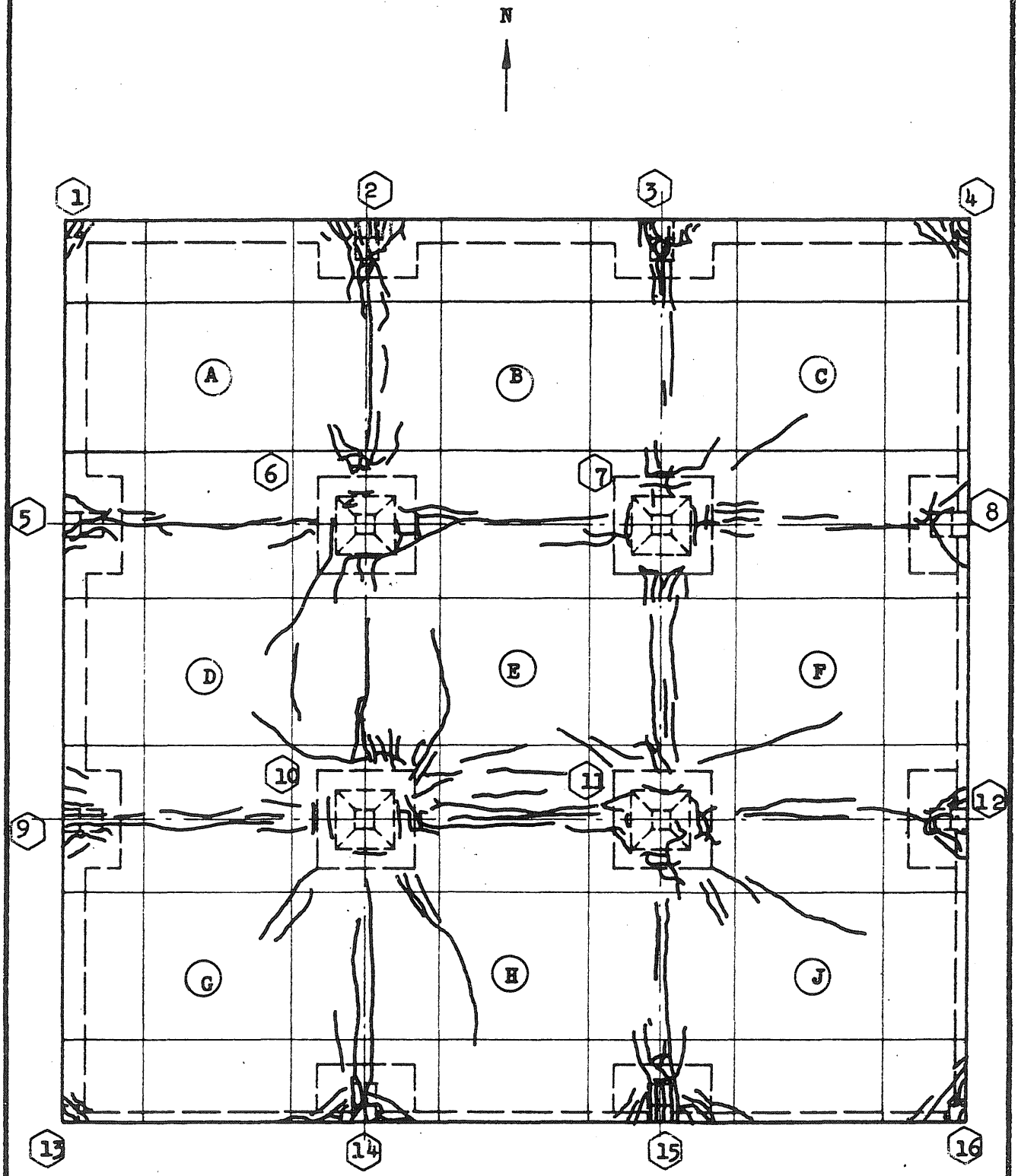

FIG. 7.22 CRACK PATTERN ON TOP OF SLAB, TEST 512

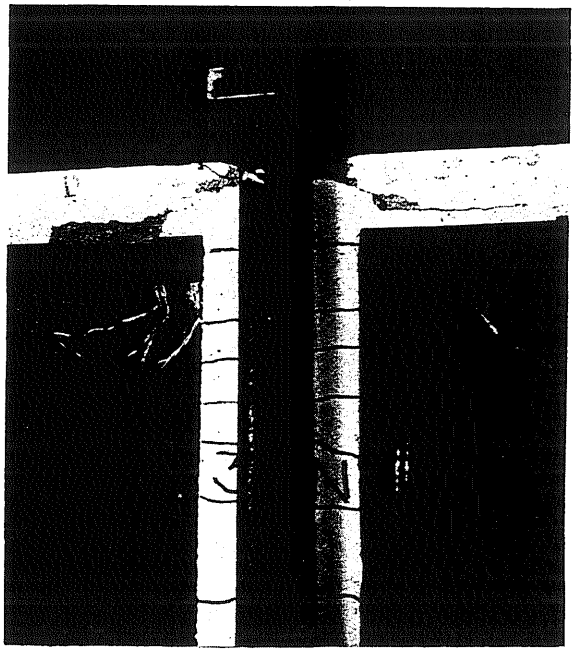

(a) Column 3

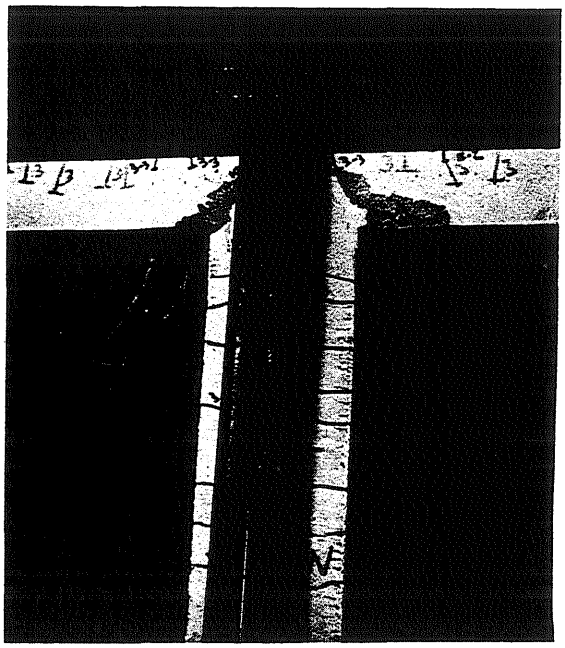

(b) Column 5

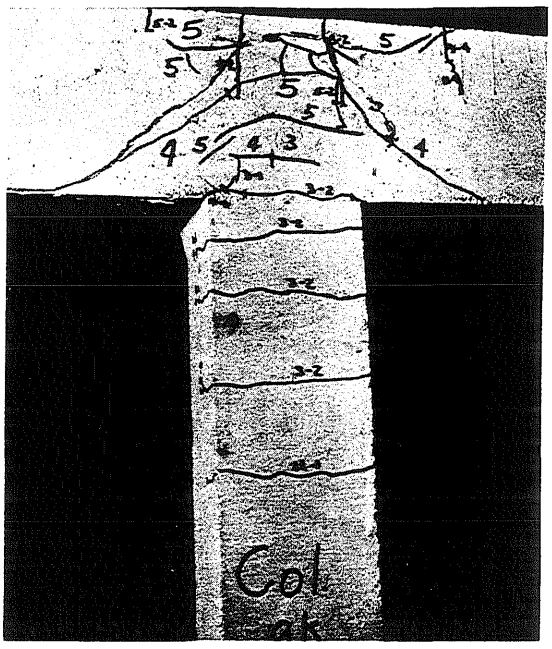

(c) Column 8

FIG. 7.23 CRACK PATTERNS AT BEAM-COLUMN CONNECTIONS

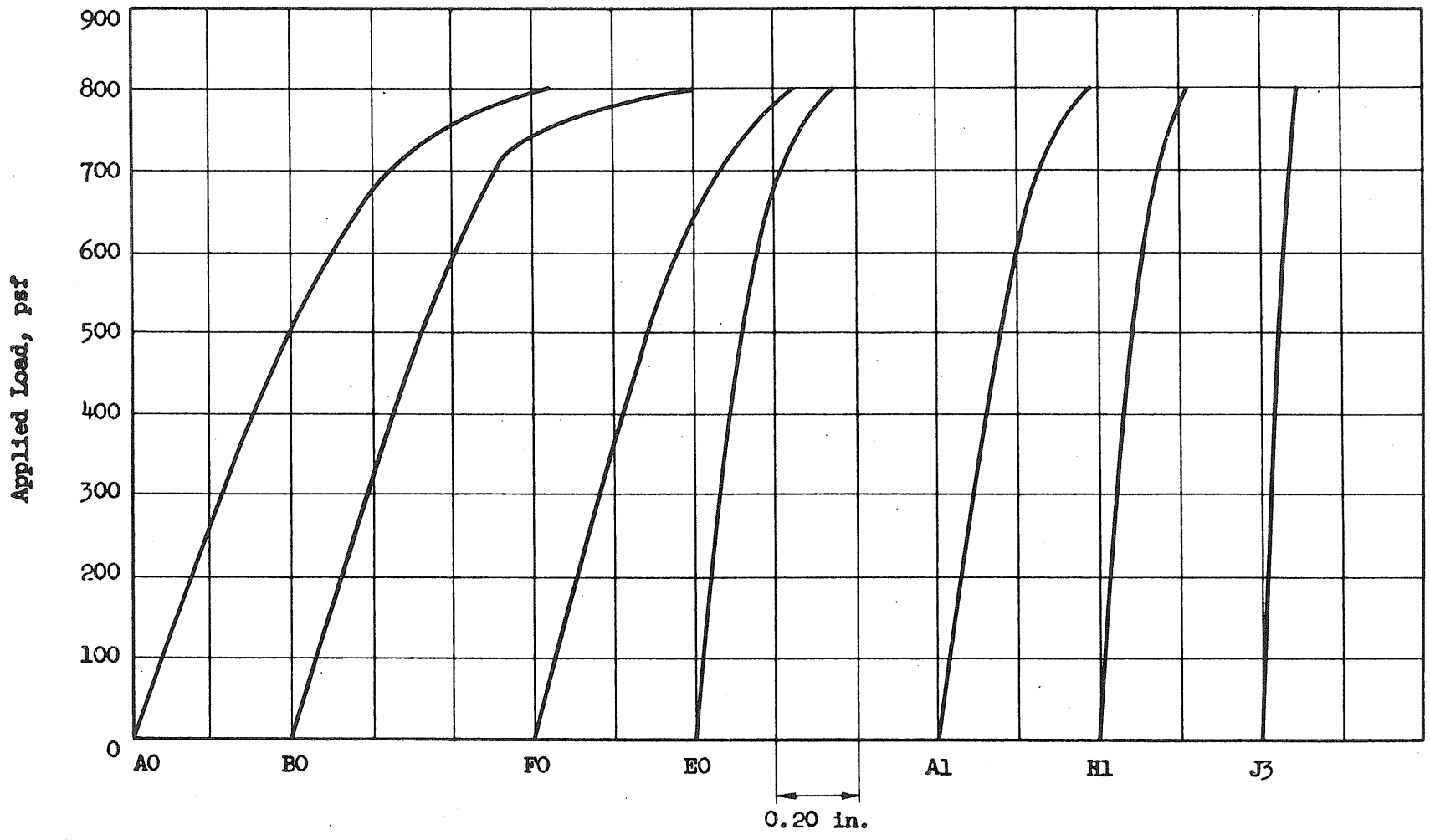

FIG. 7.24 LOAD-DEFLECTION CURVES, TEST 513

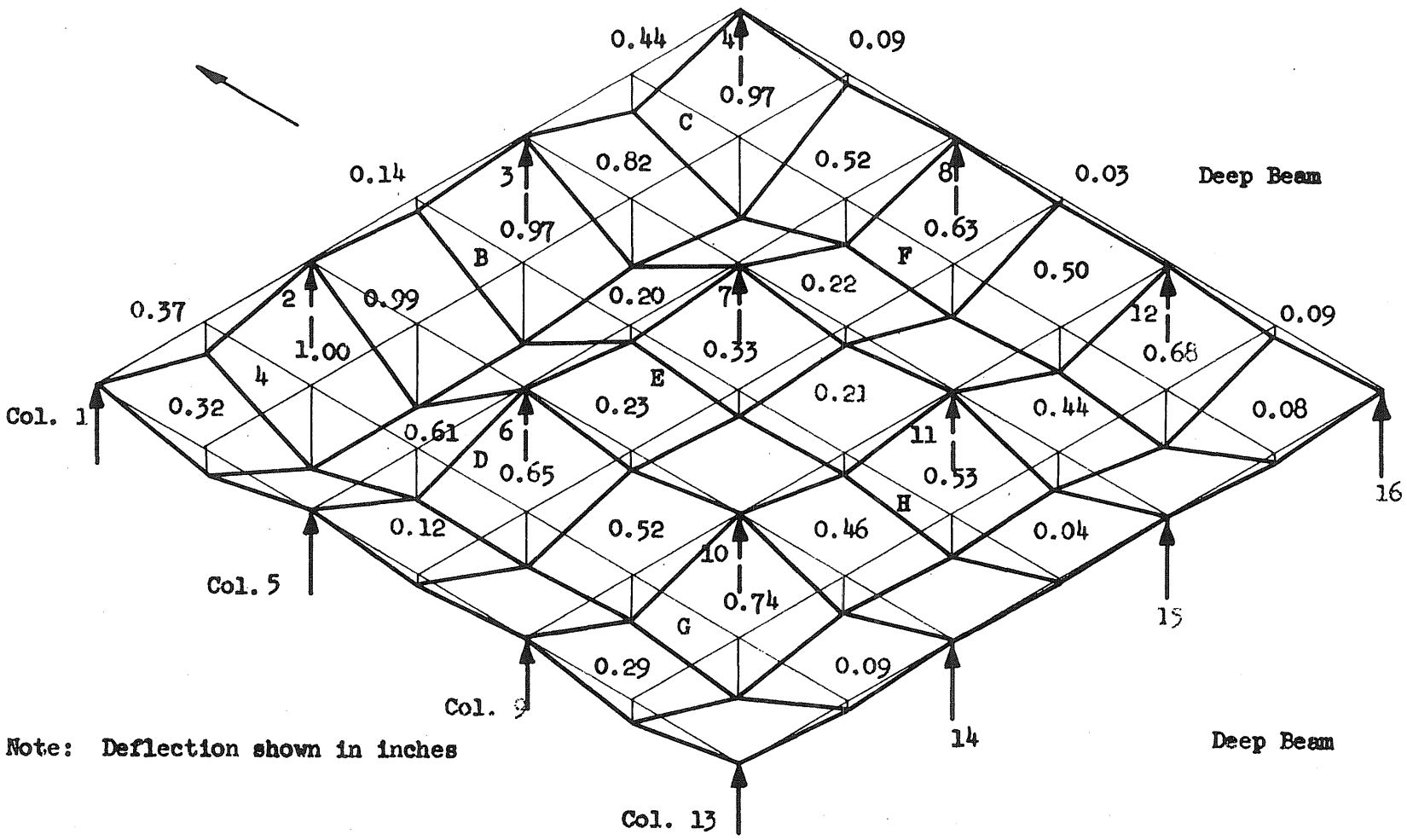

FIG. 7.25 SCHEMATIC DEFLECTION DIAGRAM, TEST 513

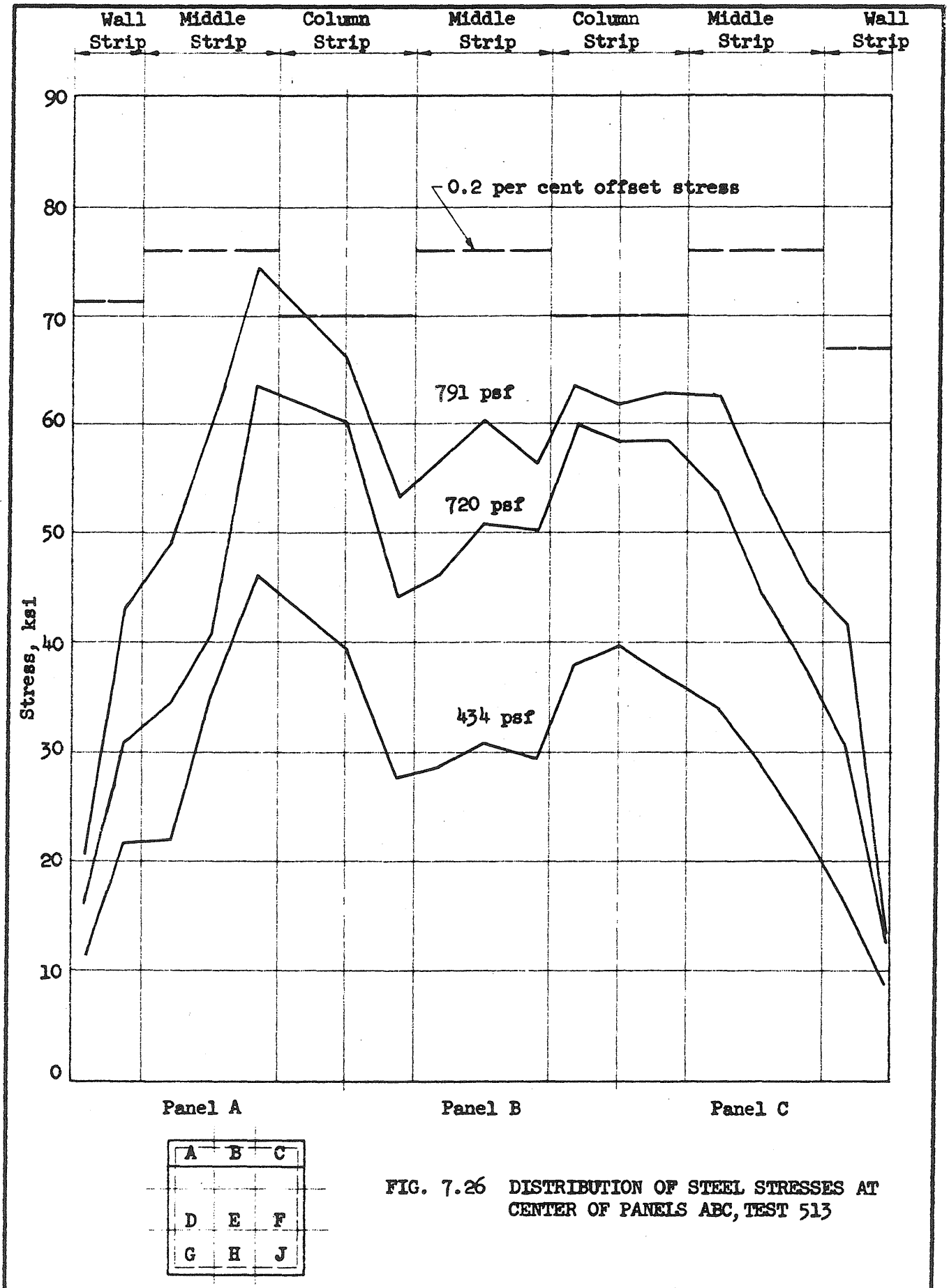

FIG. 7.26 DISTRIBUTION OF STEEL STRESSES AT CENTER OF PANELS ABC, TEST 513

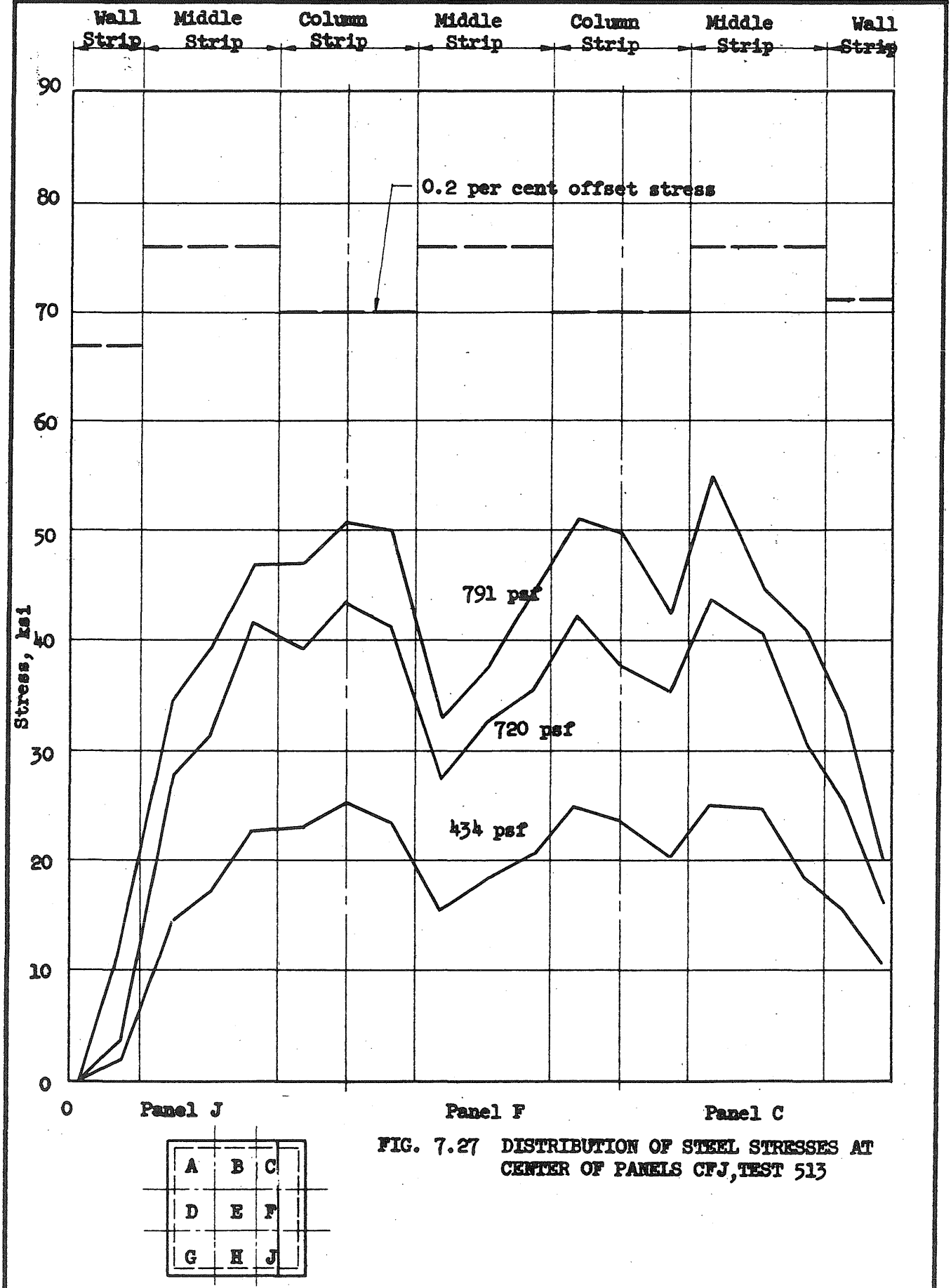

FIG. 7.27 DISTRIBUTION OF STEEL STRESSES AT CENTER OF PANELS CFJ, TEST 513

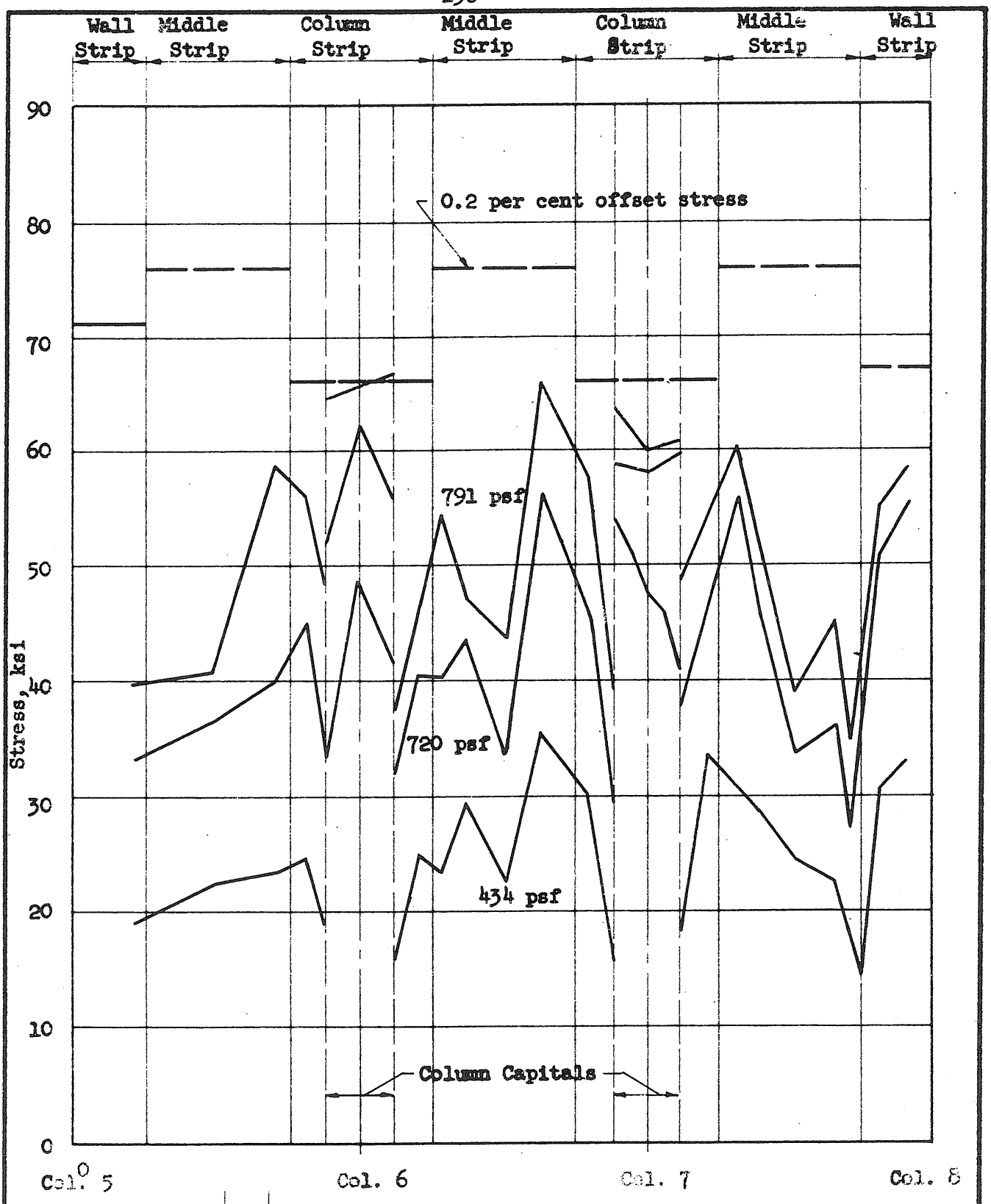

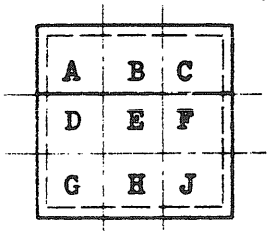

FIG. 7.28 DISTRIBUTION OF STEEL STRESS AT COLUMN LINE 5-8, TEST 513

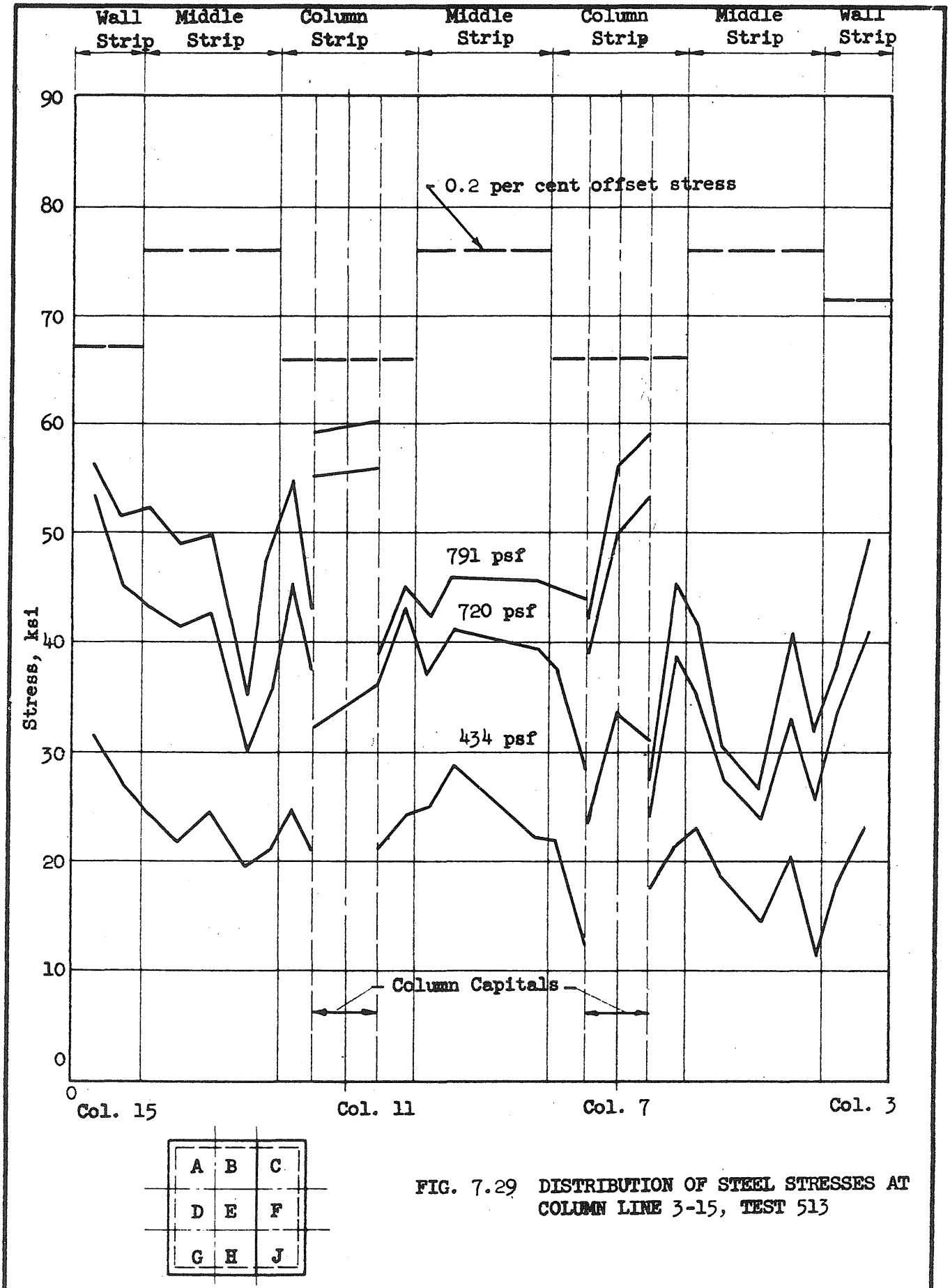

FIG. 7.29 DISTRIBUTION OF STEEL STRESSES AT COLUMN LINE 3-15, TEST 513

(a) Column 2 After Failure

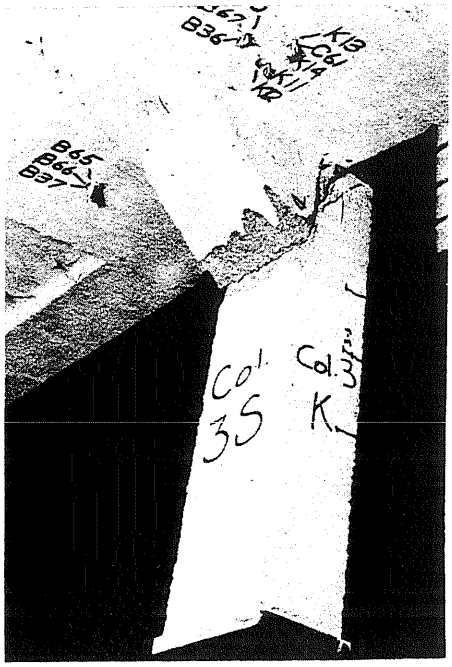

(b) Bottom View at Column 3

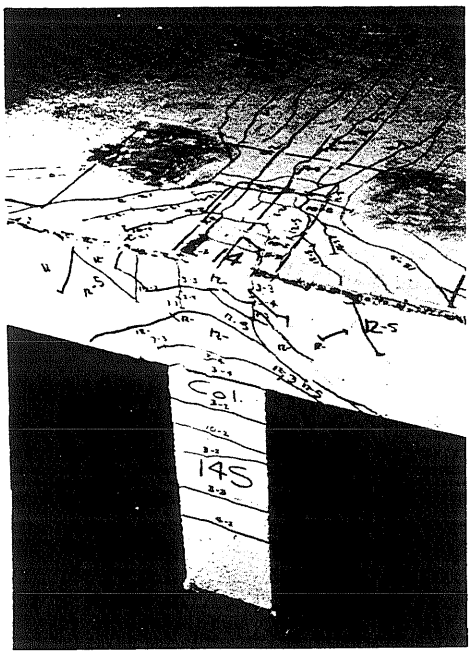

(c) Top View of Column 14

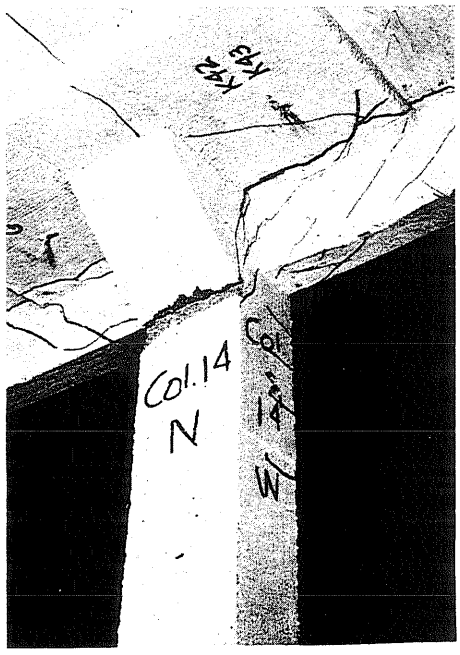

(d) Bottom View of Column 14

FIG. 7.30 PHOTOGRAPHS OF BEAM-COLUMN CONNECTIONS AFTER FAILURE

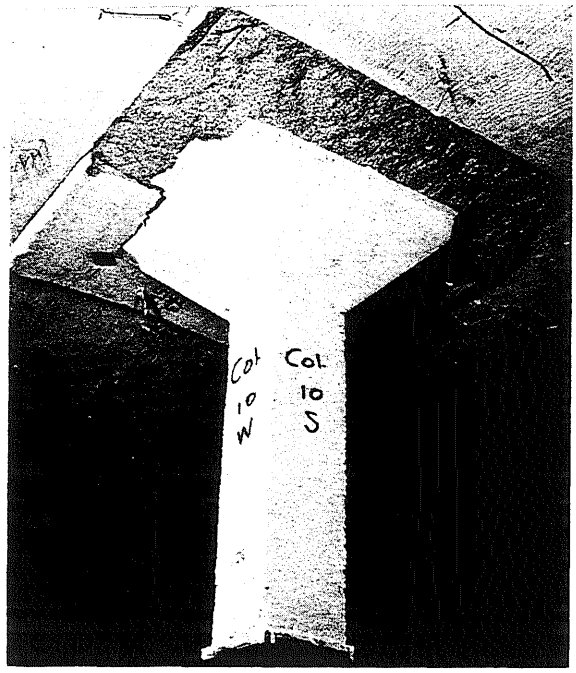

(a) View from Southwest

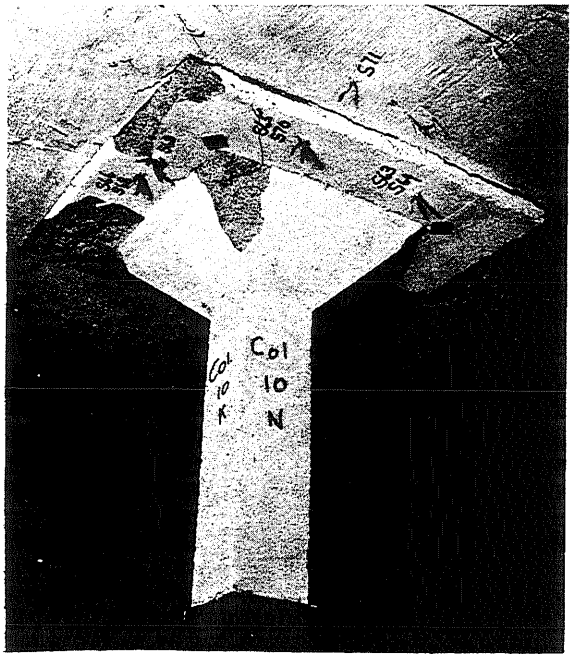

(b) View from Northeast

FIG. 7.31 PHOTOGRAPHS OF DROP PANEL AFTER TEST TO FAILURE

Shallow Beam

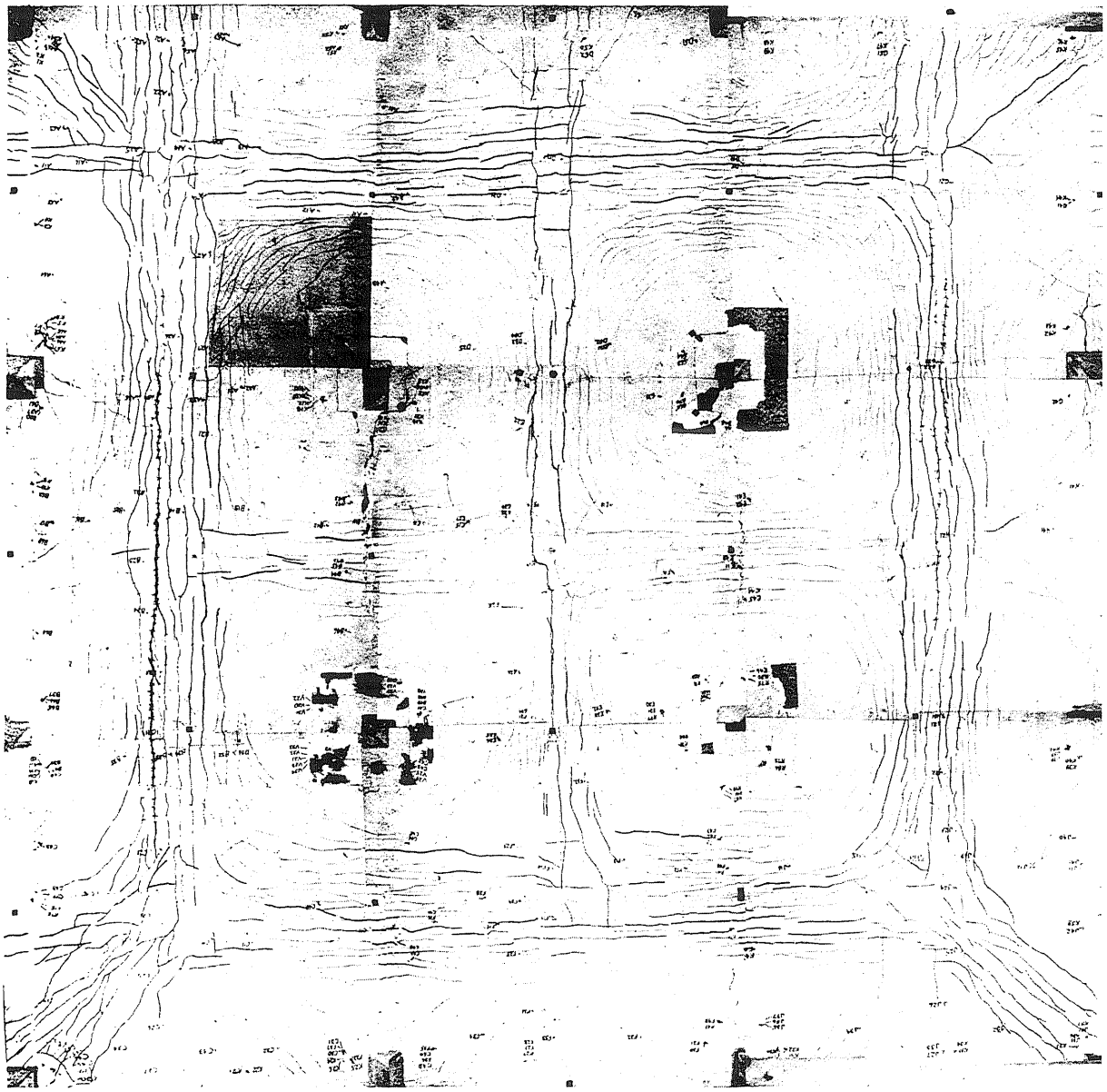

Shallow Beam

Deep Beam

Deep Beam

FIG. 7.32 CRACK PATTERN ON BOTTOM OF SLAB AFTER TEST TO FAILURE

Shallow Beam

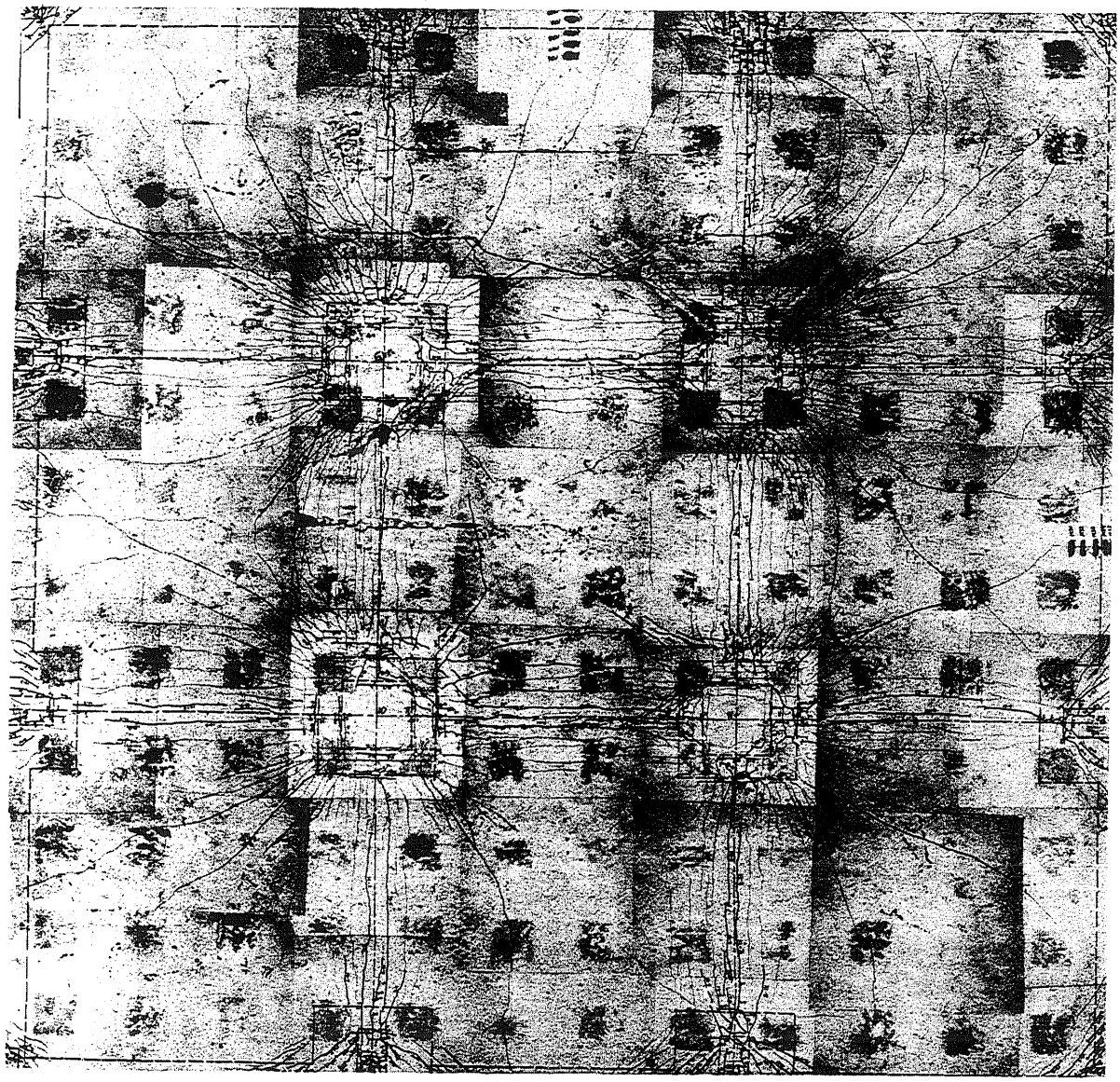

Shallow Beam

Deep Beam

Deep Beam

FIG. 7.33 CRACK PATTERN ON TOP OF SLAB AFTER TEST TO FAILURE

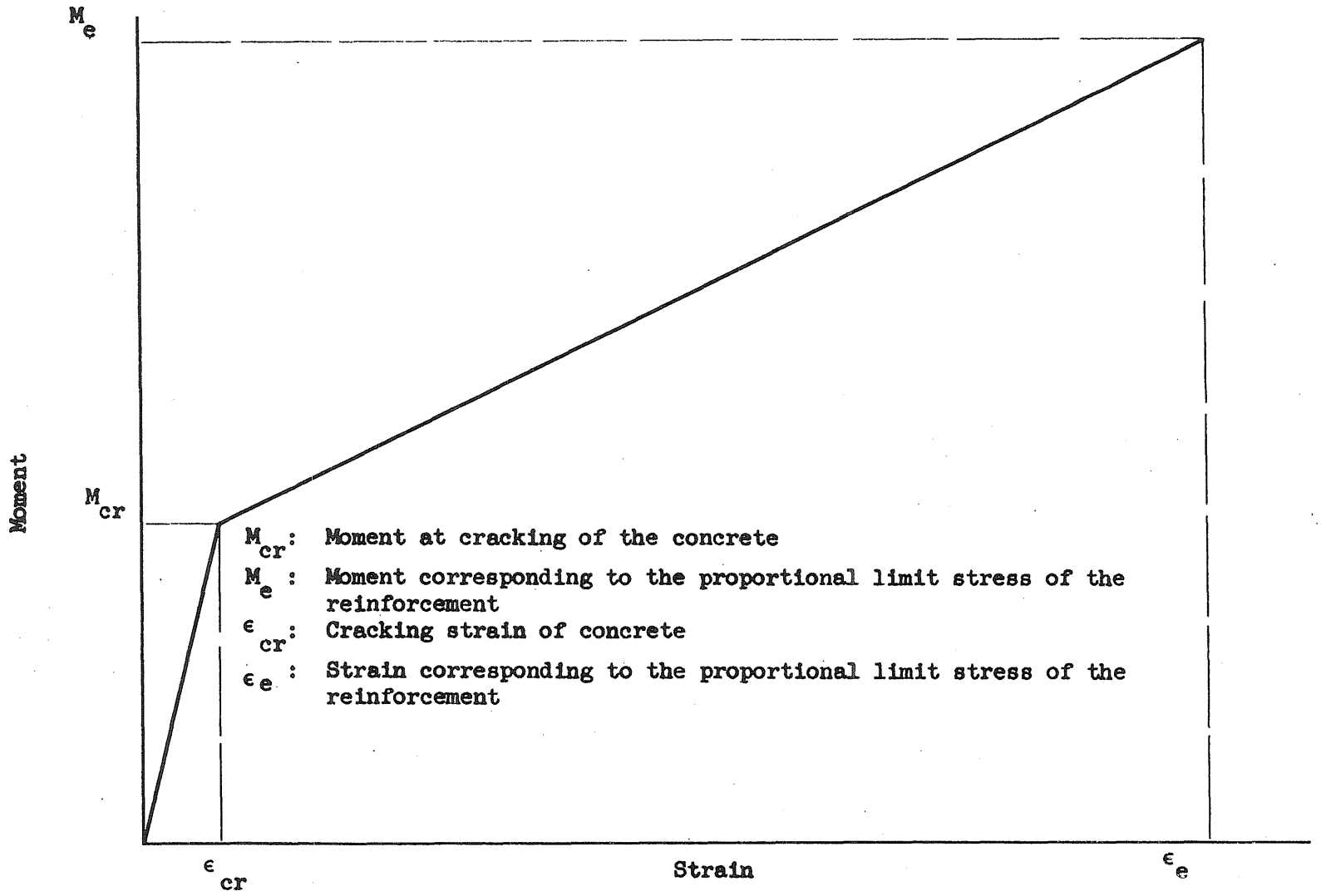

FIG. 8.1 TYPICAL MOMENT-STRAIN RELATIONSHIP FOR THE SLAB SECTIONS

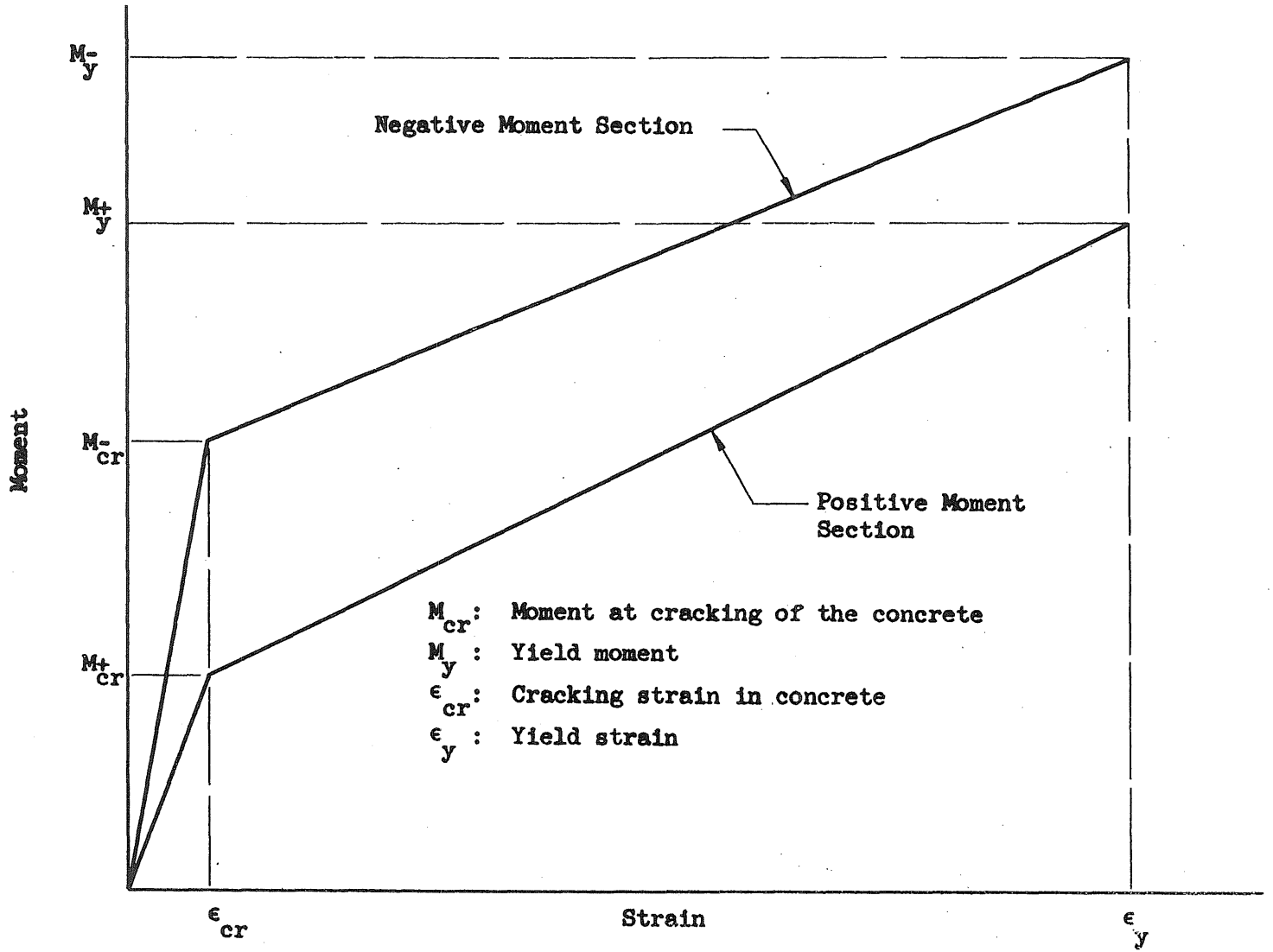

FIG. 8.2 TYPICAL MOMENT-STRAIN RELATIONSHIP FOR BEAM SECTIONS

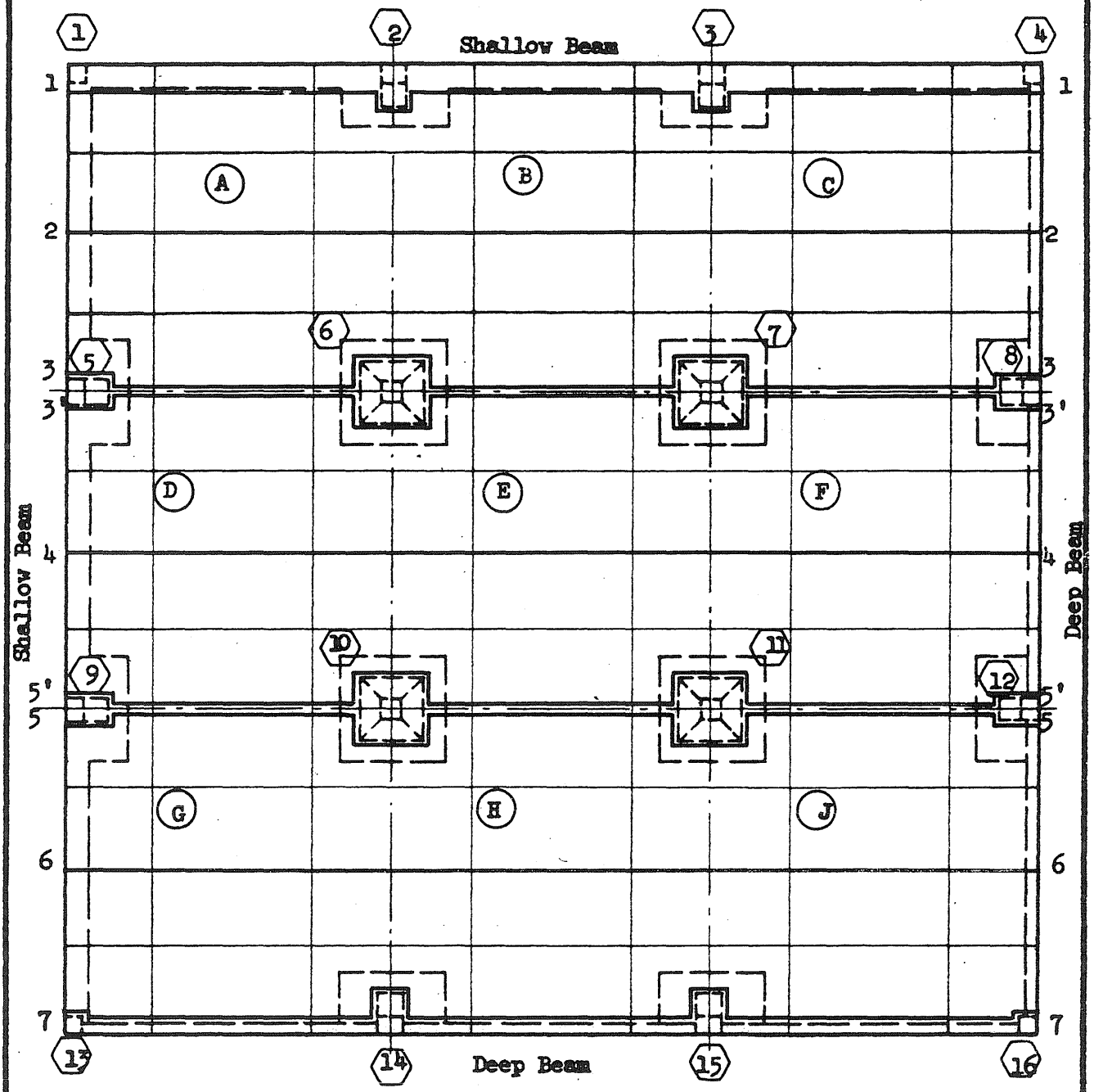

FIG. 8.3 LOCATION OF MOMENT SECTIONS

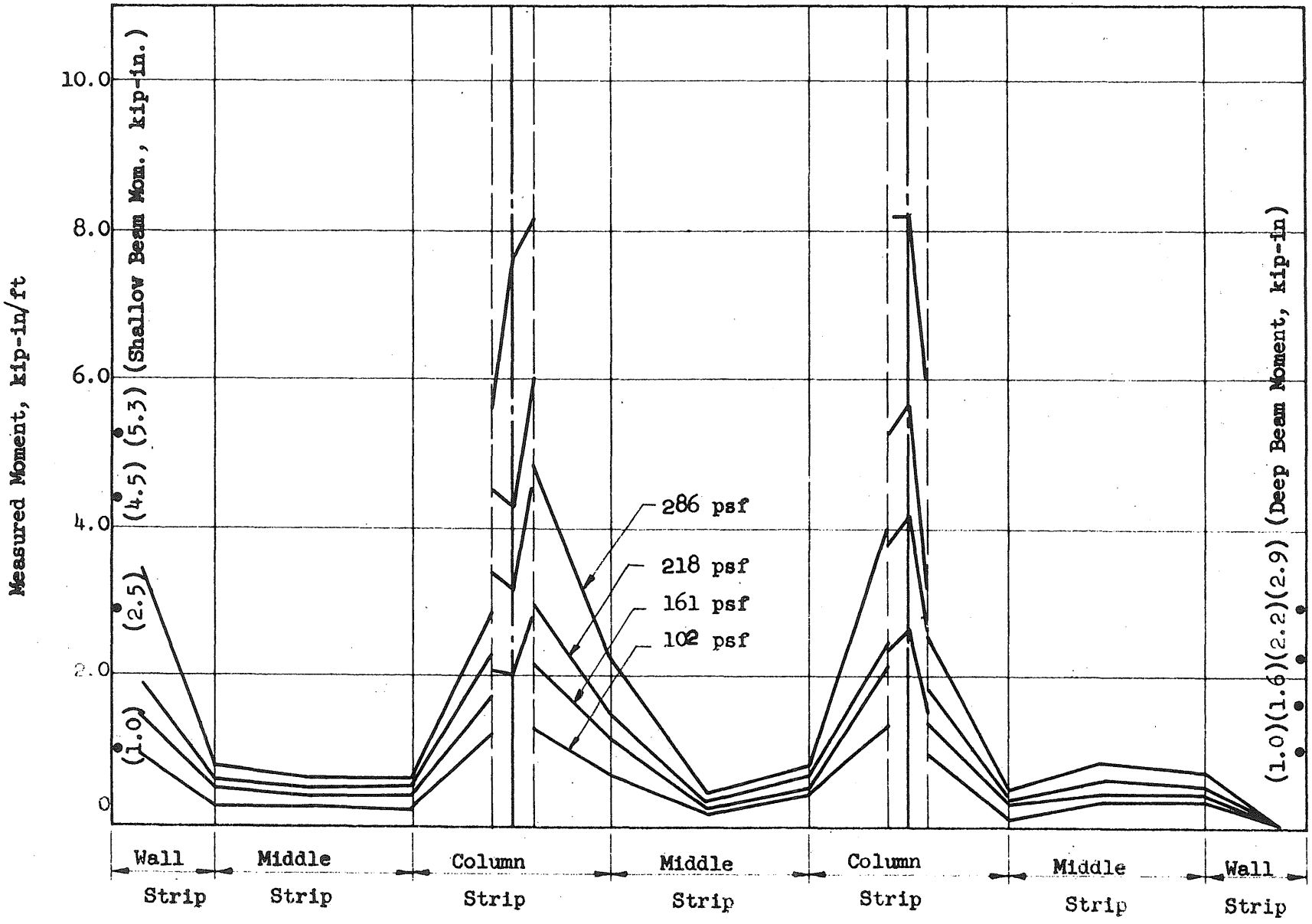

FIG. 8.4 DISTRIBUTION OF MEASURED MOMENTS, SECTION 1-1

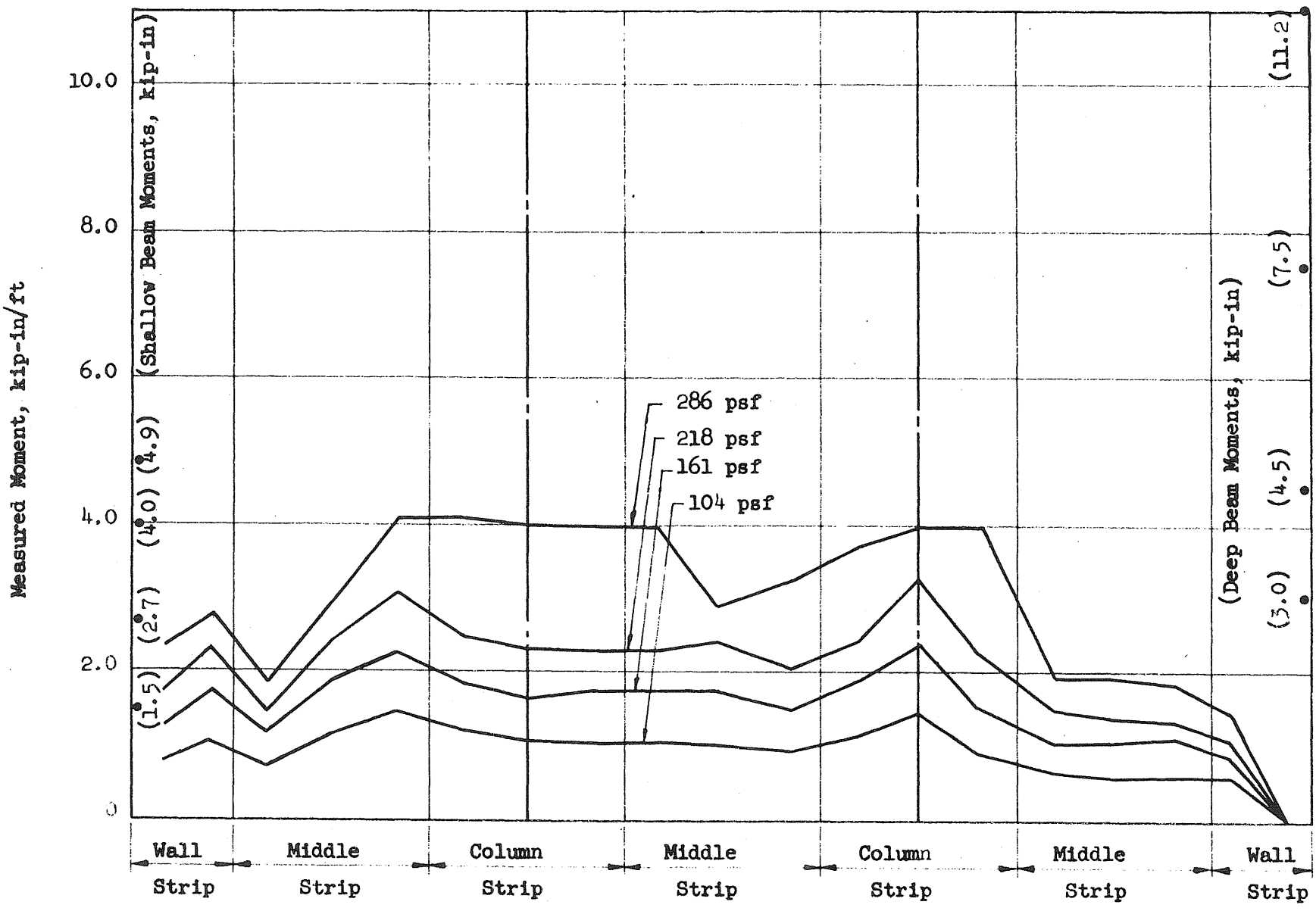

FIG. 8.5 DISTRIBUTION OF MEASURED MOMENTS, SECTION 2-2

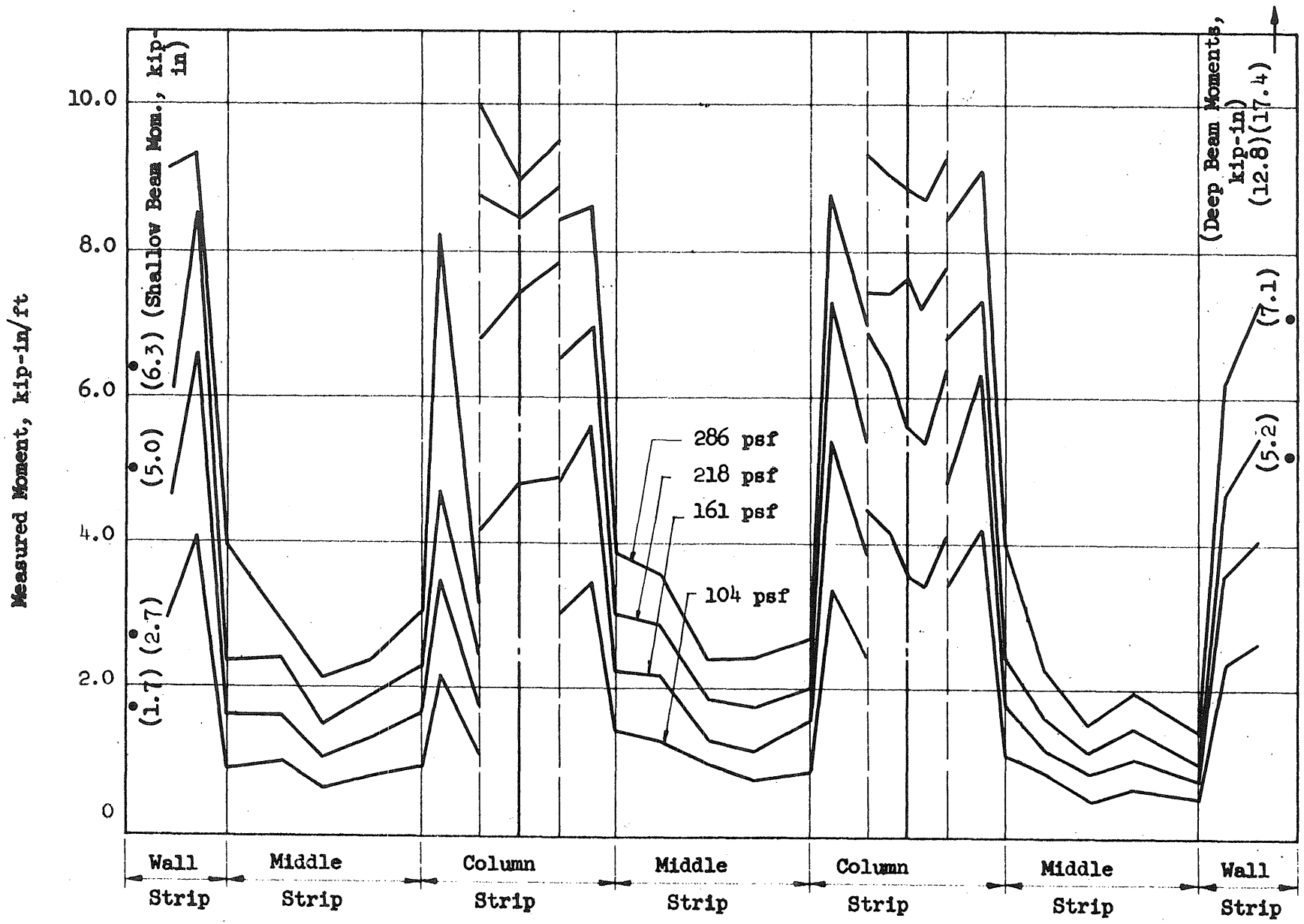

FIG. 8.6 DISTRIBUTION OF MEASURED MOMENTS, SECTION 3-3

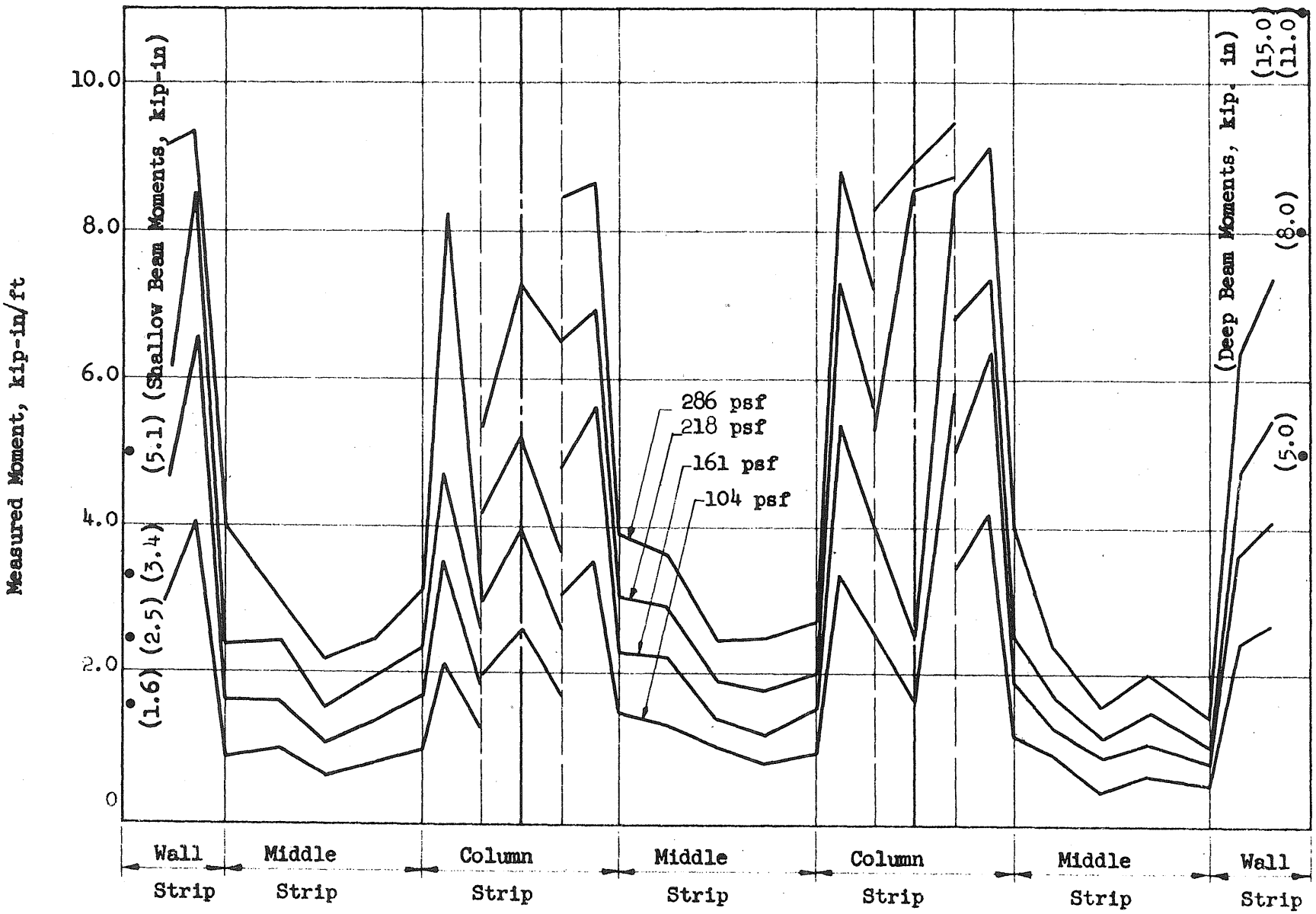

FIG. 8.7 DISTRIBUTION OF MEASURED MOMENT, SECTION 3' - 3'

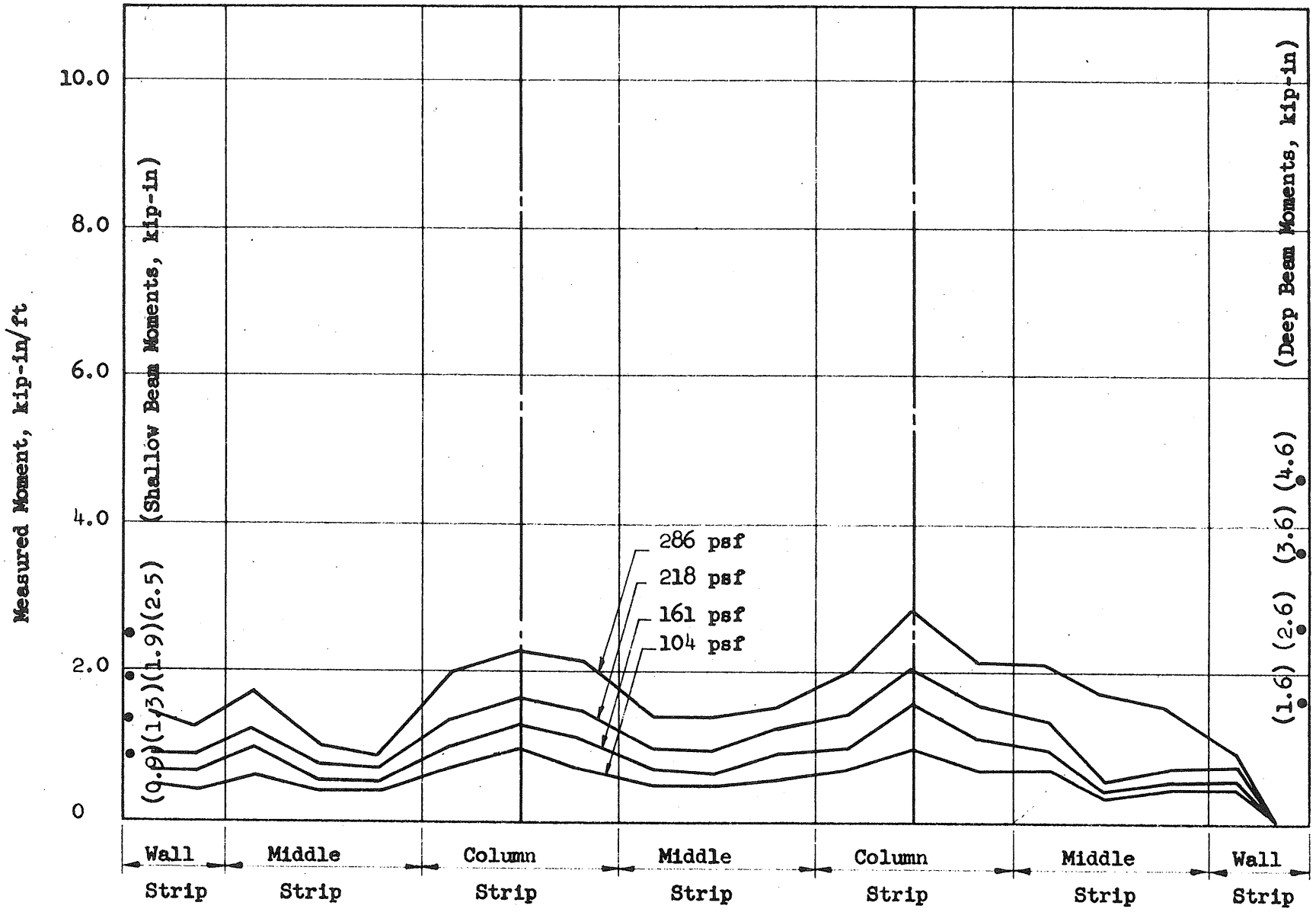

FIG. 8.8 DISTRIBUTION OF MEASURED MOMENT, SECTION 4-4

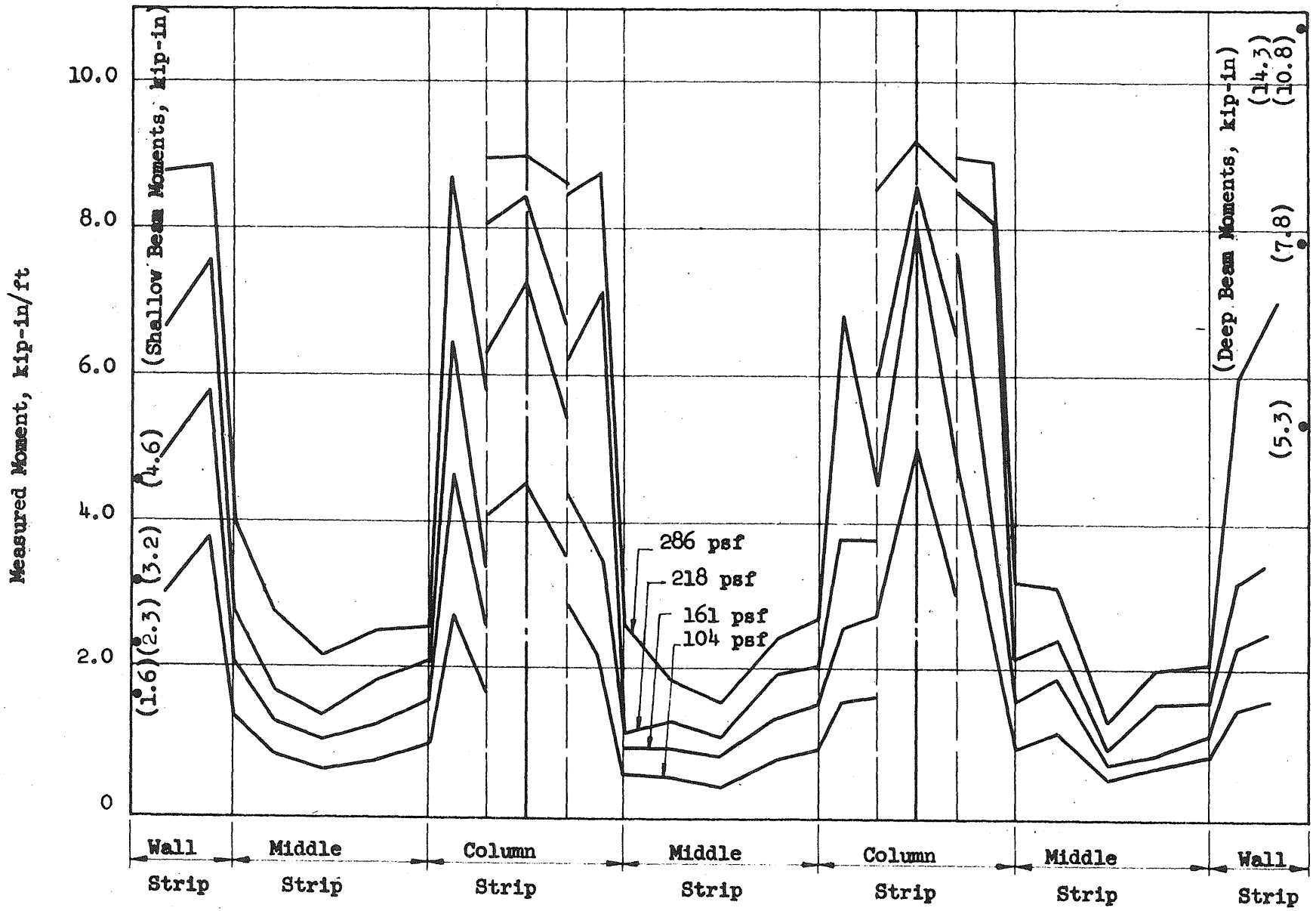

FIG. 8.9 DISTRIBUTION OF MEASURED MOMENTS, SECTION 5' - 5'

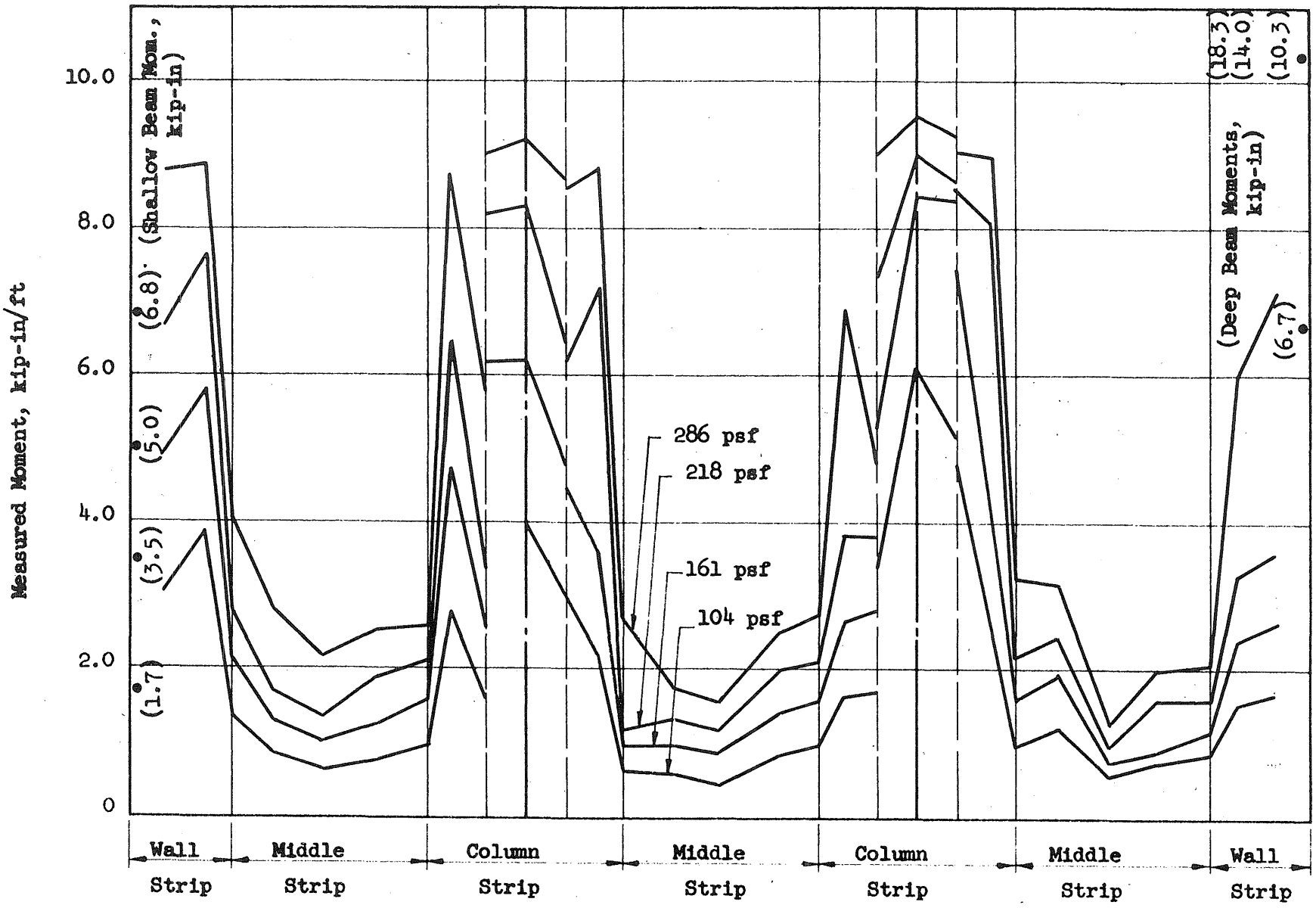

FIG. 8.10 DISTRIBUTION OF MEASURED MOMENTS, SECTION 5-5

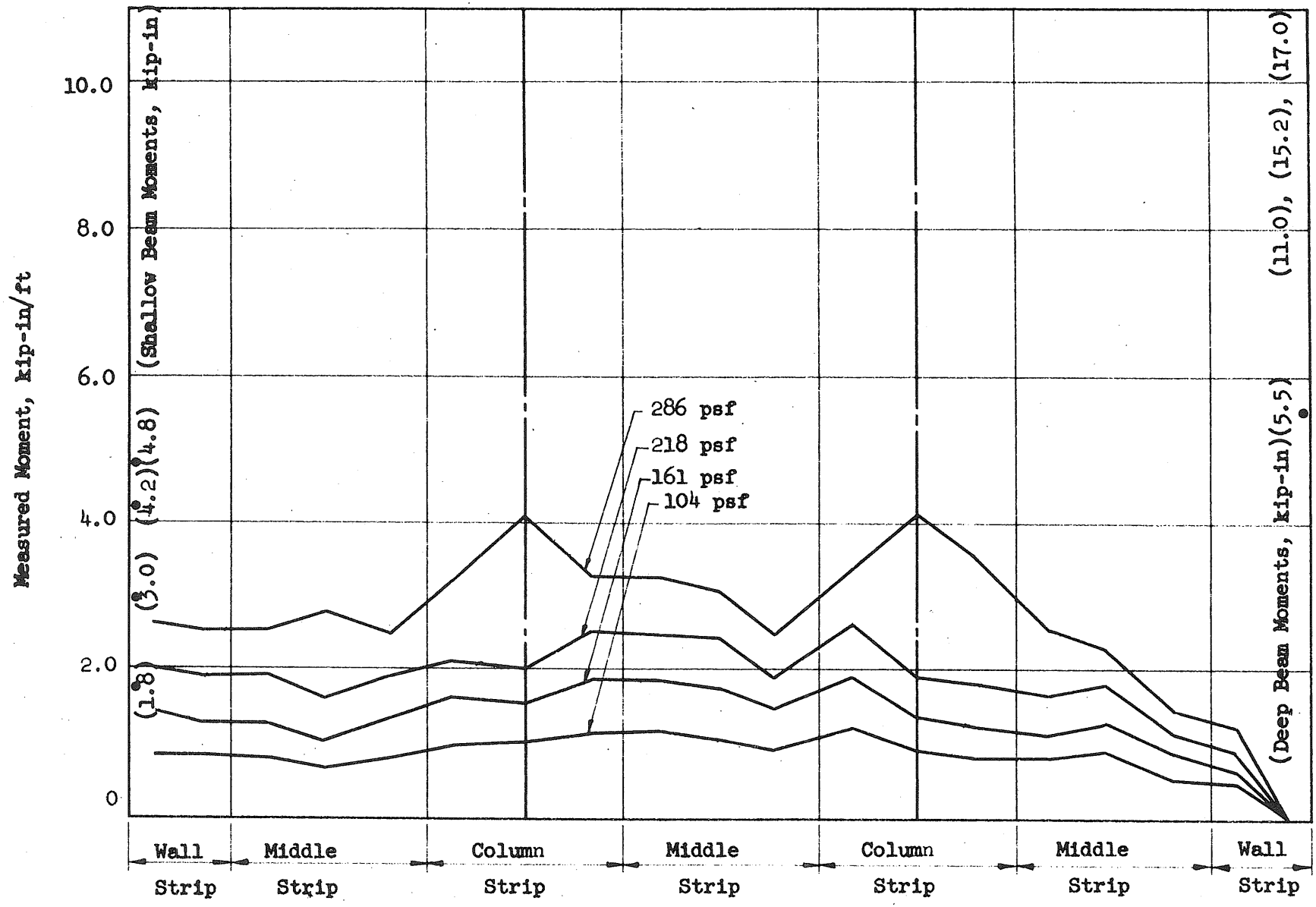

FIG. 8.11 DISTRIBUTION OF MEASURED MOMENTS, SECTION 6-6

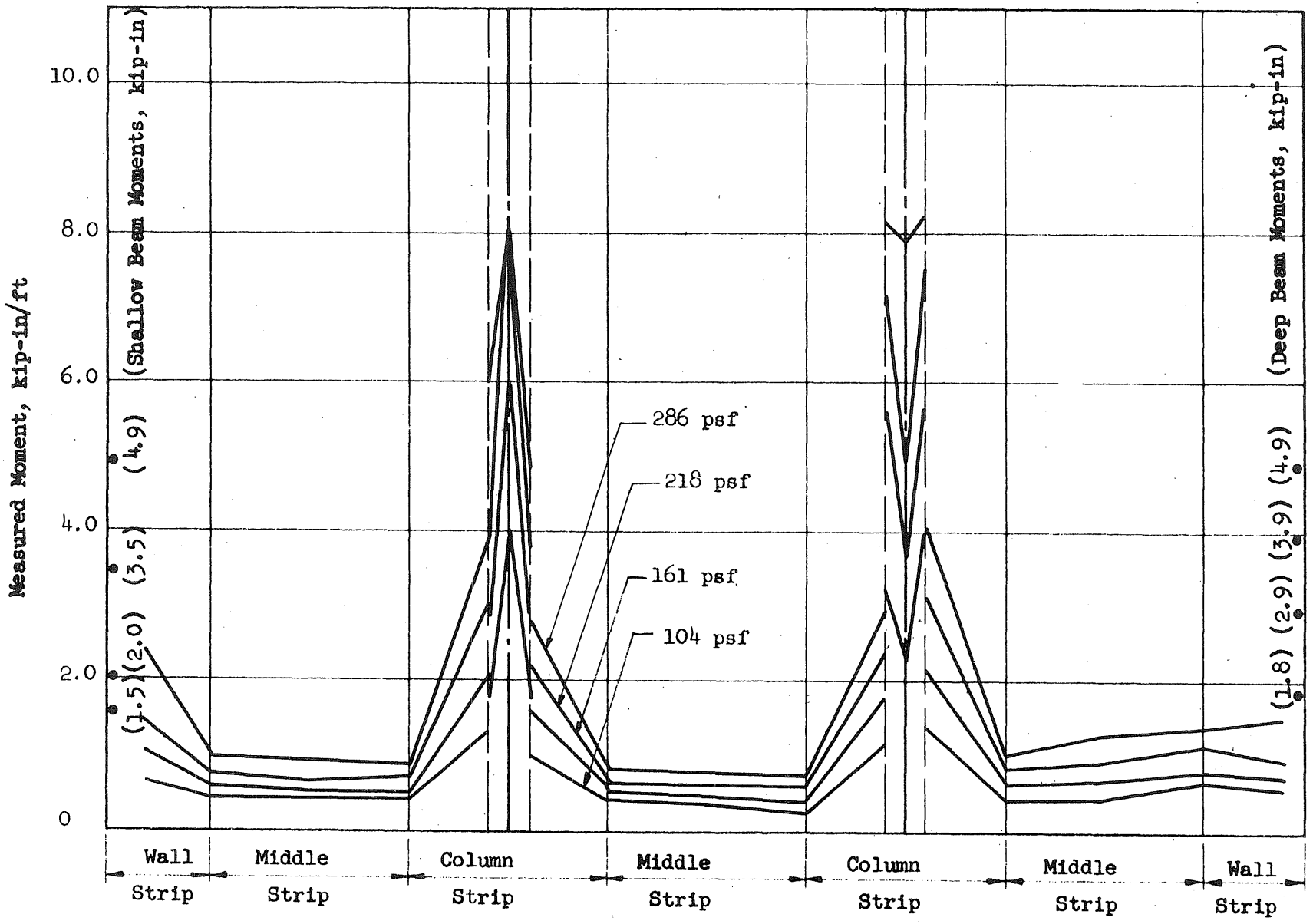

FIG. 8.12 DISTRIBUTION OF MEASURED MOMENTS, SECTION 7-7

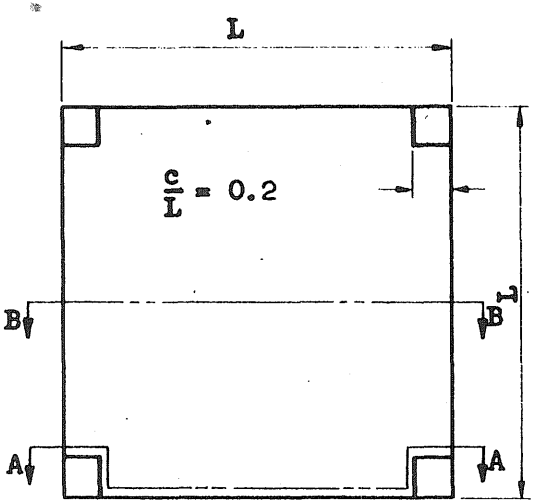

Plan View of Panel

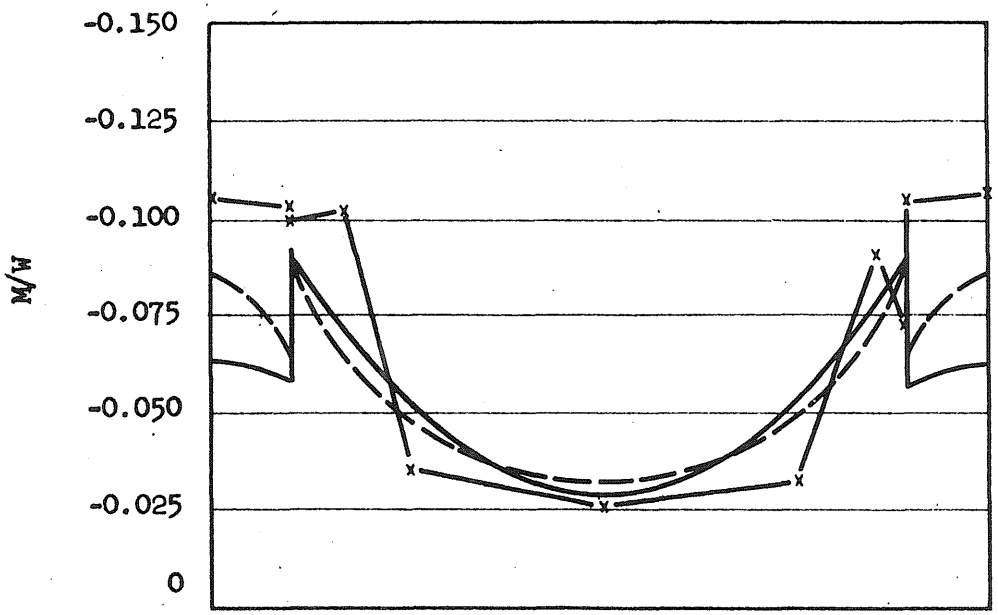

Moment Across Section AA

Theoretical Moment based on uniform distribution of reaction over capital area

Theoretical moment based on infinite stiffness of capital at midpoint

Measured moment

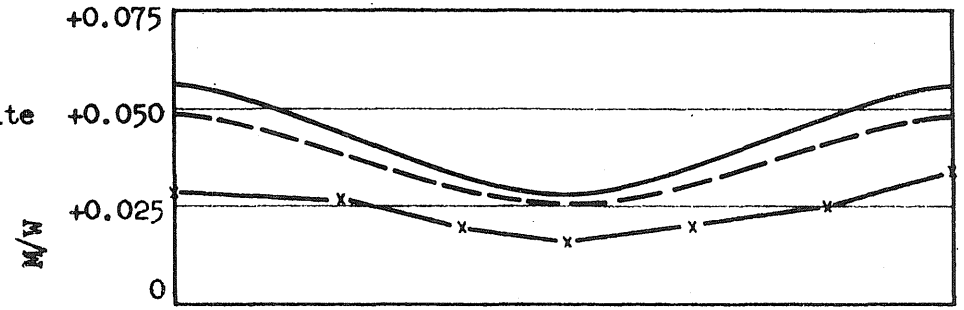

Moment Across Section BB

FIG. 8.13 COMPARISON OF MEASURED MOMENTS WITH THEORETICAL MOMENTS IN THE INTERIOR PANEL - SOLUTION BY NIELSEN

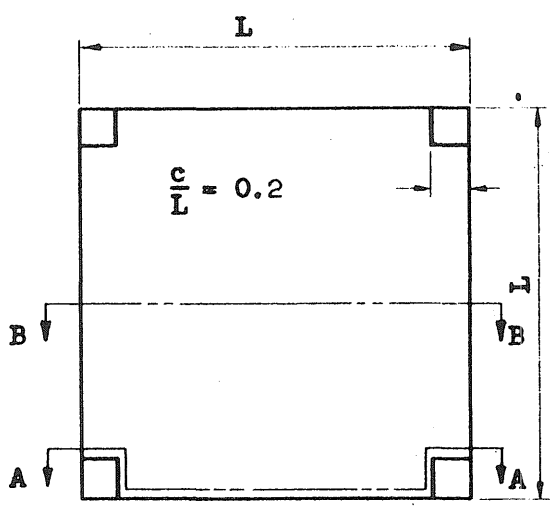

Plan View of Panel

Theoretical Moments

Measured Moments

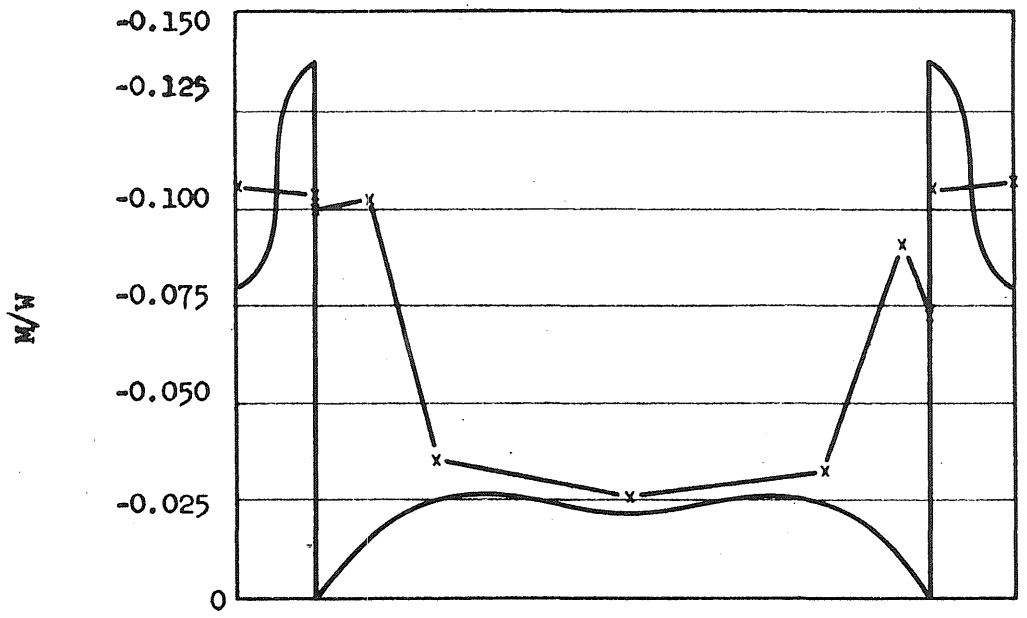

Moment Across Section AA

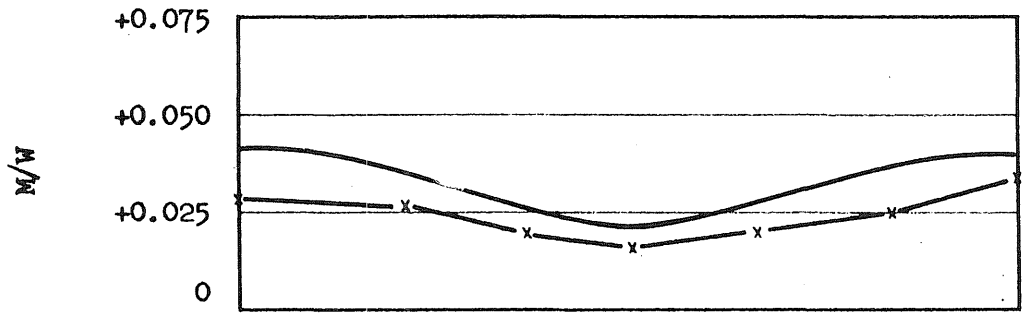

Moment Across Section BB

FIG. 8.14 COMPARISON OF MEASURED MOMENTS WITH THEORETICAL MOMENTS IN THE INTERIOR PANEL - UNIVERSITY OF ILLINOIS SOLUTION

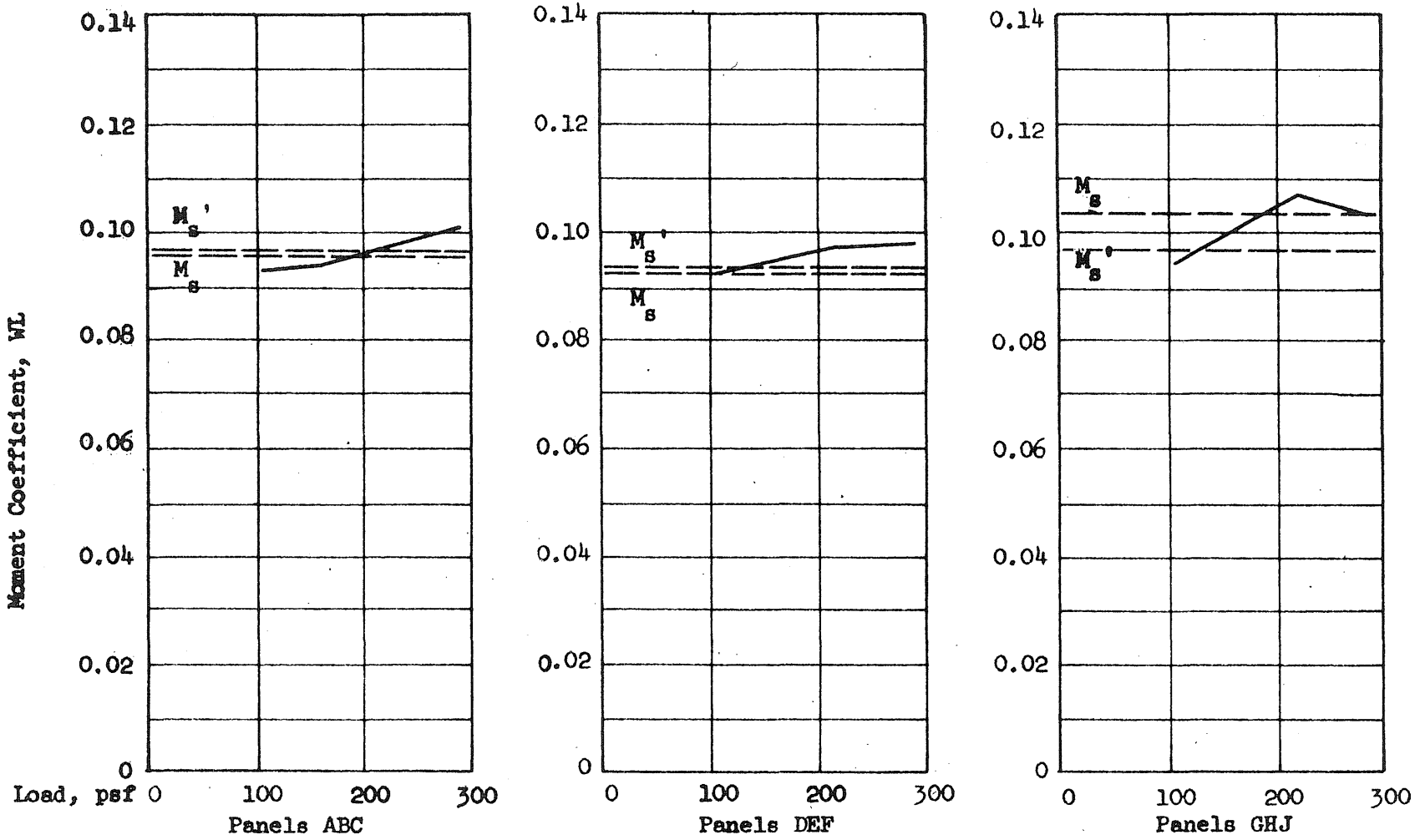

M_s: Static Moment based on uniform distribution of reaction along all supported edges.

M_s': Static Moment based on uniform distribution of reaction along edges of capitals and/or columns.

FIG. 8.15 COMPARISON OF MEASURED AND STATIC TOTAL MOMENTS COEFFICIENTS

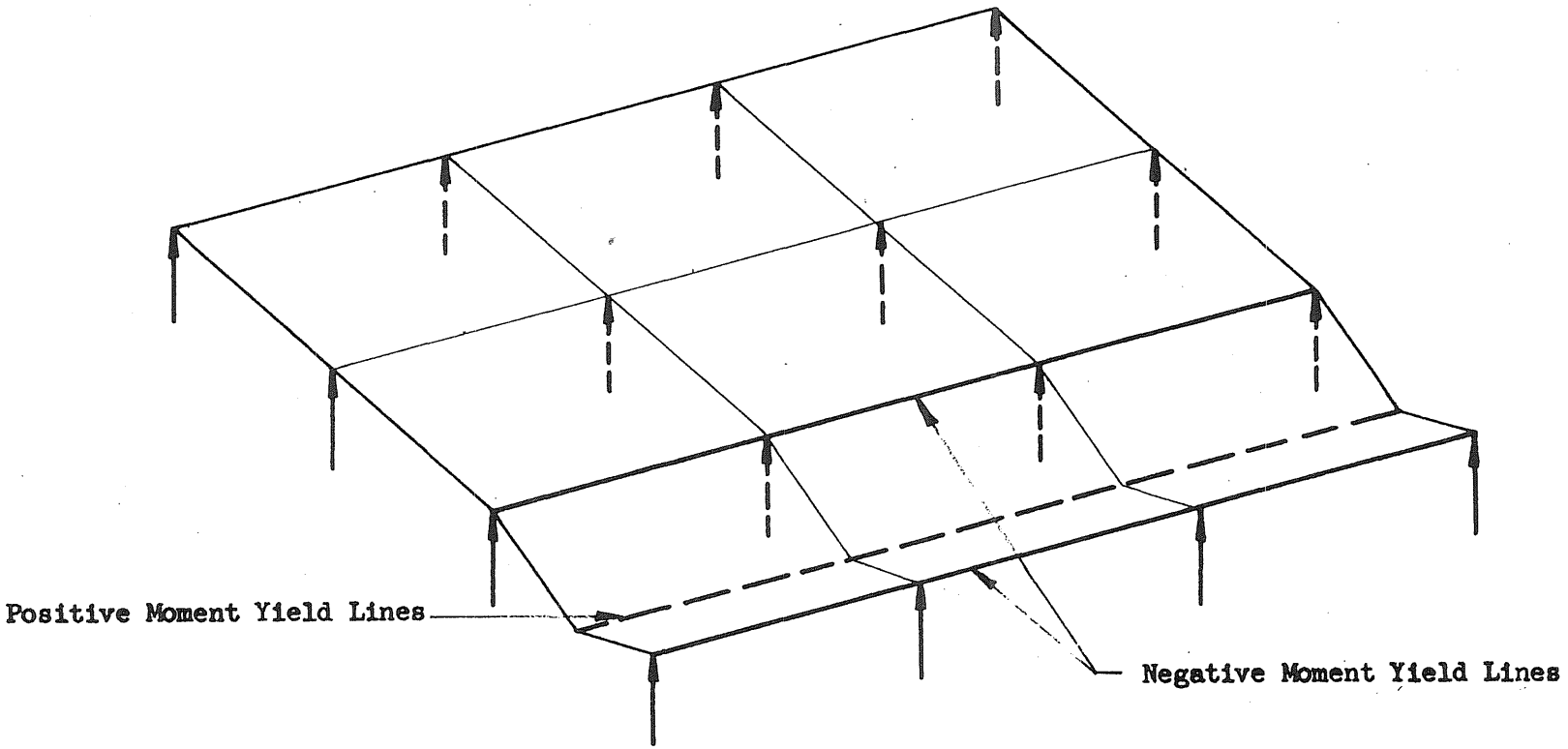

FIG. 9.1 IDEALIZED STRUCTURAL FAILURE MECHANISM

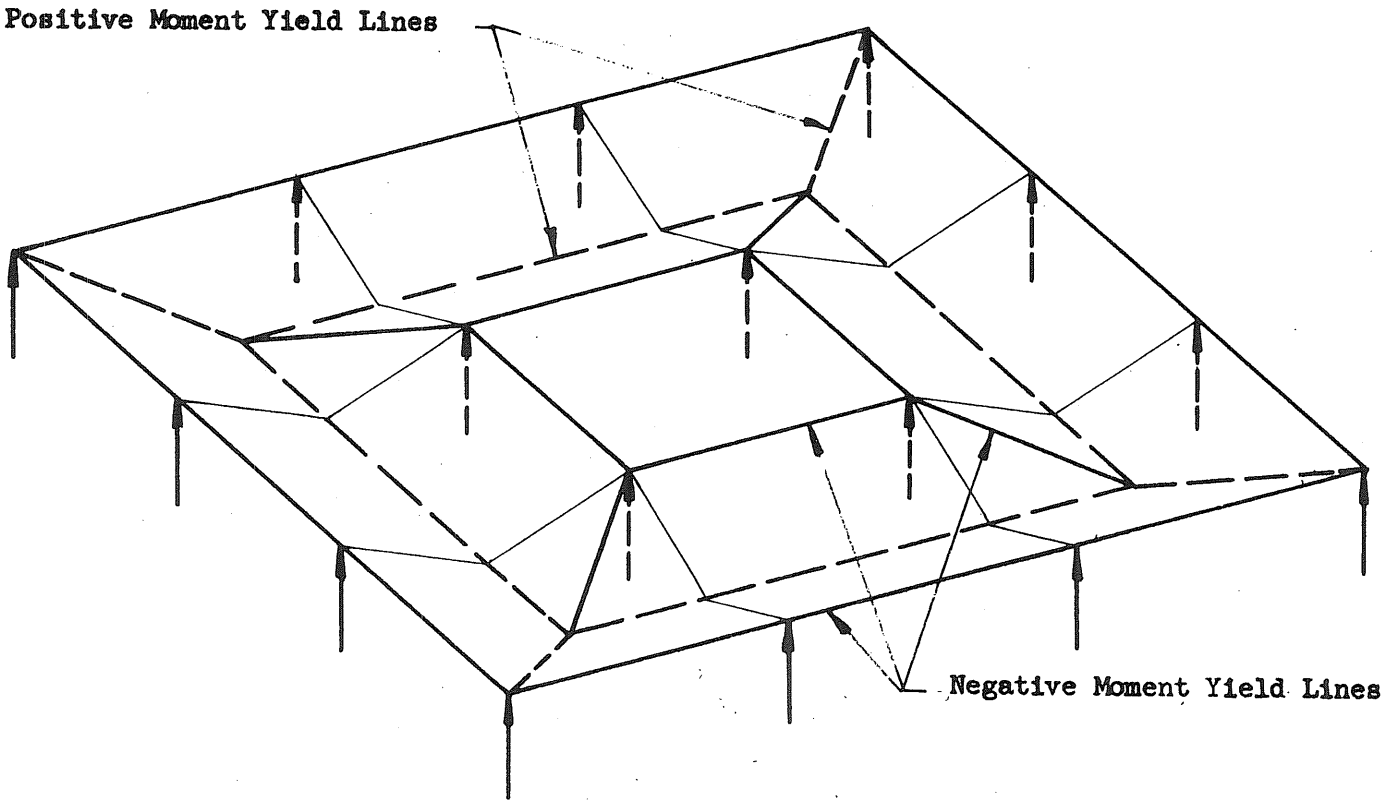

FIG. 9.2 IDEALIZED SLAB FAILURE MECHANISM

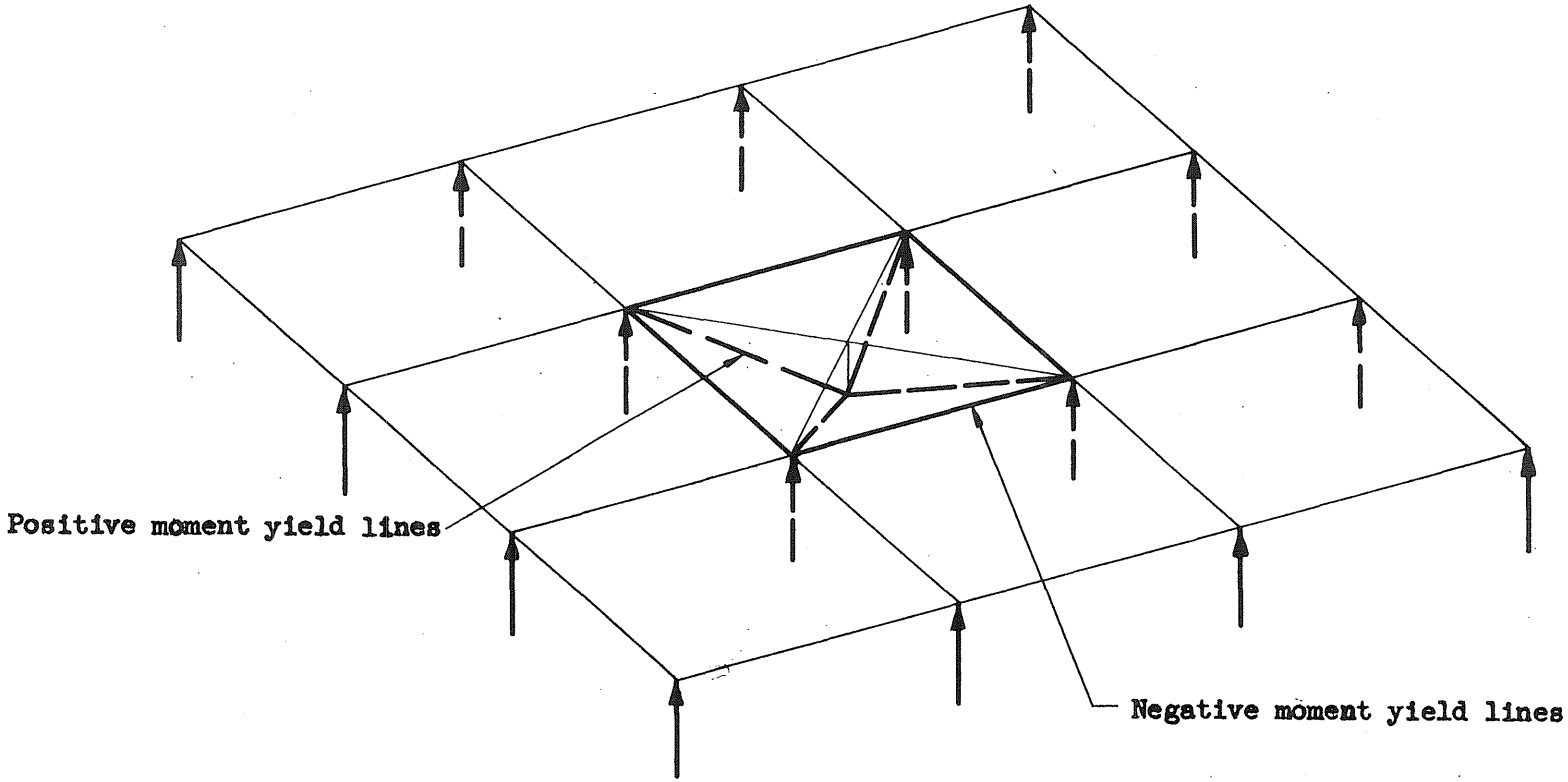

FIG. 9.3 IDEALIZED MECHANISM FOR FAILURE OF A SINGLE INTERIOR PANEL

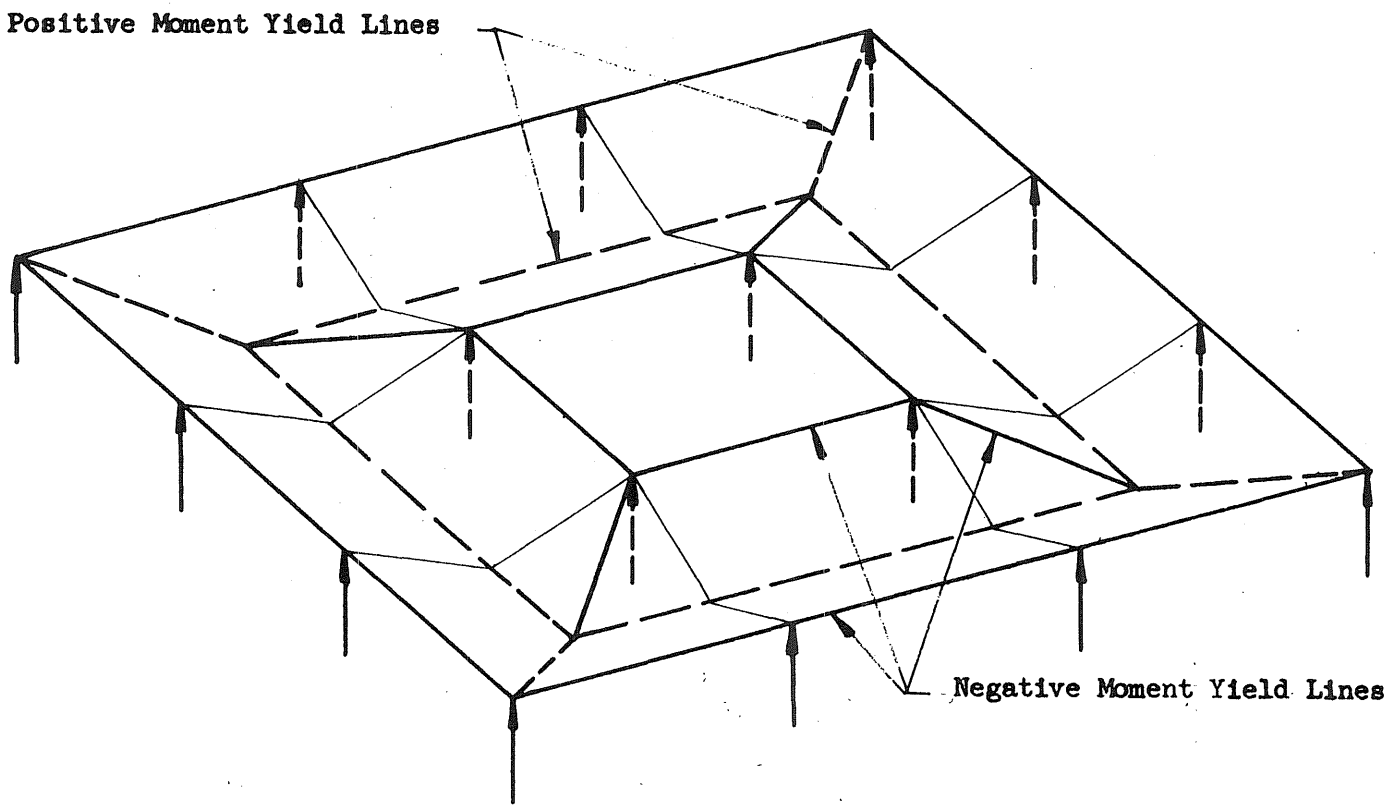

FIG. 9.2 IDEALIZED SLAB FAILURE MECHANISM

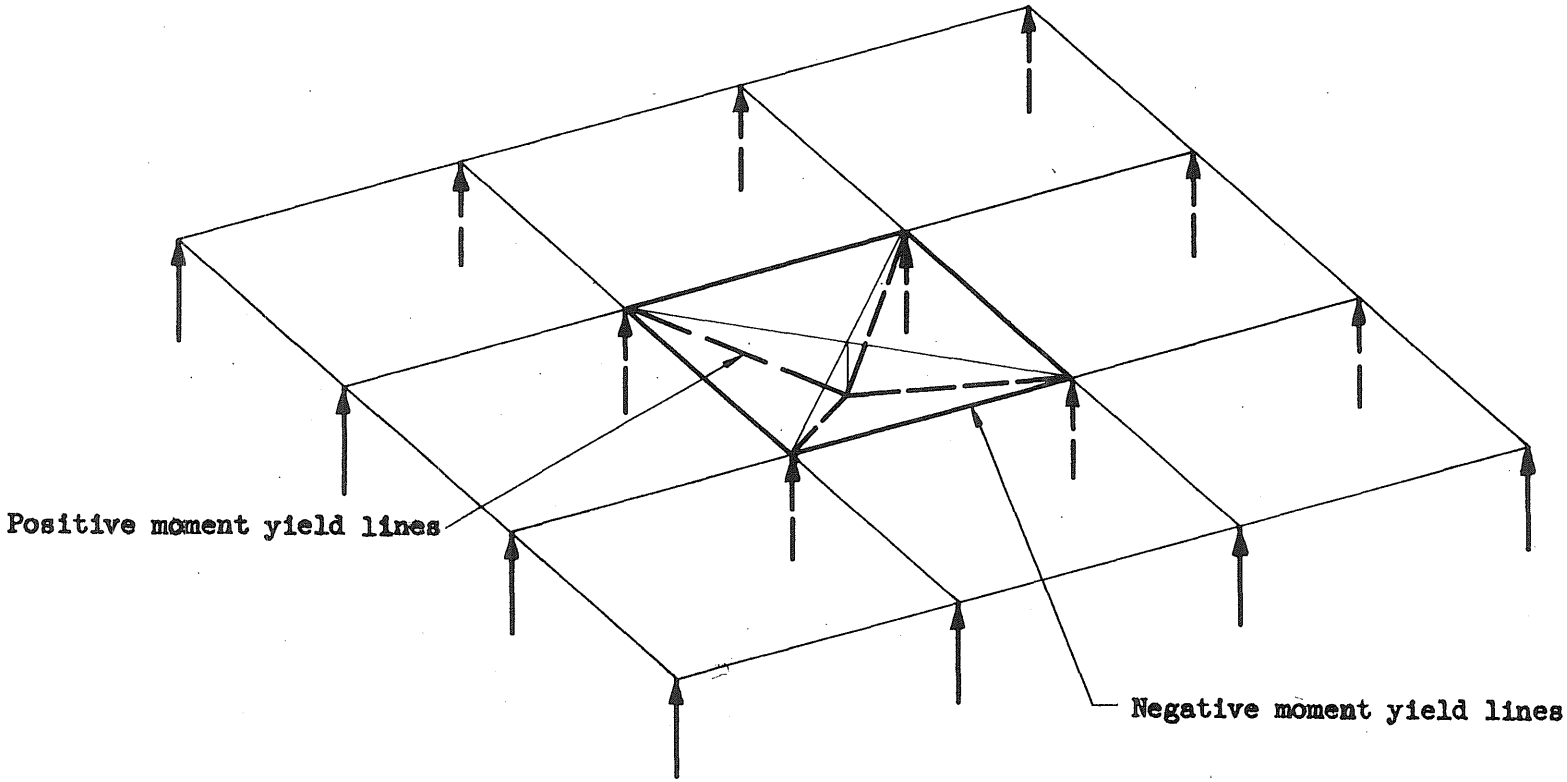

FIG. 9.3 IDEALIZED MECHANISM FOR FAILURE OF A SINGLE INTERIOR PANEL